SOLAR RADIATIVE VARIABILITY FORCING OF CLIMATE CHANGE ON SEASONAL TO DECADAL SCALES IN KENYA

JARED OCHIENG' HERA NDEDA

A Thesis submitted in fulfillment for the Degree of Doctor of Philosophy in Physics in the Jomo Kenyatta University of Agriculture and Technology

2008

DECLARATION

This thesis is my original work and has not been presented for a degree in any other University.

Signature …… Date ……

Jared O. Hera Ndeda

This thesis has been submitted with our approval as University Supervisors.

1. Signature …… Date ……

   Dr. Akeem Babatunde Rabiu

   Federal University of Technology,

   Akure, Ondo State, Nigeria.

2. Signature …… Date ……

   Dr. Livingstone Mwalugha Ngoo

   JKUAT, Kenya

3. Signature …… Date ……

   Dr. Gilbert O. Ouma

   U o N, Kenya

DEDICATION

This work is dedicated to my wife Monica and children; and to my loving, patient and understanding mother Joyce. A lot of appreciation is due to my father, the late Hezekiah Manasseh Ndeda for setting my clear direction by committing his limited resources to my education and good health all through my childhood to adulthood. To my elder brother Samuel Jalang'o for being a good role model to me on academic aspirations; his unrelenting commitment to education unveiled to me the opportunities that were available for higher education abroad. I hence risked my newly acquired job and traveled to a foreign country to pursue my undergraduate studies. This was an irreversible turning point and a firm foundation for this prestigious and pleasant conclusion. Indeed to all my brothers, sisters, relatives and friends for the various roles they have played towards my success up to now.

ACKNOWLEDGEMENT

Dr. A. B. Rabiu initiated me into the field of Solar-Atmospheric and Terrestrial Physics. Had he not, I would have missed out on the valuable experience gained through him, and perhaps may have been by-passed by opportunities granted by this research. I wish to thank him for his guidance throughout this work. His commitment to the academic duties is demonstrated in the total of six global (International) conferences that I came to know of through his involvement in them as a member of the International Organizing committee. I presented various stages of results of my work in the conferences, and received commendations and good suggestions. The conferences were held in: Bangalore India, Gaborone Botswana, Tokyo Japan, Addis Ababa Ethiopia, Akure Nigeria and Abuja Nigeria. Attendance of the Abuja conference made it possible for me to extend my stay in the Federal University of Technology Akure, Nigeria to tidy and finalize the thesis in direct consultation with Dr. Rabiu. All the conferences and workshops enhanced my deep conceptualization of this area of research and the space science in general.

I do appreciate the UNOOSA, NASA, ESA, NAOJ and ICTP for sponsoring me to most of the conferences. I also appreciate JKUAT for coming in handy to sponsor my trips in the cases where I was not able to get the external sponsors for the conferences.

My thanks further go to the UNESCO ANSTI for responding positively to our request to sponsor Dr. Rabiu for the initial stay with me at JKUAT so as to synchronize the research direction.

I appreciate the patience, advice and encouragement of Dr. L. M. Ngoo who besides offering useful insights also performed administrative duties necessary for the completion of this work. He was ready at all times to meet me whenever I needed his input. He often went out of his way to create time to give all he had, and never delayed my work at any one time.

Finally and by no means least, Dr. Ouma G. O. has been a great inspiration to me in this work. He was readily available for any meteorological related requirements, ranging from introducing me to the resourceful staff at KMD for data acquisition and retrieval to availing the relevant literature. His initial input in the development of the proposal and eventually the skillful suggestions during reorganization of the thesis are worth mentioning. His patience and friendly attitude made me comfortable as I waded through the tortuous journey to complete this work.

I have a compelling obligation to thank my dear friend, Maurice K'orowe who while on his research mission in Hyderabad India in 2004, met Dr. Rabiu who was on a post doctoral research in the same institution. Maurice introduced me to Dr. Rabiu

immediately they met. This culminated in this research project. Thank you Maurice for your love of seeing your friend through the same path you are treading on.

I must not forget to mention Dr. Otieno F. for the enormous support with the necessary computer hardware and software that started me off smoothly. He offered me all information he had on MATLAB and many other research literature. In the same note, I remember Salif Daisy for the initial statistical package information that was later advanced by Dr. Kihoro J. Thank you two for the support.

I dearly acknowledge the Director, Kenya Meteorological Department (KMD) for providing me with the KMD data. I am indebted too, to Omeny P., Agallo D., Njogu and indeed to all other staff of KMD, Nairobi for their readiness to assist me at any time of need. Bravo to Owiti Z. formerly of IGAD climate prediction centre, Nairobi for assisting me with relevant literature material from the centre. Also, I acknowledge the research committee of JKUAT for approving funding for good portion of this research and JKUAT administration for providing the study leave.

Special gratitude goes to my wife Monica and my lovely children for their patience and understanding and above all, for their relentless provision of emotional support. To my dear mother Joyce for her patience when she had to stay for several days without seeing me during the times she came to stay with me in my house.

My dear friends and colleagues: Prof. Odhiambo R the former Dean of the faculty of Science, Dr. Kinyua R the Chairman of Physics department, Dr. Lomo P; and my former student and friend Ojuang' J are here duly recognized for the various encouraging roles they played in the faces of various challenges and trying moments that I often faced in the course of this work. And to all, I say thank you!

TABLE OF CONTENTS

LIST OF TABLES

LIST OF FIGURES

LIST OF APPENDICES

LIST OF SYMBOLS

G_{sc}:	Solar constant
Hα:	Hydrogen-Alpha
R_o:	Radius of the Sun or Solar radius
R:	The Universal gas constant
R_s:	Sunspot Numbers
r:	Correlation coefficient
T:	Absolute temperature in Kelvin
ρ :	Density
σ :	Stefan – Boltzman constant = 5.669×10^{-8} Wm^{-2} K^{-4}

LIST OF ABBREVIATIONS

ACRIM:	Active Cavity Radiometer Irradiance Monitors
ANSTI:	African Network of Scientific and Technological Institutions
AVT:	Average Temperature
CAWSES:	Climate and Weather of the Sun-Earth Systems
CPEA:	Coupling Process in the Equatorial Atmosphere
DAAC:	Goddard Distributed Active Archive Centre
DC:	Dry Cold season
DH:	Dry Hot season
DTSI:	Downward Total Solar Irradiance
ERB:	Earth Radiation Budget
ESA:	European Space Agency
EURECA:	European Retrievable Carrier
EUV:	Extreme Ultraviolet
EVA:	Evaporation
FWHM:	Full Width at Half Maximum
ICPAC:	IGAD Climate Prediction and Applications Center.
ICTP:	International Centre for Theoretical Physics
IGAD:	Inter-Governmental Authority on Development
IHY:	International Heliophysical Year
IMF:	Interplanetary Magnetic Field
ITCZ:	Intra Tropical Convergence Zone

KMD:	Kenya Meteorological Department
LR:	Long Rain season
MAT:	Maximum Temperature
MBE:	Mean Bias Error
MDI:	Michelson Doppler Imager
MHD:	Magneto hydrodynamics
MIT:	Minimum Temperature
NAOJ:	National Astronomical Observatory of Japan
NASA:	National Astronautics and Space Administration
NGDC:	National Geophysical Data Centre
NOAA:	National Oceanic and Atmospheric Administration
QBO:	Quasi-biennial Oscillations
RCMRD:	Regional Centre for Mapping of Resources for Development
RH:	Relative Humidity
RMSE:	Root Mean Square Error
RNF:	Rainfall
SBUV:	Solar Backscatter Ultraviolet
SCOSTEP:	Scientific Committee on Solar-Terrestrial Physics
SEM:	Space Environment Monitor
SMM:	Solar Maximum Mission
SOHO:	Solar and Heliophysical Observatory
SOLSTICE:	Solar-Stellar Irradiance Experiment

SOVAR:	Solar Variability Radiometer
SORCE:	Solar Radiation and Climate Experiment Satellite
SR:	Short Rain season
SRA:	Solar Radiation
SST:	Sea-Surface Temperature
SUD:	Sunshine Duration
SUSIM:	Solar Ultraviolet Spectral Irradiance Monitor
TSI:	Total Solar Irradiance
UARS:	Upper Atmosphere Research Satellite
UNESCO:	United Nations Educational, Scientific and Cultural Organization
UNOOSA:	United Nations Office for Outer Space Affairs
USGS:	United States Geophysical Society
USI:	Upward Solar Irradiance
UV:	Ultraviolet
VIRGO:	Variability of solar Irradiance and Gravity Oscillations
WDC:	World Data Centre
WIS:	Wind Speed or Wind Run

ABSTRACT

The study focused on solar forcing of the Earth's climate by looking at how indices of the various solar spheres relate to the climatic parameters measured on the Earth.

The daily meteorological data for nine climatic parameters: Relative Humidity, Maximum Temperature, Minimum Temperature, Wind speed, Sunshine duration, Solar Radiation, Evaporation, Rainfall and Average Temperature obtained from the Kenya Meteorological Department (KMD) for the five representative synoptic meteorological stations covering the period 1986 to 2005 were filtered and reduced to Monthly means. The same procedure was done to the solar indices (Sunspot numbers, F10.7 cm solar radio flux and Mg II core-to-wing ratio) data obtained from NGDC, Boulder, Colorado through their website. The cross-correlation method was applied to calculate the correlation coefficients between the various meteorological variables and solar indices at each station. Significant periodicities in the meteorological variables at each station were determined from the periodograms that were obtained by applying the Fourier transform technique Scargle periodogram (Scargle, 1982) to the monthly means of the meteorological variables. Modeling of the meteorological and solar indices was done using the proposed linear Multivariate model, and the empirical coefficients determined by applying least square fittings. Validity of the models was tested using the statistical indicators: The Mean Bias Error (MBE) and Root Mean Square Error (RMSE). Periodicities in the drought occurrences were determined. Employing the stepwise

multivariate regression analysis in SPSS, the proposed model was then applied to the cases where solar indices were lagged.

Results show that above 95% level of statistically significant correlations exist between wind speed and sunspot numbers in Kericho; between minimum temperature and sunspot numbers in Kisumu; between sunshine duration and sunspot numbers in Garissa; and between solar radiation and sunspot numbers in Garissa. Above 95% level of statistically significant correlations exist between relative humidity and F10.7 cm radio solar flux in Mombasa; between wind speed and F10.7 cm radio solar flux in Kericho, Kisumu, Mombasa and Garrisa; between solar radiation and F10.7 cm radio solar flux in Nairobi and Kisumu; between evaporation and F10.7 cm radio solar flux in Garissa; and between average temperature and F10.7 cm radio solar flux in Kericho. Also above 95% level of statistically significant correlations exist between relative humidity and Mg II core-to-wing ratio in Mombasa; between wind speed and Mg II core-to-wing ratio in Kericho, Mombasa and Garissa; between solar radiation and Mg II core-to-wing ratio in Nairobi; and between evaporation and Mg II core-to-wing ratio in Kericho.

Modal periodicities of 6 and 12 months are detected in climatic parameters in all the meteorological stations apart from Kericho.

The models from the Fast Fourier analysis technique, show variations of solar forcing on climatic parameters at different locations in Kenya. Periodicities of 3.5 and 11 years in drought occurrences obtained in some meteorological stations in the drought occurrences are also comparable to the literature reports on solar activity periodicities,

thus confirming solar signature on the Kenyan climate. Stepwise regression models manifest in specific meteorological stations, and for different climatic parameters. These are seen from the above 95% level of statistically significant correlations between the observed and predicted values from the Fast Fourier analysis models. Solar control is evident on the climate of Kenya.

CHAPTER 1

INTRODUCTION

1.0 Background

We live in an exciting environment: the heliosphere, the exotic outer atmosphere of a star. The space beyond Earth's protective atmospheric cocoon is highly variable and far from gentle. It is the one part of the cosmos accessible to direct scientific investigation, our only hands-on astrophysical laboratory. Our technological society is increasingly susceptible to space weather disturbances in this curious region. A host of interconnected physical processes, strongly influenced by solar variability, affect the health and safety of Earth inhabitants and the habitability of alien environments. Heliophysics aims to explore the Sun-Earth system to understand the Sun and its effects on Earth, the solar system, and the space environmental conditions**.**

The impact of climate variability on day-to-day life systems cannot be overemphasized as nearly every aspect of the bio-system is affected by it. The climatic variability has direct influence on the Socio-Economic factors such as food security of Kenya as a country whose economy is heavily dependent on rain-fed agriculture. Over 70% of the natural disasters in Kenya are related to extreme weather and climate events such as winds, droughts and floods among others Makabana, (2003); Nyakwada, (2003). For example, the recent droughts that occurred in 1983/84 and 1998/2001 led to death of livestock resulting in malnutrition, especially among children and heavy economic

losses among communities, conflicts between communities and between wildlife and humans over the limited resources; power rationing due to low dam levels.

The 1998/2001 drought was more severe than that of 1983/84, but impacts associated with it were less severe than those of 1983/84 because of preparedness by the government in response to the early warning by the Kenya Meteorological Department (KMD). The 1997/98 El Niño related floods and 2003 floods related to the warm Sea Surface Temperature (SST) in the Indian ocean affected villages in Western Kenya leading to displacement of communities to higher grounds, disruption of economic activities such as agriculture due to submerged farms, outbreaks of water related diseases such as Cholera, Malaria and dysentery, among others, Makabana, (2003). Land slides occurred in Central Kenya and led to a number of fatalities. Many early warnings, however, are disregarded because of the previous failure of forecasts to verify. Forecasters need to come clean with regard to their capacities to forecast hazards and the confidence level of their forecasts; Alusa, (2003). A more predictable climate is bound to result in better planning of agricultural practices, hence food security for the country; safety of life and better socio-economic activities in general.

Climate Variability is the short term fluctuations in climate that may not be permanent, such as daily, monthly, annual or even decadal fluctuations. Climate change can be seen in the signals of climate variability; Dilley *et al* (2008). Recent findings on the use of El Niño/Southern Oscillation (ENSO) phenomena to forecast climate variability have

decreased to some extent the uncertainty on rainfall variability; Kitheka S. K., (2003). Empirical statistical methods are used operationally in the development of the seasonal forecasts aided by the atmospheric Global Climate Models outputs; Mungai *et al.*, (2003). The skill of weather prediction using empirical statistical climate models has been good (approximately 75% in seasonal forecast). However, there is still need to look for other indices in predicting climate variability in the country. Therefore this work is investigating the use of solar indices for the study.

Understanding the solar terrestrial interaction, including climatology and weather, starts within the context of Earth's connection to Sun's activity; Tobiska, (2000). There is a need for proper understanding of the Sun-Earth connection as an external forcing of the Earth's climate; Rabiu, *et al.*, (2004). The increasing interest in understanding the solar terrestrial relationship is evident in ongoing international programmes such as Climate and Weather of the Sun-Earth Systems (CAWSES), Scientific Committee on Solar Terrestrial Physics (SCOSTEP), Coupling Process in the Equatorial Atmosphere (CPEA) and International Heliophysical Year (IHY).

In this study, Solar radiative forcing of the Earth's climate is investigated by looking at how indices of the various solar spheres relate to the climatic parameters measured on the Earth. The solar indices include: sunspot numbers (index of the sun's photosphere), F10.7 cm solar radio flux (index of the sun's corona) and Mg II core-to-wing ratio (index of the sun's chromosphere) Viereck *et al* (2001).

1.1 Area of study and location of Kenya

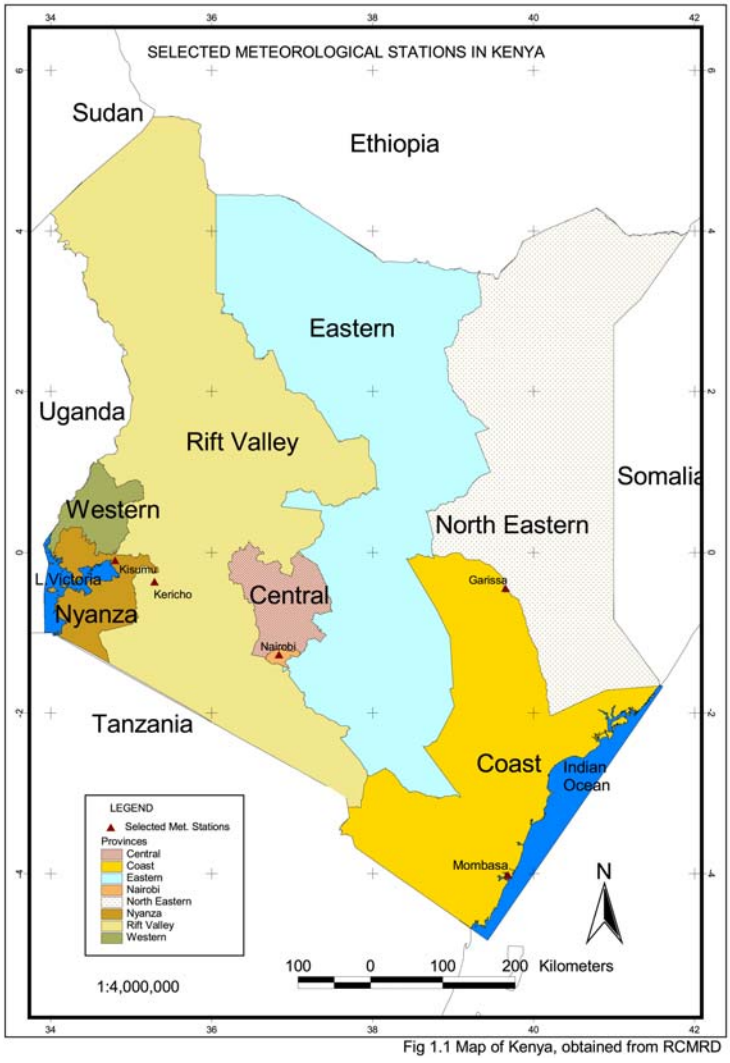

Fig 1.1 Map of Kenya, obtained from RCMRD

Figure 1.1: Map of Kenya, obtained from the Regional Centre for Mapping of Resources for Development (RCMRD), Nairobi.

.

Kenya is a country occupying the landmass bounded by latitudes 5^{o}S and 5^{o}N; and longitudes 34^{o}E and 42^{o}E as shown in Figure 1.1. Kenya is in the Eastern part of Africa,

sharing boundary with five countries: Tanzania on the Southern, Uganda on the Western, Sudan on the North Western, Ethiopia on the Northern and Somalia on the Eastern side. On the South Eastern side the country borders the Indian Ocean, where the coastal city of Mombasa is situated. On the Western side; Kenya, Uganda and Tanzania share the world's second largest fresh water Lake Victoria. The city of Kisumu is on the shores of this lake. The remaining three locations; Kericho, Nairobi and Garissa selected for this research are inland. The geographic equator passes through Kenya.

1.1.1 Climatology of Kenya

Kenya is generally a dry country with over 75% of its area classified as arid or semi arid and only 20% viable for agriculture. Inland rainfall and temperatures are closely related to altitude changes, with variations induced by local topography. Generally the climate is warm and humid at the coast, cool and humid in the central highlands, and hot and dry in the north and east.

Being an equatorial region, the rainfall of the area is expected to be associated with synoptic scale circulation patterns like the convergent low-level winds in the Inter Tropical Convergence Zone (ITCZ) surface locations; Ouma, (2000). However, superimposed on the synoptic-scale circulation patterns are meso-scale systems induced by regional factors such as complex topographical patterns, the existence of many large inland lakes and the proximity of the Indian Ocean; Ogallo, (1983); Basalirwa *et al.*, (1999).

Across most of the country, rainfall is strongly seasonal, although its pattern, timing and extent vary greatly from place to place and from year to year. Studies have shown that a higher percentage of annual rainfall over most of the study area is experienced during the March-April-May (MAM) season; Okoola, (1996). However, Camberlin and Wairoto (1997) via Ouma (2000) show that the southeasterly low lands receive most of its rainfall during the September-October-November (SON) season.

Several large-scale and synoptic-scale features influence precipitation in the study region. The most important of these features is the ITCZ that is a broad low-pressure belt in which the trade winds of the two hemispheres meet. The seasonal variations of rainfall in this region largely depend on the position, intensity and orientation of the ITCZ, which is related to the sun's movements; Ouma, (2000). The north – south movements of the ITCZ seasonally bring into the region two monsoon winds. During the Northern Hemisphere winter (December – February), southeasterly winds prevail in the region bringing a lot of moisture into the region since their tracts are predominantly over the Indian Ocean. These winds reverse direction during the Northern Hemisphere summer (June – August) and the region comes under the influence of northeasterly winds that are relatively dry because of their predominantly continental tracks. The strength of the convergence, and hence the strength of these winds, is influenced by the characteristics of the Arabian and the Azores anticyclones located to the north of the region; the Mascarene and St. Helena anticyclones located to the south; and a trough located within and around the Mozambique Channel.

During the months of July and August when the ITCZ is furthest north, there is a maximum influx of moist westerly winds from the Congo basin and the Atlantic Ocean, especially into the Western parts of the region; Thomson, (1957); Ogallo, (1989). These winds are locally known as the "Congo air mass" and, coupled with the semi-permanent thermal trough over Lake Victoria, they produce heavy rainfall over the Western parts of the region.

Precipitation in the region is also indirectly influenced by the tropical storms originating from Southern Indian Ocean during the Southern Hemisphere summer, and tropical depressions from the Arabian Sea region. These storms also influence ocean parameters such as sea-surface temperatures (SST) and ocean currents that have a bearing on rainfall in the region. Other synoptic systems which control rainfall of the region include the Easterly waves, the Sub-Tropical African jet streams, the East African low level jet stream and remnants of extra-tropical weather systems (for example fronts) that are forced further south or north into the region. A discussion on the characteristics of some of the extra-tropical systems and their effect on the region's rainfall may be found in Fremming (1970) and Njau (1982).

There are large spatial and temporal variations in climate over the study region caused by several regional features. These features include large inland lakes Victoria, Nakuru and Turkana, and topographic features including several mountain ranges (Kenya,

Aberdares, and Elgon) and the Great Rift Valley that runs north to south through the study region. These physical features induce significant modifications in the general wind patterns over the region creating variations in the rainfall; Ogallo, (1989).

1.2.2 Kenyan Homogeneous Climatic Zones

The rainfall generating mechanisms in the tropics are of smaller scales mainly dominated by orography. Ogallo (1980) confirmed that certain parts of East Africa experience rainfalls whose controls are not only the basic large-scale synoptic systems but also the mesoscale influences like the lake and sea breezes. The seasonal rainfalls in Kenya are closely linked to the physical features. However, this relationship only gives a broad overview of the probable controls that the lake, the ocean and orography has on the distribution of rainfall in Kenya. Therefore, the variability of relief from place to place yields zones on land with homogeneous seasonal rainfall.

Zoning is the process of delineating a given area of interest into sub-areas that have similar meteorological signals. Agumba (1988) and Ogallo (1989) have used Principal Component Analysis (PCA) in delineating Kenya and East Africa into homogeneous rainfall zones as can be seen in Figure 1.2 for the long rain (LR) season in March to May. The dry cold (DC) season from June to August, the short rain (SR) season from September/October to November and the dry hot (DH) season covering December, January and March also have their respective homogeneous rainfall climatological zones. A station may belong to different climatological zones in different seasons depending on the meteorological signals it displays in the season. For example KER is seen to fall in

the same climatological zone with KSM during the September/October – November (short rain) season, but falls in different zones during the long rain and short rain seasons.

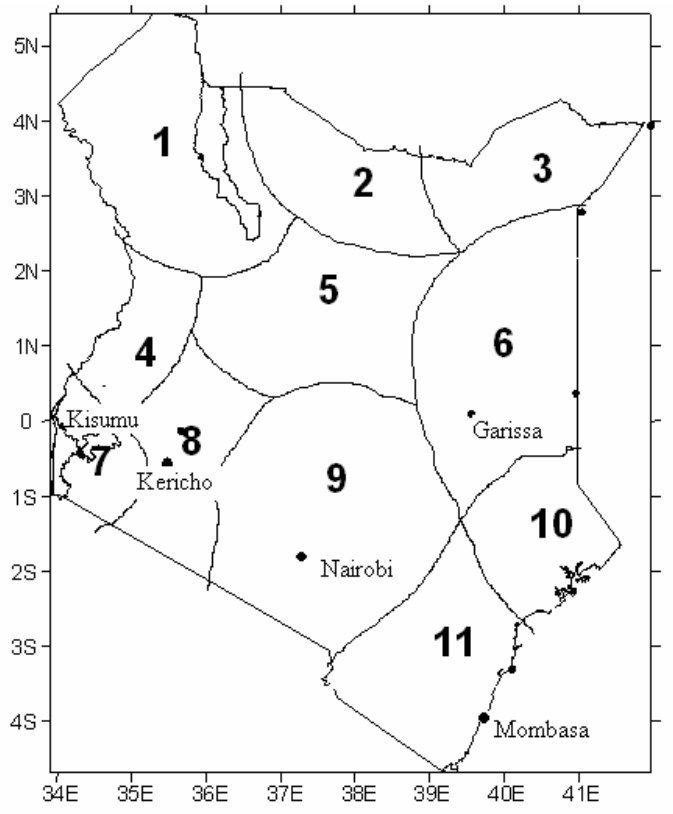

Figure 1.2: Climatological zones of Kenya derived from the March-April-May (MAM) seasonal Rotated Principal Component Analysis (RPCA) patterns (Ouma, 2000)

1.2 Statement of the problem

Kenya is a tropical country with varied climatic regimes. Climatic parameters such as Relative humidity, Temperature, Wind speed, Sunshine duration, solar radiation, Evaporation and Rainfall vary in different parts of the country. For example, the drought

patterns have been observed and reported between 1896 and 1900; Campbell, (1994); UNEP/GOK, (2000) reported by Agwata, (2003); some recent notable ones being in 1975, 1980, 1983/84, 1992-1993, 1998-2001 and 2004-2006. This is a pattern that shows lack of rain in those years. It is also notable that the variability of the onset of rains has often resulted in lack of proper timing of the agricultural activities.

Meteorologists are currently not using solar indices as climatic forcing mechanisms.

The study therefore seeks to establish link between solar variability and the variations of the climatic parameters specifically; relative humidity, temperature, wind run, sunshine duration, solar radiation, evaporation and rainfall.

1.3 Objectives

The primary aim of this study is: to enhance climate change monitoring by investigating Solar Irradiance variability Forcing on the Kenyan climate.

This has been done by looking at the following Specific Objectives:

(i). Use Correlation analysis on the climatic parameters and solar indices to establish the degree of variations of the climatic parameters with the solar indices based on the in situ data.

(ii) Use Fourier Transform technique to determine the periodicities of the meteorological variables and the periodicities in drought occurrences in Kenya.

(iii). Model each of the climatic parameters and observed Solar Irradiance using the atmospheric-solar parameters – Sunspot numbers, Mg II core-to-wing ratio and F10.7-cm solar radio flux.

(iv). Validate the developed models using the statistical models.

(v) Employ stepwise regression analysis to model each of the climatic parameters and the lagged solar indices so as to compare with models from (iii) above.

1.4 Justification

Practically all proxy records around the world show large multi-decadal and century-climate variations. The variability of climate affects every aspect of our bio-system. Agricultural activities that are central to the existence of life on Earth are naturally affected by these variations.

Various studies have also recorded the variations in solar activities over the centuries.

Hence there is a need to understand how solar radiative variability forces climate variability on seasonal to decadal scales in Kenya, East Africa. Adaptation to climate change depends on the early warning systems. Therefore, establishment of solar

variability as a forcing mechanism of climate variability is bound to improve the early warning system for the imminent climatic variations that can have devastating socio-economic effects in the country. Adaptation to the climatic changes can then be possible without severe socio-economic devastation.

CHAPTER 2

LITERATURE REVIEW

A number of researchers have attempted to study the relationship between the solar radiation and the climatic patterns. The examples include: Dickson, (1975); Eddy, (1977); Foukal and Lean, (1990); Hansen and Lacis, (1990); Dewan and Shapiro, (1991); Friis-Christensen and Lassen, (1991); Nikolaskin *et al*., (2001); Rabiu, (2003); Rabiu *et. al*., (2005); Fox, (2004); Ruzmaikin, (2004). Different models have been tested in an attempt to establish the probable relationship between Infra-Red (I-R) radiation with Water Vapor, Relative Humidity and Clearness Index; Udo, (2002). It was found that it is possible to evaluate on a daily or monthly basis, the I-R Sky radiation if Clearness Index, Water Vapor pressure and Relative Humidity are known at a location; the study did not, however, look at the influence of the short wave solar irradiance, for example, the Ultraviolet; Udo, (2002).

Ozone is a relatively active gas and is a primary absorber of solar radiation in the wavelength range between 200 and 300 nm. Changes to the stratospheric ozone concentration will therefore strongly affect the heating rates at these altitudes, and in addition, the amount of solar radiation that is able to reach the lower atmosphere and the surface. Furthermore, induced stratospheric temperature changes will be associated with an altered emission of infrared energy; Palmer M.A. *et al.*, (2004). Therefore, the overall impact on the lower atmosphere will depend on the balance between the effects at short and long wavelengths; Lacis *et al*. (1990), Shine, (2000); reported by Palmer M.A. *et al*.,

(2004). Imposed stratospheric ozone reduction has significantly increased the magnitude of the cooling at levels above the tropopause. This is because reduced ozone concentrations absorb less short wave energy, allowing more to penetrate to the troposphere and surface. While investigating the role of ozone changes in determining the climate response to solar forcing using a climate model from Hadley Center (HadSM3), Palmer M.A. *et al,* (2004) performed two experiments, both of which included a wavelength-dependent reduction in total solar irradiance (TSI) of 7.5 Wm^{-2} (0.55%). The results showed that, though the climate response to solar forcing impact on the troposphere will depend on the vertical profile of the ozone changes imposed, inclusion of stratospheric ozone changes enhances the troposphere temperature response by approximately 15-20% in the annual mean; Palmer *et al*., (2004).

Periods of low solar activity, for example Maunder Minimum, have been related to the low temperatures in Northern Europe; and a reduction of irradiance by up to 0.2% during these periods has been established; Solanki *et al*., (2001). This gives a clue on direct connection of solar irradiance variations to the terrestrial climate. While investigating the Sun-Climate interaction, Kilcik, (2005) compared solar irradiance data from the World Data Centre (WDC) to the data of Ca plage (indications of solar chromosphere) and sunspot areas (indication of the photosphere) acquired from National Geophysical Data Centre (NGDC). He compared these data sets to temperature data acquired from NGDC. Applying the cross-correlation equation of Bourke, (1996), with no time lag in the data set, 0.42 correlations for USA and 0.79 for Japan between

temperature and irradiance were obtained. In the same study, periodicity of the solar irradiance and surface temperature of each country was done using the Fourier analysis technique Scargle periodogram applied to the smoothed annual mean temperature and solar irradiance data. Both data sets showed similar periodicities, except for the disagreement in the interval 1965-1975 for both regions. The disagreement is attributed to the sulphate aerosols that cool the earth's surface and the lower solar activity cycle, 19^{th} cycle; Kilcik, (2005).

It is notable that solar irradiance changes have influence on the Earth's climate and Agriculture (JUGG, 1991-1994; Oritiz *et. al*., (1996-1998). There are predictions of climatic variations within the troposphere due to anthropogenic greenhouse gases, especially CO_2. These are demonstrated by the increase in surface air temperature, increase in global rates of precipitation and evaporation, rising sea level, and changes in biosphere. Increase in surface air temperature would lead to increase in evaporation and generally higher levels of atmospheric water vapor. It would also lead to more intense hydrological cycle, with more frequent heavy precipitation levels; Tamara *et. al*., (1999); Quark Soup, (2004).

Because of the coarse spatial resolution of the present general circulation models, simulations of the regional and seasonal distribution of precipitation are poor. Other shortcomings in climate models include the representation of aerosols, precipitation, clouds and changes in irradiance; Tamara, (1999).

Uncertainties in representation of the influence of anthropogenic aerosol forcing is a principal source in modeling climate change during the industrial period. The aerosols scatter and absorb short wave (solar) radiation and modify reflectivity of clouds. Both effects are thought to decrease the absorption of short wave radiation by the Earth, exerting a cooling on climate, despite the fact that troposphere aerosols are short lived in the atmosphere (just a few days). Improved comparisons between simulated and observed global temperature trends during the industrial period, shown by the recent climate modeling studies that included effects of aerosols may only be by chance because of the uncertainties in aerosol forcing; Tamara *et. al*., (1999); Quark Soup, (2004).

Clouds have warming and cooling effects. There is a direct influence of solar activity on cloud cover, with only one-month delay between solar strength and cloud cover. The variance in cloud cover within one sun cycle is around 2% which results in measured 0.3^{o}C variance in sea surface temperature (SST); Ferdinand-Quark Soup, (2004). But the question of whether average cloudiness would be increased or decreased in a greenhouse-enhanced world is not yet established. All these issues contribute to the present uncertainty in climate sensitivity; Tamara, (1999).

The increase of the sun's activity in the past century, which is about three times the variability within a cycle, may have resulted in 0.9^{o}C increase in SST (the measured trend in the last decades in the tropics is around 0.1^{o}C/decade), large enough to explain

the whole increase in global temperature, leaving not much room for any anthropogenic forcing; Ferdinand-Quark Soup, (2004). Model calculations by Rolf *et. al*., (2005), based on over eight years of measurements at eight radiation stations distributed over the central Alps (Central Europe, latitude ~46^{o}N), show the cloud-free long wave flux increase of +4.2 or 1.9 Wm^{-2} to be in due proportion with temperature of +0.82 or 0.41 ^{o}C and absolute humidity of +0.21 or 0.10 gm^{-3} increases, but three times larger than expected from anthropogenic greenhouse gases. After subtracting for the two thirds of temperature and humidity rises, the increase of cloud-free long wave downward radiation of +1.8 or 0.8 Wm^{-2} remains statistically significant and demonstrates radiative forcing due to an enhanced greenhouse effect; Rolf *et. al.,* (2005). Radiative forcing – measured at Earth's surface – corroborates the increasing greenhouse effect. This suggests that the anthropogenic greenhouse gases cannot be concluded as the only contributors to the climate variability, hence the need to investigate solar variability as another climate forcing factor.

The temperature of the surface and that of the air above the surface are changing at different rates due to some unknown mechanism; Dano *et. al.*-Quark Soup, (2004). This phenomenon may be due to the fact that when radiation waves fall directly on the surface-there is immense impact. This impact certainly results in higher temperature on the ground as opposed to the areas above the ground within the troposphere where there is no such impact.

Gradual temperature changes have had impacts on crop yields; Fleck-Quark Soup, (2004). Study by Pegeng *et. al.*-Quark Soup, (2004) confirms predictions from some simulation studies of substantial yield reductions caused by higher mean daily temperature. However, yield reductions caused by global warming predicted by simulation tend to be smaller. For example, the simulated yield reduction from a $3^{o}C$ rise in mean daily temperature was 16% for maize, wheat, sorghum and soybean in Central United States. For rice, simulated yield potential in the major rice-growing regions of Asia with present CO_2 concentration decreased by 7% for every $1^{o}C$ rise above current mean temperature; Pegeng *et. al*.-Quark Soup, (2004).

Accurate measurements of solar irradiance have only been available since 1978. Extrapolation to earlier periods depends upon proxies which become less and less reliable as one goes further back. Measured troposphere, land and SST, as well as proxy indicators such as glacier melt and sea ice retreat, have certainly indicated 'global warming' since 1978; Hans *et. al*-Quark Soup*,* (2004).

Irradiance variations have been connected to the sun's magnetic activity. Proof of other proxies is yet to be established. The observed variations of 0.1% expected to produce corresponding variation of $0.2^{o}C$ in globally averaged equilibrium surface temperature is not a conclusive evidence to relate solar irradiance variations to the global climate changes (Solar Irradiance and Long-Term Climatic Variability, via http://www.Org/).

Since 1979 the use of satellite-borne radiometers has enabled more accurate measurements of the TSI to be carried out. The advent of satellite-borne radiometers (ERB/Nimbus-7, ACRIM/SMM, NOAA-9, SOVAR/EURECA, VIRGO/SOHO, ACRIM/UARS, ERBS) enabled more accurate measurements of TSI to be carried out, making it clear that the absolute value of the instantaneous TSI is not known to better than a few Wm^{-2}; Varotsos *et. al.* (2004). However, over a period these trends can be observed beneath these variations and the satellite sensor data show a consistent picture of variation of about 1.4 Wm^{-2}, or approximately 0.1%, from the minimum to the maximum of the 11-year cycle; Haig, (2000), reported by Varotsos *et. al.* (2004). However, while satellite-flown instruments are very valuable in giving synoptic coverage of a large area on some sort of regular periodic basis, there are problems when one looks to them for evidence of long-term changes, for example in the climate or in variables linked to climate. Since direct measurements of TSI made by satellite instruments are available only over the past two decades, it is necessary to use other proxy measures to reconstruct variations at earlier dates; Haig, (2000).

Statistical Regression analysis has also been used to arrive at a relationship between I-R radiation and Vapor Pressure (e), Relative Humidity (RH) and Clearness Index (k_T) Udo, (2002).

Spectral analysis may be defined as the study of the distribution by wavelength or frequency of the radiation emitted by an object of interest. It includes various analyses of

solar activities and other related phenomena. Graphical representations of trends of variations of different parameters with time, called the spectra can be analyzed in spectral analysis.

Spectral analysis has been employed to study relations between solar activity and various climatic and other phenomena. Juan *et al.*, (2004) used continuous wavelet transform to examine the relationship between solar activity and the annual precipitation in the Beijing area. The results showed that there are four main periods for the annual precipitation (11, 22, 33 and 72 years) that closely correspond to the four periods of the sunspot numbers (11, 22, 33 and 78 years). This plus further correlations and statistical analysis led to their conclusion that the annual precipitation is closely related to the variation in sunspot numbers and that solar activity probably plays an important role in influencing the precipitation on land. Several other studies have been reported by Juan *et al*., (2004) stating solar output as causing significant changes in Earth's climate; for example, Pederson in 2001 as reported by Juan, (2004) found possible solar influence from the annual precipitation and other hydro-meteorological reconstructions in Northeastern Mongolia derived from the tree rings (which serve as a proxy for the varying intensity of solar activity) from 1651 to 1995. Their spectral analysis revealed significant periodicities around 12 years and 20-24 years that are believed to be solar induced.

It is well known that the water level of Lake Victoria (always considered as indirect index of tropical precipitation) is positively correlated with the 11-year period of the sunspot numbers during 1880-1930. This evidence made many people acknowledge that precipitation was closely related to solar activity. After 1930, however, it seems that the correlation ceased to exist. This is the evidence that the relationship between solar activity and precipitation is very complicated and varies with time and probably also with geographic position. On the global scale, the correlation between sunspot number and precipitation may be positive, negative, or even zero; Juan *et al*, (2004).

To examine periodicity of different kinds of solar events, Nag *et al.,* via (tukada2@vsnl.net) have used the Fourier transformation by expressing a signal g(t) by a trigonometric Fourier series over any interval of duration T_o as:

$$g(t) = a_o + \sum a_n \cos(n\omega_o t) + \sum b_n \sin(n\omega_o t) \qquad (2.1)$$

Where n = 1 to infinity and $\omega_o = 2\pi / T_o$. While a_o, a_n and b_n are the Fourier coefficients. They determined a high correlation between the daily values of sunspot number and the radio flux at the observing frequency close to 2.7 GHz (and this holds good for both sunspot maximum and minimum periods), and they came up with a regression equation after plotting the scatter diagram of the two variables: Radio flux = $I + a.N$. Where '*I'* is the basic component of the radio flux, *'a'* is an arbitrary constant and '*N'* is the sunspot number. Further modification of the regression equation and application of autocorrelation to the same time series to confirm the periodicity obtained from the Fourier transformation led to the observation that sun exhibits periodicity of both short

term and long term, in different kinds of solar activity, such as, sunspot numbers, general magnetic field, solar irradiance, flares, radio emission and high energy particle emission.

Mid-range periodicities (the regime between the long-term periodicity of 11-year sunspot cycle and the short-term 27-day periodicity) in solar flare occurrence have been analyzed by Bai, (2003) for solar cycles 19-23 using various methods.

Several mid-range statistically significant periodicities were detected from analyses of cycles 19-23: 51 days from cycle 19; 85 and 129 days from cycle 20; 153 days from cycle 21; 34 and 129 days from cycle 23. In my work also, the Fourier analysis technique; Scargle, (1982) has been employed to investigate the periodicity of the Meteorological variables and solar indices at each station.

Raspopov *et. al*., (2001) demonstrated existence of long term variations in solar activity and climate using dendrochronology or tree-ring dating (method of scientific dating based on the analysis of tree-ring growth patterns) data. Dendrochronology may simply be defined as the dating of past events (climatic changes) through study of tree ring growth, or just as "tree technology". Jona, via http://www.livius.org/, says that in areas where the climate is reasonably predictable, trees develop annual rings of different properties depending on weather, rain and temperature in different years. These variations may be used to infer past climate variations. Raspopov *et. al.* (2001) observed existence of harmonics and combinatory frequencies, besides the primary periodicities

related to the solar activity, in the radiocarbon spectrum that suggested the non linear nature of the effect of solar activity on terrestrial environment and climate (as demonstrated by results of spectral analysis of variations in tree ring widths at the Northern timberline on the Kola peninsula). They, however, did not address solar variability effects on specific climatic parameters, nor did they suggest a model to explain how solar activity relates to terrestrial environment and climate.

An increase in solar activity (more sunspots) is accompanied by an increase in the solar wind that reflects cosmic rays, and hence reduces ^{14}C production. Therefore, the ^{14}C concentration of the atmosphere (which is recorded in the wood of trees) is lower during sunspot maxima and higher during sunspot minima; USGS, (2000). The fact sheet of USGS, (2000) also reports that irradiance is greatest during sunspot maxima and lowest during sunspot minima-which appear counterintuitive because the dark sunspots might be expected to dim the sun. However, bright regions surrounding the sunspots, called faculae, cause the sun to brighten at peak activity. It is also reported that during the Maunder Minimum, the total irradiance reduced by 0.2% relative to the solar minimum (or quiet sun) of the mid-1990's, but total ultraviolet (UV) radiation was reduced by 1.04%. As reported in the Fact sheet, Crowley and Kim, (1996), estimated that the total warming of 0.8^{o} to 0.9^{o} occurred between the minimum of sunspot activity during the Maunder Minimum and maximum sunspot activity during the mid-20^{th} century. It is reported that the surface of the Earth has warmed $0.55^{o}C$ since 1860, and about half of this could be due to increased solar warming since the Maunder Minimum. However,

0.36°C of the 0.55°C increase has occurred since 1970. Solar forcing can only account for 0.11°C of the 0.36°C increase; the rest could be due to greenhouse warming or some other cause.

Thus, there appears to be a real relation between solar activity and global temperature related to solar irradiance, with colder temperatures during sunspot minima. The main problems in solar-climate influences are in the instability of the relations found. Negative and positive correlations between solar activity and surface air temperatures have been reported by different authors. Georgieva, K. *et al*. (2000) show that the sign of the correlation changes regularly in consecutive centennial solar cycles and seems determined by the North-South asymmetry of solar activity: the correlation is positive when the Northern solar hemisphere is the more active one and negative when more active is the Southern solar hemisphere. When showing that Quasi-biennial Oscillations (QBO) exist in solar North-South asymmetry, Georgieva, K. *et al.* (2000) confirmed from the displayed spectra that in the 18th century, in the vast majority of the available stations the surface air temperature was positively correlated with solar activity in the 11-year solar cycle, this correlation changed to negative in the 19th century and to positive again in the 20th century. That is in the end of 18th century; high temperatures are observed in solar minimum and low ones – at high solar activity, and about 1920-30 the situation changes to the opposite. The change in the sign of the correlation does not occur simultaneously all over the globe.

The driving force behind various terrestrial phenomena like geomagnetic storms, auroral and weather systems etcetera originate from the sun and the variations in it as reflected through sunspot numbers, solar flares, solar irradiance, interplanetary plasma, magnetic field variations and high energy solar particle events affect such phenomena. Considering SST as a better measure of global climate since it represents 70% of the planet's surface area, and is much more spatially and temporally homogeneous than the land surface; Shah *et al.*, (2005) have used it to explore whether the long period solar variations also reflect in variations of the climatic parameters. The spectra obtained by them on 100 years time scale revealed good correspondence between the sunspot activity and SST, in that the sunspot activity also reaches a minimum (Gleissberg's minimum in solar activity) around the same period as the SST. They further investigated linkage between climatic variations and geomagnetic activity (using *aa* or antipodal geomagnetic indices data), and concluded that geomagnetic activity seems to be a possible link through which the solar activity controls the earths climate. The role of the sun in forcing the climatic change still remains an open question.

From the foregoing literature review, the major focus has been on the sunspot numbers as the solar index forcing the terrestrial climate. However, there are other solar parameters that may be considered. Therefore this work aims at looking at the climate forcing due to the two other solar parameters (F10.7 cm solar radio flux and Mg II core-to-wing ratio) in addition to the sunspot numbers.

CHAPTER 3

THEORETICAL CONSIDERATIONS

3.0 Introduction

This chapter defines and discusses all the solar and climatic parameters used in this study, together with the space structure traversing the sun to the end of the solar system dubbed the "Heliosphere". It starts by defining and explaining the source of radiation; the Sun, stating its various spheres that are sources of the solar indices used. These spheres include the photosphere, the chromosphere and corona which are sources of sunspot number, Mg II core-to-wing ratio and F10.7 cm radio solar flux respectively. The indices are discussed at length, stating the sources of information about them. The SOLAR2000 model is discussed just after the solar indices. Some sections define the Heliosphere and give information on space weather. The earth's atmosphere has many spheres, beginning with the Exosphere (the outer most) to the troposphere (next to surface of the earth). These are briefly defined by stating the various activities going on in each of them. We then proceed to define and give some theoretical background of the climatic parameters: Relative Humidity, Temperature, Wind, Sunshine duration, Radiation and Rainfall.

3.1 The sun (The Active Sun)

The sun is the nearest star to us. It offers a unique celestial laboratory where a large variety of phenomena take place, ranging in temporal domain from a few milliseconds to

several decades, in spatial domain from a few hundred kilometers to thousands of kilometers, and in temperature domain from a few thousand degrees to several million degrees; Bhatnagar, (2006). Its mass motion ranges in thousands of kilometers per second. The solar radiation whose variations are envisaged to be forcing the climatic variations here on earth originates from the sun.

The sun is a sphere of intensely hot gaseous matter with a diameter of 1.39×10^9 m and is on the average, 1.5×10^{11} m from the earth. As seen from the earth, the sun rotates on its axis about once every 4 weeks. However, it does not rotate as a solid body; the equator takes about 27 days and the Polar Regions take about 30 days for each rotation; Duffie *et al.,* (2006); Tracking a solar Storm by NASA, via http://son.nasa.gov/).

The sun has been observed by the Solar and Heliophysical Observatory (SOHO), a sun-study space-craft built and operated by NASA and the European Space Agency (ESA). Irradiance measurements are made by several instruments on SOHO: VIRGO-Total Solar Irradiance, SEM (Celias)-EUV disk integrated flux from 1-770Angstroms and in He II 304 Angstrom, CDS-EUV 307-380 Angstroms and 516-632 Angstroms Spectral irradiance and 69 full disc images taken each month; Friss-Christensen *et al.*, (2001). Even the back side of the sun can be seen using the technique of holographic helioseismology; Bhatnagar, (2006).

The sun is composed of the core that contains the burning gases at very high temperatures; so it is the centre of thermonuclear fusions that power the sun. The great majority of atoms are stripped of their electrons at temperature above 15,000,000K. Each hydrogen atom weighs 1.0078 atomic mass units (amu) and each He atom is made of 4 hydrogen atoms thus weighing 4.0312 amu. During the fusion process an excess mass *m* of 0.0282 amu above the He atom of 4.003 amu is converted into energy E according to Einstein's formula:

$$E = mc^2 \tag{3.1}$$

Here *c* is the velocity of light (Solar Structure, via http:www.Columbia.edu/). Thus in each second, the sun converts 5 million tons of mass into energy which generates energy on the order of $4x10^{26}$ watts! (Solar Structure, via http: www.Columbia.edu/).

Just above the surface of the sun are charged solar gases heated to about 60,000^{o}C. The brighter areas show more density of charged material, which means greater magnetic activity. It is estimated that 90% of the energy is generated in the region of 0 to $0.23R_o$ (where R_o is the radius of the sun), which contains 40% of the mass of the sun. The region from $0.23R_o$ to $0.7R_o$ known as radiation or radiative zone (Solar Structure, via http:www.Columbia.edu/) insulates the core, helping it maintain the high temperatures needed to sustain the nuclear fusion. The gamma photons produced in the core's fusion reactions are repeatedly absorbed and re-emitted by nuclei in the radiative zone, gaining lower energies and longer wavelengths with each successive re-emission. At a distance $0.7\ R_o$ from the centre, the temperature drops to about 130, 000 K and the density to 70

kg m^{-3}; here convection processes begin to become important, and the zone from 0.7 to 1.0 R_o is known as the convective zone. Here atoms may keep their electrons because of the low temperature and ions and even neutral hydrogen exist. Here many atomic absorption processes occur, mainly bound-free transitions. The high opacity makes it difficult for photon radiation to continue outward and steep temperature gradients are established which lead to convective currents. It is in this location where sunspots and other solar activity phenomena are generated. Radiation is not as prevalent in this layer, so the matter heated by contact with the radiative zone forms giant convective cells which appear on the photosphere as granules (Solar Structure, via http:www.Columbia.edu/). The plasma is made up of charged particles which create large, prominent magnetic fields when they move with the convective cells; this plays a large part in the creation of sunspots and flares. The outer layer of the convective zone is called the photosphere (sphere of light). Within this zone the temperature drops to about 5000 K and the density to about 10^{-5} kgm^{-3}. Above the photosphere is a layer of cooler gases several hundred kilometers deep called the reversing layer; Duffie *et al.,* (2006)**,** which is just the lower chromosphere (The Structure of the Sun, via http://www.cs.berkeley.edu/).

The sun's surface appears to be composed of granules (irregular convection cells), with dimensions from 1,000 to 3,000 km and with cell lifetime of a few minutes. Other features of the solar surface are small dark areas called pores, which are of the same order of magnitude as the convective cells, and larger dark areas called sunspots, which

vary in size. The sun is controlled by powerful magnetic forces that drive its activity and can create solar storms. Huge clouds of cooler gases are propelled into the sun's atmosphere by these forces.

The sun is always changing every minute, both inside and outside. 108 earths lined up across the width of the sun approximate the size of the sun. The SOHO spacecraft is actually only 1.6 million km (one million miles) sunward from the earth. It orbits the Sun along with the Earth and sends back images and data 24-hours a day. The more we learn about the sun, our star, the more we know about all stars (This is the Sun in ultraviolet light! via www.nasa.gov). The dynamo action (dynamo model is a model for the generation of a planet's or a star's magnetic field by the organized circulation of conducting fluids in its core) of the Sun is believed to be responsible for emergence of new magnetic fields into the solar atmosphere. The wealth of solar phenomena (radiative, plasma and Magneto Hydrodynamics (MHD), popularly known as solar activity, arise due to these magnetic fields making their tortuous journey from the interior of the Sun to the solar atmosphere and into interplanetary space.

The sun is commonly divided into the solar interior or the core, the radiative zone, the convective zone and the visible surface or the photosphere. The visible surface is also the visible zone. Outside the sun's Photosphere are the chromosphere or colour sphere and the corona. Due to the gaseous nature of the sun, no sharp boundaries exist between

the various layers. The sun's interior (core) makes up all but a tiny fraction of the solar mass and unlike the outer layers; it is not accessible to direct observation.

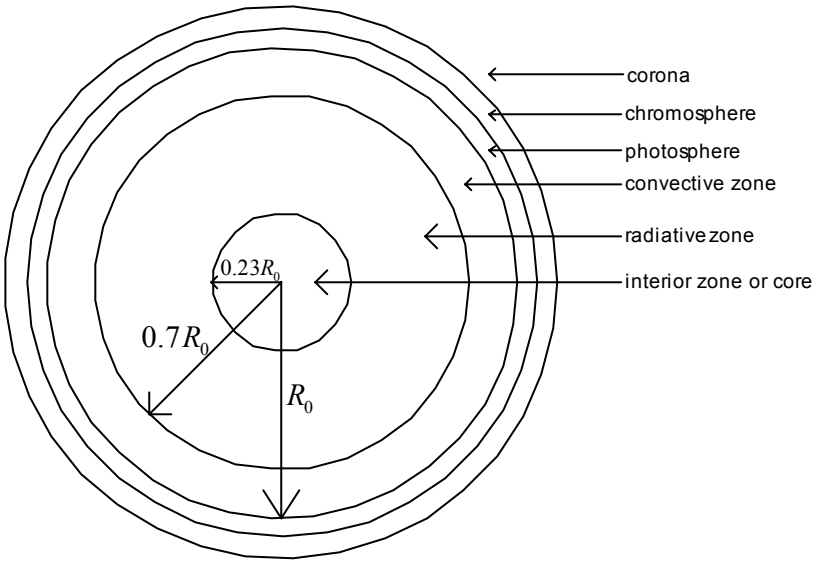

Figure 3.1: Structure of the Sun (Duffie *et al.*, 2006; and The Structure of the Sun, via http://www.cs.berkeley.edu/)

The various regions in the structure of the sun in fig. 3.1 are characterized as follows: $r<0.23R_o$ is the Solar interior or core, with 40% mass of sun and 15% of volume; 90% of energy is generated here. T = ~ 8-40x10^6K, $\rho = 10^5$ kgm^{-3}.

$0.23R_o<r<0.7R_o$ is the Radiation or Radiative zone where the temperature drops.

$0.7R_o<r<R_o$ is the Convective zone; here T = 130,000K, $\rho = 70$ kgm^{-3}.

R_o marks the boundary of the solar radius. It is the outer layer of the convective zone, known as the photosphere; T = 5000K, $\rho = 10^{-5}$ kgm^{-3}. It is the source of most solar radiation. Above the photosphere is the Chromosphere; here T = 5000k +. Lastly is the Corona where T = ~ 10^6k and ρ = very low.

3.1.1 Photosphere

Photosphere or sphere of light region is the visible surface of the sun; the region of the solar atmosphere from which visible light and solar wind escapes into space. The photosphere is composed of 73.5% hydrogen, 25% helium, 1.5% oxygen and carbon as stated by The Structure of the Sun, via http://www.cs.berkeley.edu/.

The solar wind is a stream of charged particles mostly protons and electrons that escape into the sun's outer atmosphere at high speeds. Most of the radiation from the sun originates here at its temperature, T of 5800K. This radiation is in equilibrium and the Stefan-Boltzmann law can be applied to calculate this temperature. As stated by Solar Structure via http:www.Columbia.edu/, according to the Stefan-Boltzmann law each square centimeter of the solar surface having a temperature T emits, in all directions, light of σT^4 ergs per second (σ is Stefan-Boltzmann constant). Subsequently, the total emission of the sun in one second known as luminosity,

$$L_o = 4\pi R_o^2 \sigma T^4 \qquad (3.2)$$

The fundamental relation can be used to determine L_o, R_o or T if any two of them are known.

Sunspot is a temporary cool region in the Sun's photosphere, associated with an active region (a plage), with a magnetic field intensity of fewer than 0.1 Tesla. The activity of the sun is therefore measured by the sunspot numbers. Faculae are bright regions of the

photosphere seen in white light, seldom visible except near the solar limb (Glossary of Solar-Terrestrial Terms, via http://www.swpc.noaa.gov/info/glossary.html).

The sun rotates about its own axis that has a tilt of 7.5 degrees. It completes a half cycle of the rotation in 11 years, and a full cycle in 22 years: That is, a north pole of the sun reaches the South Pole position in 11 years, and comes back to its original position in 22 years. So the 11 year cycle observed in different kinds of solar activity, 22 year cycle in the magnetic polarity reversal and 27 day periodicity in the slowly varying component of solar radio emission are well known (Nag *et al.,* via tukada2@vsnl.net). The knowledge about these periodic values helps us to know the physical state of the sun, whether it is quiet, or in disturbed phase at a particular period. During quiet or non-active period the sun emits less energy, whereas, at the time of disturbed or active phase it emits higher energy; Zeilik *et al.,* (1998). Sunspot cycle is the 11-year number cycle and a 22-year magnetic polarity cycle of the formation of sunspots. Sunspots show us where the Sun's magnetic fields are most intense. Magnetic fields above sunspots act like invisible nets, blocking the escape of electrically charged gas, or plasma that constantly boils away from the solar surface. When the pressure is too great, they burst. Solar storms then erupt with the power of millions of Hydrogen bombs. If the explosion occurs low in the solar atmosphere, the blast is short but intense. It pours out ultraviolet light, x-rays and other radiation – a solar flare. In visible radiation, the best view of the solar flares is in the Chromosphere. Solar flares release enormous amounts of energy ranging from 10^{29} to 10^{32} ergs in a few minutes, in spectral frequencies from radio, visible, extreme

ultraviolet, X-rays and Gamma rays and even particles and cosmic rays; Bhatnagar, (2006). If the magnetic "nets" stretch far into the corona before they break, a Coronal Mass Ejection (CME) occurs, a billion tons of solar plasma speeding at over a million miles per hour. Two to four days later, if the storm is aimed at earth, the results can be dramatic. Induced currents can corrode pipelines, destroy power grids, and cause blackouts. Navigation and communication satellites can be damaged. Astronauts may be exposed to high radiation doses.

Earth-directed solar storms can create aurora – shimmering curtains and swirls of light in the night sky. Some solar particles find their way into Earth's protective magnetosphere; most gather on the far side in the "magneto tail." Then, sped by a magnetic slingshot, these particles zoom in along Earth's magnetic fields and strike the upper atmosphere in ovals around the poles where atoms glow like neon lights (The Sun and Space Weather, via soho.nascom.nasa.gov/).

3.1.2 Chromosphere

The part of the sun's atmosphere just above the photosphere is known as the Chromosphere (colour sphere): It is hotter and less dense then the photosphere (10^{-9} kgm^{-3}), just about 10,000 km thick; it creates the flash spectrum seen during eclipses (The Structure of the Sun, via http://www.cs.berkeley.edu/). During a total eclipse of the sun, it appears as a thin red rim around the sun. The hydrogen atoms absorb energy from the photosphere and most of the energy is then emitted as red light. The chromosphere is

most easily viewed by filtering out all other wavelengths of light from the sun and only letting the red light from the chromosphere through (Facial Blemishes on the Sun, via http://solar.physics.montana.edu/). It is at a temperature of 4300K but can go up to 50,000K in its outer reaches. The chromosphere is also characterized by cellular convective patterns, with cells much larger than the photosphere's granules. The Chromosphere is alive with activity, mainly due to the various magnetic fields which are dominant in the sun. This causes various events, such as filaments which are large, dark regions of very dense cool gas, held in place by magnetic fields which usually appear long and thin above the chromosphere (Solar Filaments and Prominences, via http://solar.physics.montana.edu/). When filaments appear on the "edge" of the sun other than their hotter surrounding, they appear brighter than the dark outer space behind them. In that case they are called prominences. Filaments last for a few weeks or months. The gas in a filament will eventually move to a different layer in the sun and will no longer be visible in an image of the chromosphere. But at the same time, other gas may move into the chromosphere and create a new filament somewhere else. The birth and death of filaments is a mystery and the subject of the ongoing study by solar scientists (Solar Filaments and prominences, via http://solar.physics.montana.edu/). Prominences can be observed as flame like tongues of gas that appear above the limb of the sun when observed in the light of the Hα line. They occur in regions of horizontal magnetic fields, because these fields support prominences against the solar activity, and indicate the transition from one magnetic polarity to the opposite (Solar Structure, via http:www.columbia.edu/).

The other events caused by sun's magnetic fields in the chromosphere are the plage, spicules and flares (The Structure of the Sun, via http://www.cs.berkeley.edu/). Plage is the bright area surrounding the sunspot regions.

Spicules are relatively small vertical jets of material which can be as large as the earth. As stated by Solar Structure, via http://www.columbia.edu/, they look like hairs of gas rising and falling at the upper chromosphere, reaching into the corona. They last as long as 10 minutes, attaining vertical speeds of up to 20 kms^{-1} getting upwards as high as 15,000 km. Spicules array themselves into chromospheric networks establishing giant supergranulated cells with gases rising in the center and descending at their outer boundaries.

Flares are larger, explosive eruptions of solar material, emitting high energy particles and radiation in a very broad spectrum of energy. They occur near sunspots, usually along the dividing line (neutral line) separating opposite magnetic fields (Tracking a Solar Storm by NASA, via http://son.nasa.gov/). A solar flare is actually the result of an intensely hot electromagnetic explosion in the corona and produces vast quantities of x-rays which brighten the chromospheric gases (Solar Structure via http://www.columbia.edu/). Typical lifetimes of solar flares are one to two hours and the temperature in flares can reach several million degrees. Flare particles ejected into outer space reach the earth in a few hours or days and are the cause of disruptions in radio

transmission. Aurora and magnetic storms are due to strong solar flare eruptions. The peak of solar flare activity is lagged by the sunspot cycle, usually 1-2 years, but some high energy eruptions may occur at any time; the mean cycle of flare is 0.417 years (Solar Structure, via http://www.columbia.edu/).

3.1.3 Corona

This is the outermost region of the Sun's atmosphere, consisting of thin, ionized gases at a temperature of about 10^6K. The corona is very tenuous and like the chromosphere, it is visible only when the brilliant photosphere is covered. It normally extends a million kilometers from the sun.

Coronal holes are regions in the Sun's corona that lack a concentration of high-temperature plasma; here magnetic field lines extend out into interplanetary space and mark the source of the solar wind. The Coronal interstellar gas is made of high-temperature interstellar plasma made visible by its X-ray emission (the corona emits energy of many different wavelengths, from long wavelength radio waves, to short wavelength x-rays). The solar wind transports particles through space at 400 km/sec. When the solar wind reaches the earth the magnetic field of the earth will sometimes trap these electrons and protons and pull them into the earth's atmosphere (Solar Filaments and Prominences, via http://solar.physics.montana.edu/). Atoms in the earth's atmosphere interact with these high energy particles by accepting energy from them and

then releasing that energy in the form of colored light. This display of light is known as the Aurora Borealis when it occurs in the northern corona.

The Corona itself is divided into the K corona (dominating near the sun) and the F corona (evident farther out to a few solar radii). Part of the low-intensity coronal continuum matches the wavelength dependence of the photosphere. Solar activity strongly affects the appearance of the K corona; Zeilik *et al.,* (1998)

At times of Sunspot maximum, the corona is very bright and uniform around the solar limb and bright coronal streamers and other condensations associated with active regions are much in evidence. At sunspot minimum, the corona extends considerably farther at the solar equator than at the poles and the coronal streamers are concentrated at the equator. In other words, as stated by (Nag *et al.,* via tukada2@vsnl.net), during the period of solar cycle maxima, the corona becomes more or less symmetrical and spherical in shape and hence, the radio emitting layers are close to the centre and are arranged in an orderly manner. But during the solar cycle minima, the corona becomes asymmetrical in shape. So the radio sources are situated far away from the centre and are also randomly distributed. Mehul, (2005) studied Coronal rotation and its variation with height in solar atmosphere using 11 different frequencies of radio emissions, and found that the lowest frequency 275 MHz seems to originate at 15×10^4 km above photosphere while highest frequency under his study-2800 MHz originates near 6×10^4 km. The result shows that rotation period decreases from 21.4 days to 23.7 days; Vat *et al.*, (2001) as reported by Mehul, (2005).

Because the coronal gas is so hot, it emits low-energy X-rays and shows up in X-ray photographs of the sun. Some regions of the corona appear dark, especially at the top pole and down the middle part of the sun. Here the coronal gas is less dense and less hot than usual; these regions are the coronal holes. The coronal holes at the poles do not appear to change very much, but those above other regions seem somehow related to solar activity. X-ray bright points lasting only a matter of hours, are scattered within these coronal holes. These are themselves apparently short-lived active regions and are also loops, albeit very small ones; Zeilik *et al.,* (1998). It is believed that coronal holes mark areas where magnetic fields from the sun continue outward into space rather than flow back to the sun in loops. So the coronal gas, not tied down in these regions, can flow away from the sun out of the coronal holes; this flow makes the solar wind.

Solar wind is the "Corpuscular radiation". This electromagnetic emission is a well established component of the solar activity whose influence on the climate dynamics has been ignored so far; nevertheless further experimental data are needed to prove reality of direct impact of the solar wind on the Earth's atmosphere; Makarova *et al.*, (2004). The solar wind dynamic pressure as calculated by Makarova *et al.* (2004*)* is nV^2, where n and V are the density and velocity of the solar wind, respectively. Interaction of the solar wind energy with atmosphere in this scheme is as follows: under enhanced pressure of the solar wind during close approach of magnetopause to the Earth, excessive electric fields are generated. These fields induce electric current in the above-mentioned

conducting layer of the middle atmosphere as a part of the global electric circuit. The Joule heating produced by this current contributes to the warming of the stratosphere during disturbances in the solar wind; Makarova *et al.*, (2004). Short term variations of the stratospheric temperature are under influence of the solar wind energy changes; Makarova *et al*., (1997, 2000). The latter authors showed that enhanced solar wind dynamic pressure caused warming of the stratosphere above both the Northern and Southern geographic poles while quite opposite effect was observed above Antarctic station Vostok located at distance about 1,500 km from the South Pole. All these relations are found for winter months i.e. for the "polar night" conditions when the solar UV radiation impact on the polar atmosphere is minimal. Study was done by Makarova *et al.*(2004), of interrelation between the solar wind dynamic pressure and the level of the solar UV radiation presented by intensity of one of the most powerful line of the total solar irradiance – Fe XIY (λ = 530 nm), which characterizes level of the Sun flare activity. The diurnally averaged values of both parameters for period from December 1981 to January 1982 gave a very good correlation (r = 0.77) between the two data sets, although with inverse proportion here: the more the solar wind energy (the magnetopause is closer to the Earth) the less is intensity of the Fe XIY emission. It is possible to suggest that variations of the separate lines of the solar UV radiation are controlled by the Sun flare activity.

From the foregoing discussions it can be concluded that there is a direct influence of the solar wind energy on temperature variations in the Earth's stratosphere; and solar wind

is a part of the total solar activity, which is closely coupled with other kinds of this activity, such as solar UV (NGDC, via http://www.ngdc.noaa.gov/). Makarova *et al.* (2004) also found that there are at least two periods of the total solar activity: (a) a cycle of 10-12 years connected with the sun flare production; (b) a cycle of 30-40 years, which is common for both TSI level and the solar wind dynamic pressure variations.

Much of the sun's radiation is either reflected (for instance by clouds) or absorbed by our atmosphere. The eccentricity of the earth's orbit is such that the distance between the sun and the earth varies by 1.7%. At a distance of one astronomical unit (1.495×10^{11} m), the mean earth-sun distance, the sun subtends an angle of $32^{/}$; Duffie *et. al.*, (2006). The radiation emitted by the sun and its spatial relationship to the earth result in a nearly fixed intensity of solar radiation outside of the earth's atmosphere. As defined by Duffie *et al.*, (2006); the solar constant G_{sc} is the energy from the sun per unit time received on a unit area of the surface perpendicular to the direction of propagation of the radiation at mean earth-sun distance outside the atmosphere. It may be simply stated as the energy that crosses each square meter at the top of the atmosphere per second. Measurements by satellites give the value of the solar constant close to 1.35 kilowatts per square meter, with variations recorded by various scientists in periods ranging from 1954 to as late as 1983. The solar constant does in fact vary however, as a result of changes in the solar output energy. Large changes might have severe effect on the earth's climate. The Solar Maximum Mission Satellite, launched in 1980, made very accurate observations and monitored continual changes in the solar constant by 0.1 to 0.2 per cent and effects in

the earth's climate of small variations such as these are probably negligible, at the present.

Although the solar constant itself doesn't change appreciably, the amount of energy received in particular wavelength bands, for example, ultraviolet and x-rays, varies over the 11-year solar activity cycle. When cloud cover is dense for instance, only about 1 percent of the available sun's radiation actually reaches the ground. About 34 percent of the radiation from the sun is reflected back into space, mainly by clouds. The ratio between the total mount of light reflected from an object in space and the total amount of light falling on the object is the Albedo; where a perfect reflector has an albedo of 1 and the earth has an albedo of 0.34.

The simplified picture of the sun, its physical structure, and its temperature and density gradients definitely serve as a basis to appreciate the fact that the sun does not function as a black body radiator at a fixed temperature. Rather, the emitted solar radiation is the composite result of several layers that emit and absorb radiation of various wavelengths. The resulting extraterrestrial solar radiation and its spectral distribution have now been measured by various methods in several experiments.

3.1.4 Solar Ultraviolet (UV)

This is the solar electromagnetic radiation just next to the visible violet radiation in the electromagnetic spectrum (ISO 21348 information, via http://SpaceWx.com). The ultraviolet Part of the electromagnetic spectrum ranges between 5 and 400 nanometers

(nm). As stated in the ISO 21348 information, the spectral categories within the solar UV radiation include: Vacuum Ultraviolet (VUV) in the wavelength range of 10 nm to 200 nm, Extreme Ultraviolet (EUV) in the wavelength range 10 nm to 121 nm, Hydrogen Lyman-alpha (H Lyman-α) in the wavelength range 121 nm to 122 nm, Far Ultraviolet (FUV) in the wavelength range 122 nm to 200 nm, Ultraviolet C (UVC) in the wavelength range 100 nm to 280 nm, Middle Ultraviolet (MUV) in the wavelength range 200 nm to 300 nm, Ultraviolet B (UVB) in the wavelength range 280 nm to 315 nm, Near Ultraviolet (NUV) in the wavelength range 300 nm to 400 nm and Ultraviolet A (UVA) in the wavelength range 315 nm to 400 nm. As the SORCE (Solar Radiation and Climate Experiment satellite) mission states, far UV irradiance from the Sun varies by as much as 10% during the Sun's 27 day rotation, while the bright 121.6 nm hydrogen Lyman-alpha emission may vary by as much as a factor of 2 during an 11-year solar cycle, dramatically affecting the energy input into the Earth's atmosphere. Water vapor and ozone are especially sensitive to changes in the solar UV radiation. Different wavelengths of solar radiation are absorbed at different altitudes in the Earth's atmosphere, affecting different physical processes (NGDC, via http://www.ngdc.noaa.gov/). We utterly depend on solar radiation. Long term monitoring of its variations over all wavelengths is critical to our understanding of the impacts on our environments.

Makarova *et al.*, (2004) took a level of the Sun UV radiation expressed as the total solar irradiance (TSI) as the most reliable indicator of the amount of the solar energy

transferred to the Earth. This parameter has the advantage over the traditional index of the solar activity level – Sun spot number, R_s in that it is based on direct instrumental observations of the solar irradiance intensity in a wide frequency interval above the Earth's atmosphere.

3.2 Solar indices

The physical mechanisms that take place by the sun (solar activity) can be studied using various solar parameters known as solar indices. Each index is used to study and measure a particular activity of the sun in the solar interior, the photosphere, the chromosphere or the corona. These solar index observations are done by observatory satellites in space that record periodic data of solar parameters. Solar indices included the Geomagnetic activity index (*aa* index), AE index, AL index, AU index, C9 index, K_P index, sunspot index, am index, AO index, Mg II core-to-wing ratio, solar F10.7 cm and E10.7 cm solar radio fluxes. The indices of interest in this project are the Sunspot Numbers, the F10.7 cm Solar radio flux and Mg II core-to-wing ratio.

3.2.1 Sunspot Numbers, R_s

A sunspot is a relatively dark area of the sun at the photosphere, which may be as large as 50,000 miles (about 75, 000 kilometers) in diameter, at a temperature of only about 4,000 degrees Kelvin. Sunspots occur up to 0.2 percent of the sun's visible area. They move across the surface of the sun eastward, (showing that the sun rotates every 27

days), contracting and expanding as they go towards the equator before disappearing. A sunspot's life can be as short as an hour or two or as long as several months (Facial Blemishes on the Sun, via http://solar.physics.montana.edu/).

Sunspots are the most easily observed features of the solar photosphere, while at the same time they are important manifestations of solar activity; Győri *et al.,* (2004). Because of their importance, they have long been observed and measured on white-light full-disk solar images in several ground based observatories. Starting in 1996, space observations by the Michelson Doppler Imager (MDI) on SOHO have also become available; Győri *et al.,* (2004). One of the most important parameters of sunspots is their area, which is used directly or as a proxy in many fields of investigation. Precise area measurements are especially important in studies of irradiance variations.

A sunspot can be assumed as a bubble of magnetic pressure surrounded by the gas pressure of the photosphere. For the sunspot to exist, the total pressure must be in balance between the region inside and the region outside of the sunspot. A sunspot is an area that temporarily has a concentrated magnetic field. Sunspots are made up of two parts: as dark, roughly circular central disk called Umbra and a lighter outer area called the penumbra; Fischer and Dearborn, (2003).

Sunspots are seen as the centers of activity on the solar surface; Akasofu and Chapman, (1972). The number of sunspot count of the surface of the sun during certain periods, are

known as sunspot numbers. Their increase or decrease, appearances and disappearances, have been observed to follow a certain pattern known as the solar cycle. The average number of visible sunspots varies over time on a regular cycle of about 11 years; Schwabe, (1843). The part of the cycle with low sunspot activity is referred to as "solar minimum", while the portion of the cycle with high activity is known as "solar maximum". It is extremely variable in length (actually, 7 to 17 years); the highly active cycles ($\geq$ 200 spots) are generally short (9 – 10 years), and the low activity cycles (sometimes $\leq$ 50 spots) are long (12 – 13 years) (Solar Structure, via http://www.columbia.edu/). In the sunspot cycle the number of sunspots usually peaks 2 – 3 years after the beginning of each cycle and decays gradually, but low activity cycles may have a reversed asymmetry. First spots of the cycle appear at high latitudes, mostly between 20^{o} and 25^{o}, and as the spots increase in size and number they occur closest to the equator. Very few spots are observed outside the latitude range of 5^{o} – 35^{o} (Solar Structure, via http://www.columbia.edu/).

By studying the sun's magnetic field, modern astronomers have discovered that the cycle covers twenty years, with an eleven-year cycle of sunspots above the equator followed by an equal cycle below the equator. The magnetic polarity of the sunspot groups reverses in each successive cycle so that the complete cycle called “Hale cycle” lasts 22 years (Solar Structure, via http://www.columbia.edu/). R_s and *aa* are different manifestations of solar energy output; Friis-Christensen *et. al.*, (2001).

Between 1645 and 1715 very few sunspots were seen, a time period called Maunder minimum (period associated with a long cold spell in Europe, known as Little Ice Age) (Solar Structure, via http://www.columbia.edu/). From this it may be inferred that very low temperature periods are associated with low sunspot counts and therefore low solar activity periods.

3.2.2 Solar Fluxes

This is the way heat from the sun is absorbed, scattered, returned or deposited around the earth. It can be the total amount of radiation that the earth collects, emits and disperses. The ultraviolet light/radiation is of most interest to solar activity, with a wavelength shorter than that of visible light. It can be subdivided into near UV (380-200nm wavelength), far UV (200-10nm) and extreme UV (1-31nm).

The sun emits ultraviolet radiation, but because of absorption in the atmosphere's ozone layer, 99% of the ultraviolet radiation that reaches the earth is the less harmful portion of the UV radiation. The solar cycle variation is much longer in the ultraviolet part of the spectrum of solar radiation; Haigh, (1994). The solar 10.7 cm flux is the solar flux density measured at a wavelength of 10.7 cm in the ultraviolet region of the spectrum.

The radio emission from the sun at a wavelength of 10.7 centimeters (often called "the 10 cm flux") has been found to correlate well with the sunspot number. Sunspot number is defined from counts of the number of individual sunspots as well as the number of

sunspot groups and must be reduced to a standard scale taking into account the differences in equipment and techniques between observatories. On the other hand, the radio flux at 10.7 centimeters can be measured relatively easily and quickly and has replaced the sunspot number as an index of solar activity for many purposes. The 10 cm flux can be used as a daily index or averaged over longer periods to trace out the trends in solar activity. Typically the 10 cm flux is averaged over a month or a year although sometimes a 90 day average is made; the Australian Space weather Agency, (2006).

.

Even though both 10 cm flux and sunspot number indicate activity, they have quite different scales. The following equations are useful for converting between 10 cm flux (F) and sunspot number (R_s). The equations are valid on a statistical (i.e. average) basis.

$$F = 67.0 + 0.572\ R_s + (0.0575\ R_s)^2 - (0.0209\ R_s)^3 \quad (3.3)$$

$$R_s = 1.61\ FD - (0.0733\ FD)^2 + (0.0240\ FD)^3 \quad (3.4)$$

Where, $FD = F - 67.0$. (The Australian Space weather Agency, 2006).

3.2.3 NOAA Mg II Core-to-wing ratio

NOAA Mg II Core-to-wing ratio is derived from the ratio of the h to k lines of the solar Mg II feature at 280 nm to the background or wings at approximately 278 nm and 282 nm. The h and k lines are variable chromospheric emissions while the background emissions are more stable. The result is a robust measure of chromospheric activity. The ratio is a good measure of solar UV and EUV emissions (NGDC, via http://www.ngdc.noaa.gov/); so Mg II index is a proxy for UV and EUV; Viereck *et al.*,

(2001). While working on the Solar Backscatter Ultraviolet (SBUV) experiment on the NIMBUS7 satellite, Heath and Schlesinger, (1986) also showed that the core-to-wing ratio of Mg II h and k lines was a good measure of the temporal variations of the solar UV flux, including long-term variations, because the ratio is relatively insensitive to drifts in instrument sensitivity.

The Solar-Stellar Irradiance Experiment (SOLSTICE) instrument of the Upper Atmosphere Research Satellite (UARS), measures the solar UV spectra in the 119 nm – 420 nm range that are archived at the Goddard Distributed Active Archive Centre (DAAC). Version 7 of the data (Oct 1994) include among others the Mg II 280.0 nm core –to-wing ratio index. The Solar Ultraviolet Spectral Irradiance Monitor (SUSIM) on the UARS has been measuring the solar spectral irradiance from 115 nm to 410 nm since 12-October-1991 (UARS mission day 31). An Mg II index is computed from the daily mid-resolution spectrum in the vicinity of 280 nm. At this spectral resolution (1.1 nm FWHM, sampled every ~0.24 nm) the Mg II absorption doublet and the chromospheric emission line in the core of each absorption line, are blended so that the feature appears to be a single absorption "line". The SUSIM Mg II index is a ratio of a measure of the "core" of the feature to a similar measure of the wings of the feature (NGDC, via http://www.ngdc.noaa.gov/).

3.2.4 SOLAR2000 model

SOLAR2000 is an empirical solar irradiance specification tool for accurately characterizing solar irradiance variability across the solar spectrum. It is designed to be a fundamental energy input into planetary atmosphere models, a comparative model with numerical first-principles solar models, and a tool to model or predict the solar radiation component of the space environment. SOLAR2000 includes a new extreme Ultraviolet (EUV) proxy, E10.7, which has the same units as the commonly used F10.7 cm solar radio flux. E10.7 can be used in existing models where F10.7 is traditionally used, but it offers significant improvement as an index of the energy input to the thermosphere and ionosphere (NGDC, via http://www.ngdc.noaa.gov/). E10.7 is the integrated EUV energy flux (1-105 nm) at the top of the atmosphere reported in units of 10.7-cm radio flux, F10.7 (* 10^{-22} W m^{-2} Hz^{-1}); Tobiska, (2002). Use of the latest solar EUV spectrum model SOLAR2000 is strongly encouraged by Solar Spectrum experts.

3.3 Heliosphere

This is the terminology referring to the space from the sun through the Earth to the end of the solar system, the heliopause. Other than atmospheric and solar-terrestrial physics, heliophysical studies include studies of other planets, the outer reaches of the heliosphere, and its interaction with the interstellar medium; Riley and Crooker, (2004).

3.3.1 Space weather

This is a modern term to denote physical conditions in space around the Earth that are ultimately determined by solar activity. Over the past decade, there has been a growing awareness in space-and ground –system operations of the phenomena of space weather, i.e., the short-term variable impact of the Sun's photons, solar wind particles, or magnetic field upon the Earth; Tobiska, (2002). Space weather manifests itself through various physical phenomena such as enhanced intensity of hard radiation, increased strengths of electric and magnetic fields and elevated magnitude of electric currents, to name only a few. A 'magnetic storm', which may also be called 'space storm', is a rather violent phase of space weather and is often caused by solar outbursts such as flares and coronal mass ejections. Solar outbursts create disturbances of the solar wind that may impact the Earth environment with a delay of a few days after their eruption from the sun; Fernandez, (2006).

As we go further away from the sun's atmosphere towards the earth, we come to the Earth's atmosphere. The gaseous portion of the earth is known as the atmosphere; it is retained by the Earth's gravity. The atmosphere roughly contains 78% nitrogen and 21% oxygen, trace amounts of other gases (Argon, Carbon dioxide, Neon, Helium, Methane, Krypton, Hydrogen, Nitrous oxide, Xenon, Ozone, Nitrogen dioxide, Iodine, Carbon monoxide, Ammonia), and water vapor. This mixture of gases is commonly known as air. The average mass of the atmosphere is about 5,000 trillion metric tones. According to the National Centre for Atmospheric Research, "The total mean mass of the

atmosphere is 5.14×10^{18} kg with an annual range due to water vapor of 1.2 or 1.5×10^{15} kg depending on whether surface pressure or water vapor data are used; somewhat smaller than the previous estimate. The mean mass of water vapor is estimated as 1.27×10^{16} kg and the dry air mass as $5.1352 \pm 0.0003 \times 10^{18}$ kg".

Acted on by the combined effects of the earth's motions and energy from the sun our planet's formless and invisible envelop of air react by producing an infinite variety of weather, which in turn, creates the basic pattern of global climates. Weather is the term that denotes the state of the atmosphere at a given time and place. When changes in the weather are continuous and sometimes erratic, it is nevertheless possible to arrive at a generalization of these variations. A description of aggregate weather conditions is termed climate. Thus, climate is the average of all statistical weather information that helps describe a place or region.

3.3.2 Earth's Atmosphere

The Earth's atmosphere constitutes the following regions:

The Exosphere

This is the topmost region of a planet's atmosphere from which particles in the atmosphere can escape into space. It ranges from about 690 km to about 800 km from the surface of the Earth.

The Ionosphere

This is the layer of the Earth's atmosphere ranging from about 100 to 700 kilometers above the surface where oxygen and nitrogen are ionized by sunlight, producing free electrons. It is divided into three regions, D, E and F. The radio waves from the earth are reflected in the F region of the ionosphere.

The thermosphere

It is a layer of the Earth's atmosphere, above the mesosphere, heated by x-rays and Ultraviolet radiation from the sun. It ranges from 80-85 km to 640+ km, temperature increasing with height. This is the region of auroras.

The mesosphere

It is the region of the Earth's atmosphere between 50 and 100 km where the temperature falls rapidly with height. The meteors are formed in this region.

The stratosphere

This is a layer within the Earth's atmosphere in which temperature changes with altitude are small and clouds are rare. The region covers from 7-17 km range to about 50 km. The weather balloons reach this sphere within the atmosphere. It is the sphere with the largest atmospheric ozone (O_3) distribution at distance range of about 40 to 50 km above the surface, called Ozone layer or Ozonosphere. Ozone is the gas that absorbs the harmful part of the Ultraviolet radiation, and therefore protects life on Earth.

The troposphere

The name comes from the Greek word “tropos” meaning to turn or mix. This is the lowest layer of the Earth’s atmosphere starting at the surface going up to between 7 km at the poles and 17 km at the equator with some variation due to weather factors. The troposphere has a great deal of vertical mixing due to solar heating at the surface. This heating warms air masses, which then rise to release latent heat as sensible heat that further buoys the air mass. This process continues until all water vapor is removed. In the atmosphere, on average, temperature decreases with height due to expansive cooling. So it is within the troposphere that the weather takes place. The boundaries between these regions are named tropopause, stratopause, and mesopause.

The Magnetosphere

The region around a planet where particles from the solar are trapped by the planet’s magnetic field.

3.4 The Climatic parameter

3.4.1 Relative Humidity

Humidity can be defined as the amount of moisture content in air. Relative humidity is one of the types of indexes that explain what humidity is all about. Absolute humidity is expressed as the mass of water vapour in a given volume of air, (usually as grams per cubic meter). As air moves from one place to another, variations in temperature and pressure cause changes in air volume. When such changes occur, the absolute humidity

also changes even if no water vapour is added or removed. Consequently, it is difficult to monitor the water vapour content of a moving mass of air, if absolute humidity is the index being used.

Relative humidity is a term used to describe the quantity of water vapour that exists in a gaseous mixture of air and water. By definition, relative humidity is a ratio of the air's actual water vapour content compared to the amount of water vapour required for saturation at that temperature. Thus, relative humidity indicates how near the air is to saturation, rather than indicating the actual quantity of water vapour in the air. It is expressed as a percentage and calculated in the following manner:

$$RH = \frac{P(H_2O)}{P^*(H_2O)} X100\% \tag{3.5}$$

Where: $P\ (H_20)$ is the partial pressure of water vapour in the gas mixture.

$P^*(H_20)$ is the saturation vapour pressure of water at the temperature of the gas mixture; and *RH* is the relative humidity of the mixture under consideration.

Relative humidity depends not only on the temperature, but also on the absolute pressure of the system of interest. Given a closed system of air and water vapour, the relative humidity of a system will decrease if the system undergoes an isobaric increase in temperature. Also, the relative humidity of a system will increase if the system undergoes an isothermal increase in pressure.

Relative humidity is often mentioned in weather forecasts and reports, as it is an indicator of the likelihood of precipitation, dew or fog.

3.4.2 Temperature

The absolute temperature T of a gas is determined from the Kinetic theory of a gas; Mathur, (1980). From the Kinetic theory of a gas, the pressure P of the gas is given by the expression: $P = 1/3mnc^2$ (3.6)

Where, m is the mass of a molecule of the gas, n is the number of molecules of the gas and c is the root mean square velocity of the gas molecules. For a molar volume V of the gas, the gas equation can be written as:

$$PV = 1/3mnVc^2 = RT \quad (3.7)$$

Where, $nV = N$ (Avogadro's Number), is a constant. So the absolute temperature T is directly proportional to the square of the root mean square velocity of the gas molecules. The empirical scale of temperature in common use is the Kelvin scale that has the lower fixed point as the triple point of water (correspondingly, the ice point of 0^oC on the Celsius scale becomes equal to 273.15 K on the Kelvin scale), and the upper fixed point (steam point) is 373.15 K that corresponds to 100^oC, and absolute zero at 0.0 K. The absolute zero stated here is the temperature at which the gas molecules theoretically have zero kinetic energy. The Centigrade scale has been used to obtain the temperature data for this work as will be seen in the next chapter.

The temperature recorded on the surface of the earth by the ground instruments is highest. There is decrease in temperature as we go higher into the atmosphere according to the expression stated by Micolich (2006):

$$\frac{dT}{dz} = \frac{-(\gamma - 1)}{\gamma} \frac{(\mu g)}{R} \tag{3.8}$$

Where, *dT/dz* is the variation of temperature *T* with the vertical distance *z*, γ is the ratio of the specific heats of the atmospheric air or gas, μ is the molar mass of the atmospheric air or gas, *g* is the gravitational acceleration and *R* is the universal gas constant. The decrease in temperature is justified by the expression because the gas changes in composition as we go upwards, meaning that not only does μ decrease as we go up, but the effective γ increases slightly as we weed out the heavier of diatomic gases like N_2 and O_2 and thereby increase the proportional monatomic He content.

3.4.3 Wind Run

3.4.3.1 Causes of Wind

The tropics, near the equator, receive more direct rays from the sun throughout the year. As a result, near the equator, the ocean "heats up" more than at higher latitudes. This creates a temperature imbalance (warmer water near the equator and cooler water near the poles). The temperature imbalance creates a flow of heat towards the poles by way of winds and the oceanic currents. Unequal heating of the atmosphere on land and the oceans creates wind and global wind systems.

Wind is the result of horizontal differences in air pressure. Air flows from areas of higher pressure to areas of lower pressure. Differences in air pressure are caused by uneven heating of the Earth's surface. Therefore, we can say that the sun (solar energy) is the ultimate cause of wind. Wind direction is given as the direction from which the wind comes. For example, a "north wind" blows from north to south.

3.4.3.2 Land and Sea Breezes

The sea breeze during the day and land breeze at nights are caused by wind movements from sea to land during the day and vice versa at night due to the low pressures created in the directions of the flow of wind in the respective times. Water has higher heat capacity, and therefore absorbs more heat during the day and remains cooler while the land with less heat capacity gets hotter faster. The hot air therefore rises on land creating an area of low pressure on land during the day. Hence wind blows from sea (area of high pressure) to land (area of low pressure) causing the sea breeze. At night, the land cools off faster than the sea. Cooler air descends creating an area of higher pressure. Wind blows from land to sea causing the land breeze.

3.4.3.3 Global circulation and wind systems

Much of the solar energy that the earth receives causes intense heating in the equatorial regions. This intense heat produces powerful convection in these areas.

As the warm, moist air rises, it creates a zone of low pressure, clouds, and precipitation along the equator. As that warm air rises, it eventually reaches the troposphere and can

rise no higher as it meets cooler air in the higher altitudes. It spreads outwards towards the poles.

As it spreads, it cools and sinks back down to the surface at about 30 degrees north and south of the equator. This sinking air produces areas of higher pressure with drier conditions. Many of the world's deserts are located in these high pressure areas, around 30^{o} north and south of the equator. Examples are: Sahara Desert, Great Victoria Desert in Australia, Kalahari Desert, Sonoran Desert.

Some of this air, as it sinks, moves back towards the equator. This air flowing back towards the equator produces what is known as the trade winds. The trade winds obtained their name from the sailing ships that were used in foreign trade. These winds propelled the ships from Europe to the "New World". The area near the equator where these winds meet the cooler winds and then rise up is referred to as the ITCZ - doldrums.

These areas where air rises at the equator; sink at 30 degrees north and south latitude, and then flow back to the equator are known as Hadley cells. Although most of the air that sinks at 30 degrees north and south latitude returns to the equator, some of it continues to move pole-ward.

At approximately 60 degrees north and south, this air meets cold polar air. The areas where these air masses meet form polar fronts. The air moving in from the lower

latitudes is generally warmer and will rise. It then moves back towards the equator, sinking at about 30 degrees north and south. This sinking air contributes to the high pressure systems located there. The circulation cells that form between 30 degrees and 60 degrees north and south are called Ferrel cells.

Some of the air that rises at the polar fronts continues to move pole-ward, sinking at the poles and then moving back towards 60 degrees north and south. These Polar cells are weaker than the tropical ones.

As the air that sinks at these locations flows back along the surface of the earth, it does not flow in a straight north-south path. This flow of air is affected by the Coriolis force Effect.

3.4.4 Sunshine duration

Sunshine duration may be stated as the hours of bright sunshine, that is, the time in which the solar disc is visible. As can be seen in the section where instruments are discussed, the Campbell-Stokes sunshine recorder has been employed to obtain sunshine duration data for this work. This instrument uses a solid glass sphere of approximately 10 cm diameter as a lens that produces an image of the sun on the opposite surface of the sphere. A strip of standard treated paper is mounted around the appropriate part of the sphere, and the solar image burns a mark on the paper whenever the beam radiation is above a critical level. The lengths of the burned portions of the paper provide an index of the duration of “bright sunshine.” These measurements are uncertain on several

accounts: The interpretation of what constitutes a burned portion is uncertain, the instrument does not respond to low levels of radiation early and late in the day, and the condition of the paper may be dependent on humidity. The other instrument in use for measurement of sunshine duration is the photoelectric sunshine recorder.

3.4.5 Radiation

As defined by Duffie *et al*., (2006), solar or short-wave radiation is radiation originating from the sun, in the wavelength range 300 to 3000nm. It includes both beam and diffuse components. Long-wave radiation is radiation originating from sources at temperatures near ordinary ambient temperatures and thus substantially all at wavelengths greater than 3000nm. Long-wave radiation is emitted by the atmosphere, by a collector, or by any other body at ordinary temperatures. (This radiation, if originating from the ground is sometimes referred to as "terrestrial" radiation.). Solar radiation data could be obtained from instantaneous measurements (irradiance) as is the case in this work, or from values integrated over some period of time (irradiation); usually hour or day; Duffie *et al.,* (2006).

Two types of solar radiation data are widely available. The first is monthly average daily total radiation on a horizontal surface, *H.* The second is hourly total radiation on a horizontal surface, *I*, for each hour for extended periods such as one or more years.

The eccentricity of the earth's orbit is such that the distance between the sun and the earth varies by 1.7%. At a distance of one astronomical unit, 1.495 x 10^{11} m, the mean earth-sun distance, the sun subtends an angle of 32". The radiation emitted by the sun and its spatial relationship to the earth result in a nearly fixed intensity of solar radiation outside of the earth's atmosphere. The solar constant G_{sc} is the energy per unit time received on a unit area of surface perpendicular to the direction of propagation of the radiation at mean earth-sun distance outside the atmosphere. Varied values of solar constant have been reported by various scientists from before to after rockets and spacecraft era. Duffie *et. al.*, (2006) recommend the value of G_{sc} of 1367 W/m^2.

Solar radiation is scattered as it passes through the atmosphere by its interaction with air molecules, water (vapor and droplets), and dust. The degree to which scattering occurs is a function of the number of particles through which the radiation must pass and the size of the particle relative to λ, the wavelength of the radiation.

Absorption of radiation in the atmosphere in the solar energy spectrum is due largely to ozone (O_3) in the ultraviolet and to water vapor (H_2O) and carbon dioxide (CO_2) in bands in the infrared. There is almost complete absorption of short-wave radiation by O_3 in the upper atmosphere at wavelengths below 290nm. This absorption decreases as λ increases above 290nm, until at 350nm there is no absorption. There is also a weak ozone absorption band near λ = 600nm.

Water vapor absorbs strongly in bands in the infrared part of the solar spectrum, with strong absorption bands centered at 1000, 1400, and 1800nm. Beyond 2500nm, the transmission of the atmosphere is very low due to absorption by H_2O and CO_2. The energy in the extraterrestrial spectrum at λ >2500nm is less than 5% of the total solar spectrum, and the energy received at the ground for λ >2500nm is very small.

From the foregoing discussion it can be stated that the normal solar radiation incident on the earth's atmosphere has a spectral distribution of wavelength range from 200nm to above 2000nm with more energy concentrated between 300nm and 1200nm. The x-rays and other very short wave radiation of the solar spectrum are absorbed high in the ionosphere by nitrogen and oxygen, and other atmospheric components. Most of the ultraviolet is absorbed by ozone. At wavelengths longer than 2500nm, a combination of low extraterrestrial radiation and strong absorption by CO_2 means that very little energy reaches the ground. This implies that most of the radiation recorded by the ground instruments is between 290 and 2500nm wavelengths.

3.4.6 Rainfall

Rainfall is a major climate parameter over East Africa, which has the largest space-time variability yet the most important weather element. Over the region, rainfall determines the population densities and the agricultural productivity of large areas of the countries in general.

CHAPTER 4

RESEARCH DATA AND METHODOLOGY

4.0 Introduction

This chapter discusses the data and research methods adopted in this work. Section 4.1 states the parameters whose data are used in the research; and proceeds to discuss the Meteorological data of the nine climatic parameters in each of the five representative meteorological stations. A table of topography of the five meteorological stations, and tables giving summaries of their data period and length in months are given here. Pictures of the meteorological instruments used to obtain the meteorological data of the nine climatic parameters are also displayed. The section also talks about the three solar indices; stating the spheres of the sun from which each of them originates, and the prominent satellites used to collect their data. A table of the solar indices data period and length in months is also in this section.

Section 4.2 introduces the methods of analysis adopted in the work. It starts by mentioning the data quality control followed by a statement on data reduction and why it was necessary. The data reduction has been done on the basis of Monthly means for the meteorological parameters and the solar indices. The methods include: Correlation analysis giving the cross-correlation equation by Bourke (1996), Spectral analysis stating application of Fourier analysis technique Scargle periodogram to the monthly means to determine periodicity of the meteorological variables. The section then states the proposed empirical linear multivariate model for the meteorological and solar

variables and the use of least square fitting to evaluate the coefficients in the model. It further gives the statistical tools used to test performance of the models, and hence to validate them.

In section 4.3, a further investigation of solar connection to the earth's climate has been done by investigating solar signature in the drought occurrences in Kenya because drought is a very significant element of climate. This has been achieved by subjecting drought indices to Fast Fourier Transform to reveal the spectral characteristics from which the prominent periodicities are obtained. An extension of the work in section 4.4 gives the application of stepwise regression analysis to the lagged solar indices on the climatic parameters. This is an attempt to see prediction models obtained when lagged indices are used, but by adopting the stepwise regression approach.

4.1 Data

The data used in the study consist of daily values of some meteorological variables and three solar indices taken over the same period. In situations where data were missing we interpolated so as to reconcile with the data set.

4.1.1 Meteorological Data

The meteorological parameters that span through 1986 to 2005 include relative humidity, maximum temperature, minimum temperature, wind speed, sunshine duration, solar

radiation intensity, evaporation, rainfall and average temperature. The meteorological data were obtained from the archives of the Kenya Meteorological Department (KMD). The data were independently and simultaneously recorded from five synoptic meteorological stations in different climatic zones within Kenya; the geographical coordinates of the stations are listed in Table 4.1 and illustrated in Fig. 1.1.

Table 4.1: Topography of the meteorological stations

Stations	Code	Latitude (°S)	Longitude (°E)	Altitude (m)	Climatic zone, LR season (Fig. 1.2)
Kericho	KER	0.4	35.3	1946.85	8
Dagoretti (Nairobi)	NBI	1.3	36.8	1771.77	9
Kisumu	KSM	0.1	34.8	131.83	7
Mombasa	MSA	4.0	39.6	5.41	11
Garissa	GRS	0.5	39.6	120.13	6

The experimental sites represent the different climatic variations of the country. The Nairobi site represents the central highland region that spans the central, Nairobi and parts of Eastern provinces. Mombasa site represents proximity of the large Ocean environment that covers the whole of the coast province bordering the Indian Ocean; and the Garissa site represents the arid and semi arid features that span the whole of North Eastern province of the country. Kisumu site represents the influence of the smaller water body proximity of Lake Victoria, which is largely in Nyanza and parts of the Western provinces; while Kericho site represents the western highlands of the rift valley province.

The observation at various centers is being coordinated by the Kenya Meteorological Department (KMD) personnel with headquarters at Dagoretti Corner, Nairobi. The KMD is a renowned centre of excellence for meteorological observations and has long standing historical records of observations. KMD maintains dedicated daily records of the meteorological variables throughout the duration considered in this study. The data holdings at different centers are highlighted in Tables 4.2 – 4.6. In these tables, the dates are given in four numbers. The first two numbers represent the day of the month. The next two numbers represent the month and the last two numbers represent the year. For example, 011088 mean 1st October Nineteen eighty-eight.

Table 4.2: Data holding at KERICHO (KER).

Variable	Begin date	End date	File length (months)
HUMIDITY	010186	311203	216
TEMP (max)	010186	100606	246
TEMP (min)	010186	100606	246
WIND RUN	010186	310506	245
SUNSHINE	010186	311203	216
SOLAR RAD	010186	100606	246
EVAPORATION	010186	310506	245
RAINFALL	010773	300406	388

Site is located near Kericho town, in the western high lands of the rift valley, about 87 km from Lake Victoria. These features give it a fairly cold weather and persistent rains throughout the year. It is a tea zone area. Access is by road.

Table 4.3: Data holding at DAGORETTI CORNER, NAIROBI (NBI)

Variable	Begin date	End date	File length (months)
HUMIDITY	010186	300403	208
TEMP (max)	010186	100606	246
TEMP (min)	110186	100606	246
WIND RUN	010186	310506	245
SUNSHINE	010186	310506	245
SOLAR RAD	010186	310506	245
EVAPORATION	010186	310506	245
RAINFALL	010660	310606	553

The site is located within the premises of the KMD headquarters, four kilometers from the Nairobi city centre. It is in the central highlands of Kenya that influences the weather patterns here. It is accessible by road network throughout the year. Being within the city of Nairobi, the area is not forested. But it is within the neighborhoods of the forested Karen and Ngong' estates. The soil type is loamy, and can support coffee and other seasonal food crops like maize and beans.

Table 4.4: Data holding at KISUMU (KSM)

Variable	Begin date	End date	File length (months)
HUMIDITY	010186	311205	240
TEMP (max)	010186	311205	240
TEMP (min)	010186	311205	240
WIND RUN	010186	311205	240
SUNSHINE	010186	311205	240
SOLAR RAD	010186	280290	50
EVAPORATION	010186	311205	240
RAINFALL	020160	311205	551

The site is located within the shores of Lake Victoria, within the Kisumu city airport. It is a fairly hot region with a long rainy season from March to May, and short rainy

season in September/October to December every year. It is accessible throughout the year by road network and by air. It is within the precinct of the Equator. The soil type is firm and rocky, and supports food crops such as sorghum, maize, beans and yams. Sugarcane and Cotton are also grown in the neighborhood of the station.

Table 4.5: Data holding at MOMBASA (MSA).

Variable	Begin date	End date	File length (months)
HUMIDITY	010186	130902	81
TEMP (max)	010186	200902	81
TEMP (min)	010186	200902	81
WIND RUN	010186	200902	81
SUNSHINE	010186	200902	81
SOLAR RAD	010186	200902	81
EVAPORATION	010186	300601	186
RAINFALL	010160	100606	558

The site is located within the coastal city of Mombasa. This is the city bordering the Indian Ocean which gives it a unique humidity. The area is known for cashew nuts, cassava, palm trees and sisal.

Table 4.6: Data holding at GARISSA (GRS).

Variable	Begin date	End date	File length (months)
HUMIDITY	010186	311202	204
TEMP (max)	010186	100606	246
TEMP (min)	111088	100606	213
WIND RUN	010186	310506	245
SUNSHINE	010186	310506	245
SOLAR RAD	010186	030894	103
EVAPORATION	010186	300506	245
RAINFALL	010160	300606	246

The site is located within the North Eastern part of Kenya in the semi arid area. The semi arid features make the place have characteristic long periods of no rain. Sporadic rains are, however, experienced in this region. The region is also famous for raising livestock such as camels, goats and indigenous cattle.

4.1.1.1 Meteorological Instrumentation

The instruments used in taking the measurements of various meteorological variables are listed as appropriate in Table 4.7 and shown in Figures 4.1 – 4.7

Table 4.7: The instruments for measuring meteorological variables

Meteorological variable	Instruments
Relative Humidity	Thermo hygrograph (Negretti – Zambra type); Fig. 4.1
Maximum Temperature	Mercury-in-glass thermometer with a constriction in the capillary; Fig. 4.2 (upper horizontal)
Minimum Temperature	Alcohol-in-glass thermometer with long glass indicator immersed in alcohol; Fig. 4.2 (lower horizontal)
Wind speed	Cup anemometer and cup-counter anemometer; Fig. 4.3
Sunshine Duration	Campbell sunshine recorder; Fig. 4.4
Solar Radiation	Solarimeter; Fig. 4.5
Evaporation	The standard evaporation pan; Fig. 4.6
Rainfall	The standard rain gauge; Fig. 4.7

Figure 4.1: Thermo hygrograph for measuring Humidity

Figure 4.2: Maximum (upper horizontal) and Minimum (lower horizontal) thermometer

Figure 4.3: Cup- counter anemometer for measuring wind speed

Figure 4.4: Campell sunshine recorder for measuring sunshine duration

Figure 4.5: Solarimeter for measuring solar radiation

Figure 4.6: Standard evaporation pan

Figure 4.7: Standard rain gauge

4.1.2 Solar Indices data

The daily solar indices covering the same period as the climatic parameters (1986 -2005) were obtained from the National Geophysical Data Center (NGDC), Boulder, Colorado, U.S.A through their website (NGDC, via http://www.ngdc.noaa.gov/). The data period covers solar cycles #22 and #23.

The three solar indices used in this work are the daily values of sunspot number, solar Ultraviolet F10.7 cm solar radio flux, and Mg II core-to-wing ratio. The sunspot number is the photospheric index, F10.7 cm solar radio flux is the coronal index and the Mg II core-to-wing ratio is the chromospheric index. The Mg II core-to-wing ratio is derived by taking the ratio of the h and k lines of the solar Mg II feature at 280 nm to the background or wings at approximately 278 nm and 282 nm. The h and k lines are variable chromospheric emissions while the background emissions are more stable. The result is a robust measure of chromospheric activity. This ratio has been shown to be a good measure of solar UV and EUV emissions; Viereck and Puga, (1999). Daily Solar Flux Values give measurements of the integrated emission from the solar disc at 2800MHz (10.7cm wavelength) in solar flux units (1 s.f.u. = 10^{-22} $Wm^{-2}Hz^{-1}$).

The data on variations of solar irradiance are obtained from the satellites, the prominent ones being the: - (i) Nimbus-7

(ii) Solar Maximum Mission (SMM) Space craft

(iii) Earth Radiation Budget Satellite (ERBS)

(iv) NOAA-9 and 10 platforms

(v) Upper Atmospheric Research Satellite (UARS)

Lee III *et. al*. (1978-1997); Wilson, (1991-1994).

The data from the various satellites have been compared and are available; Lee III *et*. *al*., (1978- 1997).

Table 4.8: Solar activity indicators in this analysis

Activity Indicator	Duration	(%) of days of data obtained
International Sunspot Number (Belgium)	1986 – 2005	100
F10.7 cm solar radio flux (Canada)	1986 – 2005	100
Mg II core-to-wing ratio (Viereck and Puga, 1999).	1986 – 2005	95

4.2 Methods of Analysis

4.2.1 Data quality control

The recorded daily data were inspected across the stations to ensure that there were no inconsistencies in the records. Data suspected of irregularity were replaced appropriately using interpolation to reconcile them with the data set.

4.2.2 Data reduction

The data reduction was done to get the monthly, seasonal to decadal scales. Data reduction was also necessary because the daily data had noise that could not be useful. The noises in the daily data appear as frequent and irregular fluctuations that do not give predictable patterns.

4.2.2.1 Monthly means of the meteorological variables

The monthly means of the daily values of the meteorological variables and solar indices were evaluated by taking the averages of all the days in every month for each year of the data. The daily average temperature was evaluated by taking mean value of the maximum and minimum temperature for any day, and its monthly means evaluated as stated above alongside the other parameters. The monthly variations of the meteorological variables were plotted across the stations and shown in Figure 5.1 (a - i).

4.2.3 Correlation Analysis

The correlation method was applied to calculate the correlation coefficients between the various meteorological variables and solar indices at each station. The cross-correlation equation given by Bourke (1996), and employed by Kilcik (2005), as:

$$r = \frac{\sum_i \left[\left(x_i - M_x \right) \left(y_i - M_y \right) \right]}{\sqrt{\sum_i \left(x_i - M_x \right)^2 \left(\sum_i \left(y_i - M_y \right)^2 \right)}} \qquad (4.1)$$

for any two series x_i and y_i (i = 0, 1, 2,……..N -1); where r is the cross-correlation between x and y , M_x and M_y are the means of the corresponding series.

A suitable program written in MATLAB was developed to evaluate the entire cross correlation and their levels of significance. Tables 4.9 – 4.13 present the results. In the tables: RH=Relative humidity; MAT=Maximum temperature; MIT=Minimum temperature; WIS=Wind speed; SUD=Sunshine duration; SRA=Solar radiation; EVA=Evaporation; RNF=Rainfall; AVT=Average temperature; SNN, R_s=Sunspot numbers; F10.7=F10.7cm solar radio flux and Mg II=Mg II core–to-wing ratio.

Table 4.9: Correlation matrix among the climatic parameters and solar indices at KER

	RH	MAT	MIT	WIS	SUD	SRA	EVA	RNF	AVT	SNN, R_s	F10.7	Mg II
RH	1											
MAT	-0.792**	1										
MIT	0.379**	-0.067	1									
WIS	-0.588**	0.308**	-0.385**	1								
SUD	-0.554**	0.611**	-0.395**	0.406**	1							
SRA	-0.559**	0.634**	-0.182**	0.292**	0.597**	1						
EVA	-0.729**	0.812**	-0.186**	0.533**	0.651**	0.583**	1					
RNF	0.483**	-0.325**	0.457**	-0.368**	-0.431**	-0.368**	-0.217**	1				
AVT	-0.532**	0.873**	0.428**	0.091	0.36**	0.485**	0.645**	-0.071	1			
SNN, R_s	0.026	0.022	0.027	-0.205**	-0.094	-0.018	-0.052	0.007	0.033	1		
F10.7	-0.058	0.106	0.027	-0.171**	-0.068	0.059	0.018	-0.011	0.109*	0.965**	1	
Mg II	-0.007	0.101	0.094	-0.228**	-0.075	0.1	-0.015	0.008	0.138*	0.928**	0.962**	1

** Correlation is significant at the 0.01 level (2-tailed). * Correlation is significant at the 0.05 level (2-tailed).

Table 4.10: Correlation matrix among the climatic parameters and solar indices at NBI

	RH	MAT	MIT	WIS	SUD	SRA	EVA	RNF	AVT	SNN, R_s	F10.7	Mg II
RH	1											
MAT	-0.775**	1										
MIT	0.093	0.37**	1									
WIS	-0.479**	0.681**	0.433**	1								
SUD	-0.694**	0.783**	0.34**	0.641**	1							
SRA	-0.718**	0.85**	0.305**	0.686**	0.786**	1						
EVA	-0.79**	0.936**	0.34**	0.751**	0.833**	0.867**	1					
RNF	0.324**	0	0.642**	0.066	0.027	-0.015	-0.006	1				
AVT	-0.489**	0.881**	0.766**	0.692**	0.715**	0.744**	0.821**	0.327**	1			
SNN, R_s	0	-0.02	-0.103	-0.034	-0.026	0.075	-0.045	0.014	-0.066	1		
F10.7	-0.068	0.068	-0.044	0.033	0.068	0.166**	0.043	0.028	0.025	0.965**	1	
Mg II	-0.045	0.044	-0.049	-0.038	0.036	0.162**	-0.002	0.026	0.006	0.928**	0.962**	1

** Correlation is significant at the 0.01 level (2-tailed). * Correlation is significant at the 0.05 level (2-tailed).

Table 4.11: Correlation matrix among the climatic parameters and solar indices at KSM

	RH	MAT	MIT	WIS	SUD	SRA	EVA	RNF	AVT	SNN, R_s	F10.7	Mg II
RH	1											
MAT	-0.827**	1										
MIT	0.165**	0.111*	1									
WIS	-0.565**	0.603**	0.24**	1								
SUD	-0.586**	0.541**	-0.112*	0.505**	1							
SRA	-0.464**	0.641**	0.244**	0.605**	0.462**	1						
EVA	-0.693**	0.758**	0.242**	0.734**	0.541**	0.606**	1					
RNF	0.509**	-0.299**	0.452**	-0.088	-0.319**	0.063	-0.062	1				
AVT	-0.631**	0.9**	0.533**	0.619**	0.412**	0.652**	0.752**	-0.056	1			
SNN, R_s	0.055	-0.019	-0.149*	0.012	-0.019	0.033	-0.033	-0.08	-0.081	1		
F10.7	0.005	0.033	-0.096	0.114*	0.037	0.12*	0.032	-0.063	-0.014	0.965**	1	
Mg II	0.041	0.008	-0.063	0.099	0.015	0.07	0.006	-0.049	-0.021	0.928**	0.962**	1

** Correlation is significant at the 0.01 level (2-tailed). * Correlation is significant at the 0.05 level (2-tailed).

Table 4.12: Correlation matrix among the climatic parameters and solar indices at MSA

	RH	MAT	MIT	WIS	SUD	SRA	EVA	RNF	AVT	SNN, R_s	F10.7	Mg II
RH	1											
MAT	-0.799**	1										
MIT	-0.527**	0.827**	1									
WIS	-0.405**	0.238**	0.193**	1								
SUD	-0.71**	0.558**	0.328**	0.2**	1							
SRA	-0.762**	0.646**	0.391**	0.075	0.813**	1						
EVA	-0.825**	0.817**	0.619**	0.378**	0.698**	0.778**	1					
RNF	0.475**	-0.228**	0.06	-0.198**	-0.53**	-0.478**	-0.35**	1				
AVT	-0.708**	0.965**	0.945**	0.228**	0.477**	0.556**	0.762**	-0.104	1			
SNN, R_s	-0.044	-0.031	0.009	0.087	0.002	-0.073	0.002	-0.028	-0.014	1		
F10.7	-0.154**	0.073	0.085	0.117*	0.081	0.011	0.087	-0.065	0.082	0.965**	1	
Mg II	-0.11*	0.046	0.082	0.135*	0.047	-0.042	0.042	-0.062	0.065	0.928**	0.962**	1

** Correlation is significant at the 0.01 level (2-tailed). * Correlation is significant at the 0.05 level (2-tailed).

Table 4.13: Correlation matrix among the climatic parameters and solar indices at GRS

	RH	MAT	MIT	WIS	SUD	SRA	EVA	RNF	AVT	SNN, R_s	F10.7	Mg II
RH	1											
MAT	-0.06	1										
MIT	0.295**	0.743**	1									
WIS	-0.673**	-0.482**	-0.601**	1								
SUD	-0.36**	0.301**	0.168**	0.281**	1							
SRA	0.185**	0.71**	0.706**	-0.466**	0.339**	1						
EVA	-0.635**	0.021	-0.199**	0.669**	0.475**	0.04	1					
RNF	0.588**	-0.005	0.369**	-0.367**	-0.114*	0.337**	-0.281**	1				
AVT	0.101	0.95**	0.915**	-0.571**	0.26**	0.758**	-0.08	0.169**	1			
SNN, R_s	-0.06	0.008	-0.1	-0.085	-0.127*	-0.11*	-0.06	0.034	-0.042	1		
F10.7	-0.012	0.098	-0.025	-0.183**	-0.137*	-0.043	-0.117*	0.055	0.048	0.965**	1	
Mg II	-0.044	0.087	-0.04	-0.138*	-0.103	-0.074	-0.07	0.022	0.034	0.928**	0.962**	1

** Correlation is significant at the 0.01 level (2-tailed). * Correlation is significant at the 0.05 level (2-tailed).

4.2.4 Spectral Analysis

According to Bai, (2003), to study periodicity in a regular time series $X_j + X(t_j)$, a series of measurements made at times t_j separated by regular intervals, one often uses Fourier spectral analysis. For an irregular time series, Scargle (1982) developed a periodogram calculated by the following equation:

$$P_x(\upsilon) = \frac{1}{2}\left\{\frac{\left[\sum_{j=1}^{N} X_j \cos 2\pi\upsilon\left(t_j-\tau\right)\right]^2}{\sum_{j=1}^{N}\cos^2 2\pi\upsilon\left(t_j-\tau\right)} + \frac{\left[\sum_{j=1}^{N} X_j \sin 2\pi\upsilon\left(t_j-\tau\right)\right]^2}{\sum_{j=1}^{N}\sin^2 2\pi\upsilon\left(t_j-\tau\right)}\right\} \quad (4.2)$$

Where τ is defined by the relation:

$$\tan 4\pi\upsilon\tau = \left(\sum_{j=1}^{N}\sin 4\pi\upsilon t_j\right) \Big/ \left(\sum_{j=1}^{N}\cos 4\pi\upsilon t_j\right) \quad (4.3)$$

For this periodogram, the probability that the value P_x is greater than z by chance is given by $\Pr\left(P_x \geq z\right) = \exp(-z)$, if a time series X_j satisfies the following three conditions.

(1) The mean of the time series is zero. (2) Its standard deviation is 1. (3) Each element of the time series is statistically independent Gaussian noise.

To investigate the periodicity of the meteorological variables and solar indices at each station, the Fourier analysis technique Scargle periodogram; Scargle, (1982) has been applied to the monthly running means of the meteorological variables and solar indices. Applying a suitable program in MATLAB, the power spectra (periodograms) of the various meteorological parameters at all the stations were obtained and reported in Figures 5.2 – 5.6, with the prominent periodicities observed in the periodograms for various variables indicated in Table 5.3.

4.2.5 Modeling the Meteorological and solar variables

Assuming the meteorological variable y is expressible in terms of the solar indices R_s, $F_{10.7}$ and Mg II such that: $y = y(R_s, F_{10.7}, MgII)$, an empirical linear multivariate model of the form below is proposed:

$$y = A + B\,Rs + C\,F_{10.7} + D\,MgII \tag{4.4}$$

Where *'y'* is any of the meteorological variables; R_s is the sunspot number; $F_{10.7}$ is the *F10.7* cm solar radio flux index and Mg II is the Mg II core-to-wing ratio index respective values. A, B, C and D are empirical coefficients that are determined by least square fittings. The values of these coefficients are presented on Tables 4.14 – 4.22.

4.2.6 Performance of Models

The validity of the model was tested using the statistical indicators proposed by Stone (1993); engaged by Falayi (2005) and El-Metwally (2005). The Mean Bias Error (MBE) and Root Mean Square Error (RMSE) were evaluated using the following equations for all the meteorological variables at the five stations:

$$MBE = \sum \frac{(y_{pred} - y_{obs})}{N} \tag{4.5}$$

$$RMSE = \left[\sum \left(\frac{(y_{pred} - y_{obs})^2}{N} \right) \right]^{1/2} \tag{4.6}$$

y_{pred} is the calculated value from the model. Y_{obs} is the observed value and N is the total number of observations. The test of RMSE provides information on the short – term performance of studied model as it allows a term by term comparison of the actual deviation between the calculated value and the measured value. Iqbal, (1993) and Halouani *et al.,* (1993) have recommended that a zero value of RMSE is ideal while a low MBE is desirable. This was used because of its suitability for the kind of data used. The MBE and RMSE values obtained are presented in Tables 4.14 – 4.22.

Table 4.14: Model parameters A, B, C and D together with Performance Indicators MBE and RMSE from estimated Relative Humidity (%) using monthly means

	A	B	C	D	MBE	RMSE
KER	-33.7938	-0.1391	0.0628	382.5959	8.5081e-016	0.0954
NBI	18.3722	0.1385	-0.1714	273.4407	-1.849e-016	0.0944
KSM	-50.4949	0.0894	-0.1383	477.1217	1.3297e-015	0.1206
MSA	58.5081	0.114	-0.1375	117.3244	-2.0706e-016	0.0687
GRS	167.7331	-0.0454	0.0888	-388.261	-9.8022e-016	0.0538

Table 4.15: Model parameters A, B, C and D together with Performance Indicators MBE and RMSE from estimated Maximum Temperature (^{0}C) using monthly means

	A	B	C	D	MBE	RMSE
KER	88.8943	0.0417	-0.0061	-251.6985	-2.3192e-015	0.0680
NBI	57.8234	-0.0545	0.0733	-144.8584	-5.9650e-016	0.0765
KSM	48.5030	-0.0112	0.0198	-75.5191	-7.0070e-016	0.0576
MSA	6.1165	-0.0495	0.0391	84.6753	-3.2399e-016	0.0970
GRS	47.4955	-0.0316	0.0447	-60.0679	-4.491e-016	0.0829

Table 4.16: Model parameters A, B, C and D together with Performance Indicators MBE and RMSE from estimated Minimum Temperature (^{0}C) using monthly means

	A	B	C	D	MBE	RMSE
KER	46.5722	0.0118	-0.0003	-139.1391	-2.1582e-015	0.0575
NBI	11.7282	-0.0232	0.0202	2.2811	-6.8160e-016	0.1156
KSM	6.9808	-0.0100	0.0031	39.0746	2.1280e-017	0.0649
MSA	-53.8120	-0.0057	-0.0310	297.5030	1.0102e-015	0.2872
GRS	60.9028	-0.0094	0.0305	-149.5705	-1.4039e-015	0.1734

Table 4.17: Model parameters A, B, C and D together with Performance Indicators MBE and RMSE from estimated Wind Speed (km/day) using monthly means

	A	B	C	D	MBE	RMSE
KER	-415.1341	0.1767	-0.3321	2172.8378	1.7322e-015	0.1201
NBI	1267.7286	-0.5733	1.0974	-4600.6233	-6.3705e-015	0.2543
KSM	335.8195	-0.7290	0.8961	-1019.3638	-1.3595e-016	0.1817
MSA	-435.5342	-0.1853	0.0103	2206.1649	1.9560e-015	0.2075
GRS	-3137.4157	1.0270	-2.5723	13274.0143	6.6998e-015	0.3841

Table 4.18: Model parameters A, B, C and D together with Performance Indicators MBE and RMSE from estimated Sunshine Duration (Hours/day) using monthly means

	A	B	C	D	MBE	RMSE
KER	40.6050	0.0234	-0.0004	-130.0465	-3.2636e-015	0.1563
NBI	44.8362	-0.0845	0.1063	-168.3219	-2.9146e-015	0.3132
KSM	12.4588	-0.0179	0.0218	-21.3620	-6.1615e-016	0.1280
MSA	-51.7240	-0.0258	-0.0003	229.2170	2.9928e-015	0.3153
GRS	11.4541	0.0281	-0.0261	-4.5036	-5.5153e-016	0.3503

Table 4.19: Model parameters A, B, C and D together with Performance Indicators MBE and RMSE from estimated Solar Radiation (MJ/m^2-day) using monthly means

	A	B	C	D	MBE	RMSE
KER	91.1397	0.0617	-0.0100	-270.0257	-2.2076e-015	0.1363
NBI	-14.9340	-0.1005	0.1048	104.1790	5.9962e-016	0.1952
KSM	56.8440	-0.0385	0.0560	-137.6061	-7.8024e-016	0.0833
MSA	109.7347	-0.0464	0.0898	-358.3198	-2.0031e-015	0.1178
GRS	32.4426	-0.0327	0.0263	-42.0080	-5.4114e-016	0.1018

Table 4.20: Model parameters A, B, C and D together with Performance Indicators MBE and RMSE from estimated Evaporation (mm/day) using monthly means

	A	B	C	D	MBE	RMSE
KER	41.0370	0.0261	-0.0048	-139.6113	-4.7307e-015	0.1982
NBI	37.5828	-0.0327	0.0048	-136.2027	-3.2935e-015	0.2697
KSM	16.2239	-0.0198	0.0240	-43.5316	-8.0694e-016	0.1752
MSA	-23.4720	-0.0097	0.0009	107.2436	2.9507e-015	0.4006
GRS	-35.6684	0.0068	-0.0285	169.5269	2.9395e-015	0.2012

Table 4.21: Model parameters A, B, C and D together with Performance Indicators MBE and RMSE from estimated Rainfall (mm/day) using monthly means

	A	B	C	D	MBE	RMSE
KER	8.0958	-0.0323	-0.0126	2.2351	-1.2549e-015	0.8324
NBI	22.9796	-0.0053	0.0079	-75.7304	-2.4606e-015	1.3311
KSM	-1.8352	-0.0147	0.0094	19.9973	1.9560e-016	0.6935
MSA	0.5408	0.0244	-0.0307	16.6751	-6.9692e-016	1.1252
GRS	22.0315	-0.0057	0.0158	-82.9920	-8.9950e-015	1.7108

Table 4.22: Model parameters A, B, C and D together with Performance Indicators MBE and RMSE from estimated Average Temperature (^{0}C) using monthly means

	A	B	C	D	MBE	RMSE
KER	67.7332	0.0267	-0.0032	-195.4188	-2.4412e-015	0.0439
NBI	-105.7111	-0.0942	0.0239	472.5642	2.9072 e-015	0.5904
KSM	27.7419	-0.0106	0.0115	-18.222	-5.1509 e-016	0.0456
MSA	-23.8478	-0.0276	0.0040	191.0892	6.6653 e-016	0.1669
GRS	54.1991	-0.0205	0.0376	-104.8192	-9.9624 e-016	0.1171

4.3 Determination of Solar Signature in drought occurrences in Kenya

Drought indices were estimated from the rainfall data obtained from the five observatories and subjected to Fast Fourier Transforms in order to obtain the periodicities associated with the indices at various locations.

Table 4.23 below shows drought classification by expressing each observation as a percentage of the long-term average given by the drought index expression:

$$Index = 100 * X_i / \overline{X} \qquad (4.7)$$

Where X_i is the i^{th} observation and $\overline{X}$ is the long-term average.

Table 4.23: Drought Classification

Index	Category	Code
<25%	Extremely dry	1
25% to 75%	Dry	2
75% to 125%	Normal	3
125% to 175%	Wet	4
>175%	Extremely wet	5

The yearly drought indices were calculated by employing the INSTAT software, courtesy of KMD, for a total of 46 years (1960 to 2005) for the five terrestrial stations representing the regional climatic zones under the management of the KMD. The indices were then subjected to fast Fourier transform in order to obtain their spectra characteristics.

The Fourier coefficients derived from the respective time series by adopting the principle employed by (Nag *et al.*, via tukada2@vsnl.net.) and reported by Rabiu *et al*., (2007) revealed the most prominent peaks in spectral characteristics of drought as seen in Fig.5.7 and reported on Table 5.5.

4.4 Stepwise multiple regression analysis of lagged solar indices on climatic parameters

As an attempt to get comparable linear models, the stepwise multiple regression analysis in SPSS was done using the lagged solar indices instead of the non lagged indices. Just as it is known that evaporation enhances rain by forming the clouds that fall as rain some

times in the future, it is also possible that the previous month's solar activities could be responsible for the currently observed climatic parameter variations. The lagging was done in this case up to the third month backwards. This lagging could be done further, but the choice of third month was adopted based on how rain is caused by the rise of moist air in the direction of low pressure areas resulting from the sun radiation. The lag period in this case is about three months (ICPAC, through private discussion). Only statistically accepted models based on 2-tailed, $p<0.05$ level of significance, and the stations in which they are found are reported on Table 5.6.

CHAPTER 5

RESULTS AND DISCUSSIONS

5.0 Introduction

This chapter presents the results of the methodologies in chapter 4, and discusses them. Section 5.1 discusses the trends of the monthly and seasonal variations of the climatic parameters. The unique cases noted in the variations in each parameter are given suggested explanations.

Section 5.2 discusses the correlations between the solar parameters and the climatic parameters. Power spectra and periodicities of the meteorological variables in relation to solar activities are mentioned in section 5.3. The models and their validity are discussed under section 5.4 giving details of the models for all the parameters. General forcing trends of the solar indices of the climatic parameters in each station are discussed and suggested explanations given to the cases of meteorological stations with deviating trends.

Section 5.5 gives brief discussions of the periodicities of drought occurrence. Periodicities in drought occurrence that are closer to the literature reports of the solar periodicities are stated here. Section 5.6 discusses the inferences that are drawn from results of stepwise regression analysis between the climatic parameters and the lagged solar indices.

5.1 Mean monthly and seasonal variations of the Meteorological parameters.

The plots of monthly variations of the meteorological variables across the stations are shown in Figure 5.1 (a - i).

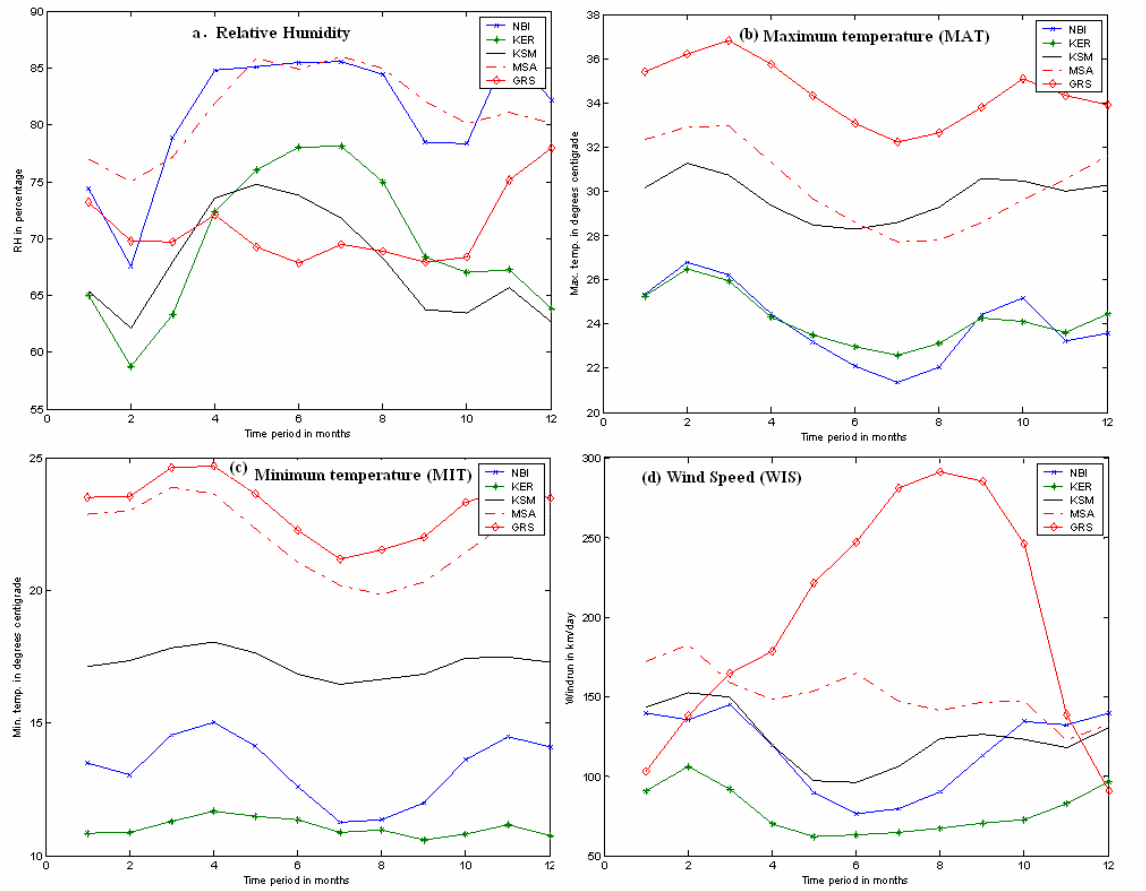

Figure 5.1: (a – d) Monthly daily variations of the meteorological variables at different stations for the duration of study

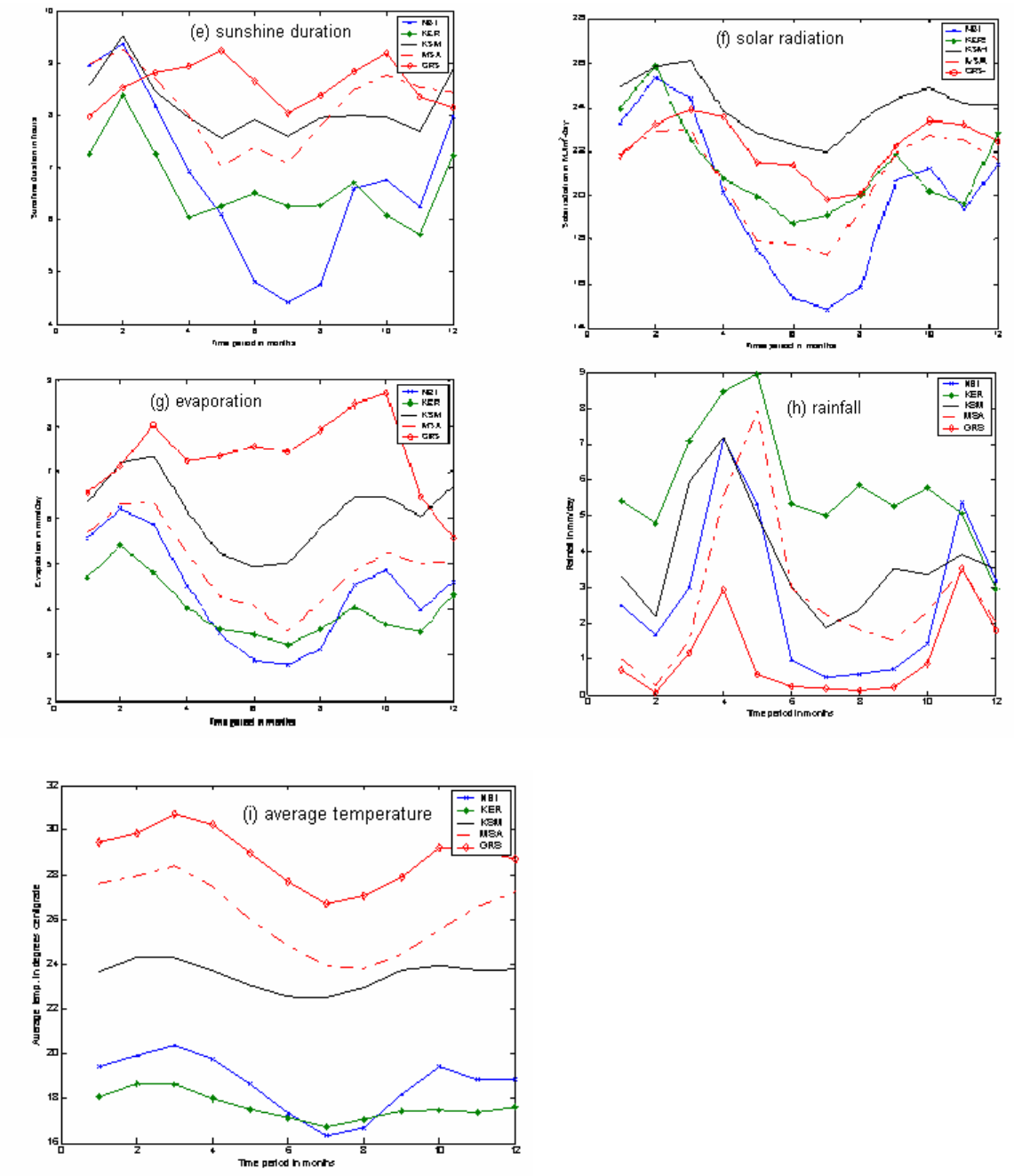

Figure 5. 1: (e – i) Monthly daily variations of the meteorological variables at different stations for the duration of study

5.1.1 Mean monthly and seasonal variations of Relative Humidity.

From Figure 5.1 *a*, it can be seen that the general trend for all the stations is that there is minimum RH in the month of February during the dry hot period. This is followed by a general rise with a maximum during March to August for all stations except GRS. The peak period includes the long rains and the dry cold seasons. NBI and MSA have the highest peak values followed by KER then KSM, while GRS does not have high RH during this period. KER, KSM and MSA tend to have lower values of RH during the dry hot (DH) period while NBI and GRS tend to have decreasing values of RH in the same period.

In NBI the values of RH range from 67% to 86%. For KER the range is from 58% to 78%. For KSM, it ranges from 62% to 73%. For MSA, it ranges from 75% to 86%.

In GRS, RH value is low in February-March, but higher than the minimums of NBI, KER and KSM, but lower than that of MSA. It is higher in January and December and finally rises in April, decreases during the dry cold (DC) period and short rains (SR) with steep rise in November to December. The range for GRS is 69.8% in March to 77.9% in December. RH values in GRS are lower than those of the other stations during the DC period but overtakes KSM and KER during the short rains to the DH period. The unique variation of RH in GRS is attributed to its lowland semi arid features that make the area receive unpredictable rainfall pattern, hence lack of a pattern in RH values.

5.1.2 Mean monthly and seasonal variations of Maximum Temperature

From Figure 5.1 *b*, a general trend of the highest maximum temperature is in February-March-April. There is general decrease from April through May with the lowest value of maximum temperature in June-July-August (DC period). A trend of general increase starts after August through September with a peak around September-October. A slight decrease is noted after the brief peak in KER, KSM and NBI, then a steady increase from November though December to January. In MSA, there is no peak in October, but a steady increase after the minimum of July-August through to December and January. GRS on the other hand registers a decrease in MAT after the brief October peak through December. Reducing temperatures in GRS during the later months of the year is explainable in terms of movements of the sun. The temperatures generally follow the apparent movement of the sun. Since the Sun is further south at this time, and GRS is in the north, it is bound to register reduced maximum temperatures.

The maximum temperature of NBI varies from 21^{o}C to 27^{o}C and of KER from 22^{o}C to 27^{o}C, which are more or less the same; except that the lowest value for NBI is lower at 21^{o}C in July than that of KER at 23^{o}C in the same month. The peak value of maximum temperature during the short rains in NBI, which is in October at 25^{o}C, is higher than that of KER at 24^{o}C in the same month. The two stations register the lowest values of maximum temperature. The general lower temperature values observed in KER and NBI highland areas in comparison to KSM, MSA and GRS are due to the high altitudes of KER and NBI as supported by reports of Ogallo, (1989).

The maximum temperature of KSM varies from 28^{o}C to 32^{o}C while that of MSA varies from 27^{o}C to 33^{o}C, which are more or less the same, but higher than the maximum temperature values of KER and NBI, while lower than those of GRS. However, the peak maximum for KSM is lower at 31.3^{o}C in February when compared to that of MSA at 32.9^{o}C in the same month. The minimum values of maximum temperature during DC period are close to each other, being 28.3^{o}C for KSM in June and 27.7^{o}C for MSA in July-August. A distinct high value of maximum temperature during the short rain is noticed in KSM (30.6^{o}C), while a continuous increase in maximum temperature is in MSA during the same period.

The similarity observed in maximum temperature trends for KSM and MSA is attributable to the fact that the two meteorological stations are located within the precincts of large water bodies (Fig 1.1). The kinds of breezes that are due to the water bodies have direct influence on the climatic features of the nearby locality. The sea breezes during the day when maximum temperatures are recorded are caused by wind movements from sea to land during the day as explained in chapter three. Water has higher heat capacity, and therefore absorbs more heat during the day and remains cooler while the bordering land with less heat capacity gets hotter faster. Hence, we get higher temperatures during the day on the land within the neighborhood of the large water bodies as observed in KSM and MSA meteorological stations.

GRS station records the highest values of maximum temperature (32^{o}C to 37^{o}C) as compared to the other stations. Being in the lowland semi arid area with very little rainfall and less cloud formation, the direct radiation impact leads to higher temperatures.

5.1.3 Mean monthly and seasonal variations of Minimum Temperature

From Figure 5.1 *c*, the trend of variation of minimum temperature is quite similar to that of the maximum temperature with a few notable differences in terms of station range similarities. KER has the lowest values ranging from 10^{o}C to 12^{o}C. This is attributable to its mountainous terrain, about 87 Km from Lake Victoria that makes it get frequent rains. The hills (1946.85m above sea level; Table 4.1) create good barrier for the moist high temperature winds from the lake that form overcast clouds resulting in frequent rains and low temperatures; Aming'o, (2005). The forestry environment within the region is also a factor in the low temperatures experienced here.

Minimum temperature of NBI varies from 11^{o}C to 15^{o}C, which is higher than that of KER but lower than those of the other three stations. The low values of minimum temperature in NBI are due to the fact that it is within the central highlands (1771.77m above sea level; Table 4.1). It is not forested and is just four km from the Nairobi city centre. It is still not close to the Industrial area of the city that would otherwise increase temperatures due to the green house gases produced by the industries. NBI and KER are both in highlands but NBI minimums are modified by the Urban Heat Island effect.

Minimum temperature of KSM that varies form 16^{o}C to 18^{o}C is much higher than that of KER and NBI. KSM is within the lake shore at a low altitude (131.83m above sea level; Table 4.1); just a few kilometers from the Nandi hills. Its minimum temperature should be same as that of MSA; however, the influence of Nandi hills helps in lowering the minimum temperature through the Mountain/Valley winds.

Minimum temperature of MSA, which varies from 19^{o}C to 24^{o}C, is higher than those of the stated three stations, but lower than that of GRS, which varies from 21^{o}C to 25^{o}C. MSA is at the lowest altitude (5.41m above sea level; Table 4.1), with high values of relative humidity. The Relative Humidity of MSA ensures higher minimum temperatures.

GRS has the highest values of minimum temperature compared to the other four meteorological stations. Though GRS has higher elevation (120.13m above sea level; Table 4.1) than MSA, its unique semi arid features make it have higher temperature values compared to the other stations.

5.1.4 Mean monthly and seasonal variations of Wind Speed

The wind patterns in Figure 5.1 *d* indicate that there is maximum wind speed in the months of February and March during the onset of the long rains for all stations apart from GRS. Except for MSA and GRS, the wind speed for the other three stations steeply decreases in the months of April and May; it is lowest in June and July during the DC

period for these three stations. There is a general rise of the wind speed for the three stations in August through the short rains (September- November) and the DH period (December, January, February).

Specifically, KER experiences the lowest values of wind speed that range from 62.00km/day in May to 104.626km/day in February, as compared to the other stations. This is explainable in terms of its height above sea level stated earlier. The forest coverage and the orography (mountainous terrain) act as barriers to the high speed winds.

The wind speed values for KSM, which range from 96.219km/day in June to 152.299km/day in February, are slightly higher than those of NBI (76.559km/day in June to 146.065km/day in March). Both stations are located within the cities of Kisumu and Nairobi respectively. The screening effect of tall buildings is certainly a factor. KSM being on the shore of Lake Victoria within the Lake basin region has the moist winds coming from the great lakes (ICPAC, Nairobi through private discussion), and therefore has higher wind speed values compared to NBI. Being a much bigger city with taller buildings within the central highland area, NBI experiences more screening effect against the winds. Hence the apparent less values of wind speed.

The wind speed values for MSA range from 122.868km/day in November to 181.902km/day in February, which is higher than those of the three stations, but lower than those of GRS (90.732km/day in December to 291.012km/day August). Apart from

GRS the maximum wind speeds in the other stations occur in February-March. The minimum wind speed is generally in May - June, save for MSA and GRS that have their minima in November and December respectively.

MSA wind speed reveals an oscillating pattern with reducing maxima and minima. The highest maximum is in February (181.902km/day), followed by highest minimum in April (148.524km/day); next high value is in June (158.337km/day) and higher minimum in August (141.389km/day). The next high maximum is in October (146.990km/day) and the lowest minimum in November (122.868km/day). The lowest maximum is in December (132.610km/day) and the next minimum in January (169.818km/day). This pattern can only be explained in terms of the sea breeze pattern of the Indian Ocean. These could have the oscillating pattern seen in the observed wind pattern in MSA.

The minimum wind speeds for GRS experienced in December (90.731km/day) and January (100.905km/day) during the DH period is lower than the ones observed in the other stations. However, there is a steady increase of the wind speed from January, overtaking speed for other stations by the month of March-April (LR season). The parabolic curve peaks in the month of August (291.012km/day) during the DC period of the country. Then we observe a steep parabolic decrease until the lowest minimum in December. The semi arid land nature of this area is likely to be a factor in the unique wind speed pattern observed because the synoptic systems like the Ocean are far away

and mountains that can modify the wind patterns are not in this area. The Chalbi desert in northern Kenya- Southern Ethiopia area, the Somali current and the East African low level jet are all factors in the observed wind patterns in GRS. When the sun is in the North, there are high heating rates in the deserts to the north. Temperature differentials create pressure differentials, hence high winds.

5.1.5 Mean monthly and seasonal variations of Sunshine Duration

From Figure 5.1 *e*, it can be seen that the maximum sunshine hours is in the month of February to March for all the stations, except GRS whose maximum sunshine hours is in May. Having maximum number of sunshine hours around March can be explained in terms of the position of the sun during that period. At that time, the sun is within the equator (23rd March) on its way northwards, and most of the stations being within the equatorial region, are bound to have more sunshine hours in that period. Cloudiness during the rainy season (ITCZ) is slightly delayed from the actual solar position, so maximum sunshine hours in February - March just during the onset of long rains are expected. Generally the minimum sunshine hour is between April and August with slight variations in KER, KSM, and MSA; but with major variation in GRS.

During the DC period when most of the stations experience least sunshine hours, the sun is in the extreme north within the tropic of Cancer (21st September), the South-Easterlies create the blocking systems leading to inversion and extensive cloud cover from low level clouds; hence the chilly climate in most parts of the country (ICPAC, Nairobi

through private discussion). We therefore experience the least hours of sunshine during this period for most of the stations.

For KER, the sunshine hours values, which range from 5.720 hours/day in November to 8.367 hours/day in February are fairly close to those of NBI that range from 4.410 hours/day in July to 9.373 hours/day in February, but NBI maximum (9.373 hours/day in February) is more than KER maximum both of which are in February. While KER has several months of low sunshine hours such as April (6.050 hours/day), July to August, and Nov (5.720 hours/day), NBI has steady drop in the number of sunshine hours, having the extreme minimum in July (4.410 hours/day) during the DC period. Both stations register high sunshine hours just before the short rain period with KER in September (6.711 hours/day) and NBI in October (6.760 hours/day). There is a drop in the number of sunshine hours for both stations at the end of the short rain season in November, with KER registering (5.720 hours/day) and NBI registering (6.257 hours/day) in that month. They both register a sharp increase in the DH period from December to February.

KSM range of sunshine hours is from 7.563 hours/day in May to 9.533 hours/day in February. The number of sunshine hours for KSM is more than that of KER in all months of the year, but the trend is quite similar to the KER trend. These two stations are only 87kms apart but have totally different terrain as has been explained earlier.

The values of sunshine hours in MSA, which range from 6.999hours/day in May to 9.242 hours/day in February are close to those of KSM, except that the minimum number of sunshine hours for MSA (6.999 hours/day in May) is less than that of KSM in the same period, and MSA tends to have high number of sunshine hours in October (8.779 hours/day) with KSM having generally less hours of sunshine in that month. In December, MSA registers less number of sunshine hours (8.448 hours/day) while KSM registers more (8.882 hours/day). General similarities in sunshine duration trends are observed in the two stations, perhaps due to their proximity to the large water bodies. However, the disparity observed in both stations towards the end of the year may be attributed to the tides of the Indian Ocean for Mombasa station.

GRS range of sunshine hours is from 7.964 hours/day in January to 9.235 hours/day in May. It has its minimum number of sunshine hours in the month of January (7.964 hours/day), while its maximum number of sunshine hours is in the month of May (9.235 hours/day). All the stations except GRS have their maximum number of hours in February during the DH period. The May maximum for GRS is attributable to the fact that the sun is moving northwards in that period, it is probably closer to the sun's position in May. The minimum hour in December is apparently due to the fact that the sun is in the extreme south while GRS is in the northern part.

5.1.6 Mean monthly and seasonal variations of Solar Radiation

From Figure 5.1 *f*, the trend of solar radiation for all the stations is that there is high radiation in December and January with a steady increase, peaking in February-March, with different maxima for different stations. KSM registers the highest radiation (26.13MJ/m^2-day in March) in this period followed by KER (25.73MJ/m^2-day in February), NBI (25.27MJ/m^2-day in February), GRS (23.93MJ/m^2-day in March) and MSA (23.05MJ/m^2-day in March) in that order. This period lies mostly at the end of the DC period (February) – to the onset of the Long rain period in March. It also corresponds to the period of highest maximum temperature, highest minimum temperature and highest sunshine duration (Figures: 5.1 *b*, 5.1 *c* and 5.1 *e*). It may hence be inferred that the long rains (Fig 5.1 *h*) are preceded by high solar radiation period, high temperature and long sunshine duration. A steep decrease in solar radiation is observed during the Long rain season (March-May).

Minimum radiation is observed for all the stations in the DC (January-August) period with different minima for different stations. KSM still receives the highest amount of radiation (21.98MJ/m^2-day in July) during this period, followed by GRS (19.83MJ/m^2-day in July), KER (19.50MJ/m^2-day in June), MSA (17.29MJ/m^2-day in July) and NBI (14.88MJ/m^2-day in July) in that order. So the Dry Cold period characterized by least rain in virtually all the stations is also having the least amount of solar radiation received by all the stations.

There is increase in the amount of radiation recorded for each station in the short rain season (September-November) with KSM recording the highest (24.85MJ/m^2-day in October) followed by GRS (23.44MJ/m^2-day in October), MSA (22.74MJ/m^2-day in October), KER (21.90MJ/m^2-day in September) and NBI (21.21MJ/m^2-day in October) in that order. So the onset of the short rains that varies from September to October is characterized by substantial amount of solar radiation and good amount of temperature in general (Figs: 5.1 *b*, 5.1 *c* and 5.1 *i*). During the short rain period there is sharp decrease of solar radiation in KER and NBI but the other stations register gradual decrease in solar radiation.

Solar radiation values for KER range from 19.13MJ/m^2 -day in July to 25.73MJ/m^2-day in February, NBI values range from 14.88MJ/m^2-day in July to 25.23MJ/m^2-day in February, KSM values range from 21.98MJ/m^2-day in July to 26.13MJ/m^2-day in March, MSA values range from 17.29MJ/m^2-day in July to 23.05MJ/m^2-day in March and GRS values range from 19.83MJ/m^2-day in July to 23.93MJ/m^2-day in March.

5.1.7 Mean monthly and seasonal variations of Evaporation

As seen in Figure 5.1 *g*, evaporation in all the stations shows increase after November through December-January with maximum in February-March covering mostly the DH period. GRS, however, shows steep decrease after October through December with an increase from January and a maximum in March.

All stations show broad minima from end of May through July-August covering the DC period for virtually all the stations. A general increase in evaporation is observed after August with a narrow peak in September-October during the short rain season. This also corresponds to the peaks observed in sunshine duration and solar radiation in the same period.

The values of evaporation in NBI range from 2.816mm/day in July to 6.173mm/day in February, while those of KER range from 3.278mm/day in July to 5.388mm/day in February. The two stations have the least evaporation values in a year after the MSA values that range from 3.573mm/day in July to 6.335mm/day in March. KSM has higher evaporation values that range from 4.939mm/day in June to 7.341mm/day in March; but GRS has the highest values that range from 6.549mm/day in January to 8.717mm/day in October.

5.1.8 Mean monthly and seasonal variations of Rainfall

From Figure 5.1 *h*, the long rain season (March- May) registers maximum rainfall in all the stations, with KER having the highest in May (8.167 mm/day) followed by MSA (7.930 mm/day), then NBI and KSM in April (7mm/day). The highest amount of rainfall recorded in GRS in this season (2.900mm/day) is still the lowest compared to the rain received in the four stations.

The rainfall amount drops steeply from May in all the stations with a broad minimum from June till September covering the DC period. The minimum rainfall received by

KER (5.0 mm/day) in this period is still the highest of all the stations followed by KSM (1.88mm/day) in July, and then MSA (1.521mm/day) in September. NBI minimum in July-September (0.480mm/day) is only more than the broad Min of GRS (0.115mm/day) in June-September.

While all the stations register steep increase in rainfall in October to peak in November during the short rain season, KER registers a sharp decrease in the same period. The maximum rain received by GRS during this period is in November (3.5mm/day), and is the same as that received by MSA in the same month. This is still the lowest compared to rain received by the other stations in that period. NBI receives the highest (5.377mm/day) in November followed by KER (5.064mm/day) then KSM (3.923mm/day). At the end of the short rain season in November, there is a sharp decrease in rainfall in all the stations, a scenario that continues throughout the DH period in December-January with a sharp minimum in February at the end of this period.

The ranges of rainfall for the five stations are: KER from 2.957mm/day in December to 8.167mm/day in May, NBI from 0.593mm/day in July to 5.357mm/day in May, KSM from 1.883mm/day in July to 7.186mm/day in April, MSA from 0.259mm/day in February to 7.998mm/day in May and GRS from 0.068mm/day in February to 3.538mm/day in November. KER receives the highest mount of rainfall while GRS receives the least amount in a year. KSM and MSA get nearly same amount, except

during the early and late months of the year when KSM receives more. The amount received by each of the two stations in a year is more than what NBI gets in a year.

The general trends of long rains in March-April-May (MAM) and the short rains in September-October-November (SON) observed in Fig. 4.8 *h*, referred to as bimodal rainfall pattern, have also been reported by Ogallo, (1989); Ouma, (2000) and Aming'o, (2005)

5.1.9 Mean monthly and seasonal variations of Average Temperature

Figure 5.1 *i* shows that variation of average temperature in a year has similar trend for maximum and minimum temperature seen in Figures 5.1 *b* and 5.1 *c*. All the five meteorological stations show highest average temperature in the DH period with the peak in March at the beginning of the long rain period. This steadily drops as we begin the long rain period in March with a broad minimum during the DC period. The average temperature begins to rise again in August at the end of the DC period, peaking around October for all stations except MSA whose second peak is in December-January.

KER (16.72^{o}C in July – 18.65^{o}C in March) has the least average temperature over the year followed by NBI (16.31^{o}C in July – 20.37^{o}C in March) except in July when NBI (16.31^{o}C) minimum average temperature goes below that of KER (16.72^{o}C). KSM (22.52^{o}C in July – 24.33^{o}C in February) has higher average temperature than the two, and MSA (23.82^{o}C in Aug – 27.92^{o}C in Feb) still has higher average temperature than KSM. GRS (26.71^{o}C in July – 30.70^{o}C in March) has the highest average temperature in

a year. Since the average temperature is obtained from the average of maximum temperature and minimum temperature, the observation of average temperature across the stations can be explained in the same way the maximum and minimum observations have been explained in this thesis. High altitude influence on low temperature values in KER and NBI can again be confirmed here, and supported by Ogallo, (1989). The reason for using minimum, maximum and average values was to take a holistic observation of temperature in the stations.

5.2 Correlations between the solar indices and the climatic parameters

Tables 5.1 to 5.3 show how the solar indices: sunspot numbers (R_s), F10.7 cm solar radio flux and Mg II core-to-wing ratio respectively vary with each of the nine climatic parameters at the five meteorological stations. The correlation coefficients and their statistical significant levels for the three solar parameters and the nine climatic parameters are indicated in the tables, and discussed below.

5.2.1 Correlations between the sunspot numbers (R_s) and the climatic parameters

Table 5.2 1: Correlations between Sunspot numbers and the climatic parameters

		Meteorological stations			
	KER	NBI	KSM	MSA	GRS
RH	0.026	0.000	0.055	-0.044	-0.06
MAT	0.022	-0.02	-0.019	-0.031	0.008
MIT	0.027	-0.103	0.149*	0.009	-0.1
WIS	-0.205**	-0.034	0.012	0.087	-0.085
SUD	-0.094	-0.026	-0.019	0.002	-0.127*
SRA	-0.018	0.075	0.033	-0.073	-0.11*
EVA	-0.052	-0.045	-0.033	0.002	-0.06
RNF	0.007	0.014	-0.08	-0.028	0.034
AVT	0.033	-0.066	-0.081	-0.014	-0.042

** Correlation significant at the 0.01 level (2-tailed). * Correlation significant at the 0.05 level (2-tailed).

As seen on Table 5.2.1, the correlations between sunspot numbers and RH, MAT, MIT, EVA and AVT are not statistically significant in the stations, except in KSM where there is a significant (at 0.05 level, 2-tailed) correlation between sunspot numbers and MIT. The influence of Lake Victoria and influence of the neighboring Nandi hills that helps in lowering the minimum temperature through the Mountain/Valley winds are responsible for the significant correlation between R_s and MIT in KSM.

Sunspot numbers (R_s) has a very significant negative correlation with WIS only in KER (significant at the 0.01 level, 2-tailed). The other negative correlations in NBI and GRS; and the positive correlations in KSM and MSA are not statistically significant. It can be inferred that the proximity of the water bodies in KSM and MSA influence wind pattern in such a way that some insignificant positive correlation between sunspot numbers and

wind speed is detectable. The modification of general wind patterns by these physical features has been reported by Ogallo, (1989) and Ouma, (2000). The lowest wind speeds in the Western highlands of the rift valley area of KER is certainly influenced by the sunspot numbers as supported by the highly significant negative correlation here. The central highlands of NBI and the low land semi arid area of GRS features favor some insignificant negative correlation between R_s and WIS.

A negative correlation between sunspot numbers and SUD is observable in most of the stations, but only the one in GRS is statistically significant at the 0.05 level (2-tailed). It can be inferred that R_s has some negative correlation with SUD in the country, but the correlation is more pronounced in the low land semi arid area of GRS. The unique variation of sunshine hours in GRS can therefore be attributed to the inverse influence of sunspot numbers as supported by the statistically significant negative correlation between the two parameters in GRS.

Sunspot numbers, R_s correlates negatively with SRA in KER, MSA and GRS; but it correlates positively with SRA in NBI and KSM. Only the negative correlation in GRS is statistically significant at the 0.05 level (2-tailed), the correlations in the rest of the stations are not statistically significant. It can therefore be said that R_s has some negative correlation with SRA in most parts of the country, but the negative correlation is more pronounced in the low land semi arid area of GRS. The high amount of radiation in the lowland semi arid area is therefore linked to sunspot numbers as supported by the

significant correlation. The central highland area of NBI and the lake influence in KSM make the two areas have some insignificant positive correlation between R_s and SRA.

Low positive correlation between R_s and RNF is observed in KER, NBI and GRS; but a low negative correlation is in KSM and MSA. None of the correlation coefficients are statistically significant at any acceptable levels. Juan *et al.*, (2004), while examining the relationship between solar activity and the annual precipitation in the Beijing area concluded that the annual precipitation is closely related to the variation in sunspot numbers, and that solar activity probably plays an important role in influencing the precipitation on land. However, Pederson, (2001) as reported by Juan *et al.*, (2004) states that relationship between solar activity and precipitation is very complicated and varies with time and probably also with geographic position; on the global scale, the correlation between sunspot numbers and precipitation may be positive, negative, or even zero. Their finding was based on long term observations covering several decades. Similar scenario is seen in this work when investigating the short term correlations between sunspot numbers and rainfall in Kenya.

5.2.2 Correlations between F10.7 cm solar radio flux and the climatic parameters

Table 5.2 2: Correlations between F10.7cm solar radio flux and the climatic parameters

		Meteorological stations			
	KER	NBI	KSM	MSA	GRS
RH	-0.058	-0.068	0.005	-0.154**	-0.012
MAT	0.106	0.068	0.033	0.073	0.098
MIT	0.027	-0.044	-0.096	0.085	-0.025
WIS	-0.171**	0.033	0.114*	0.117*	-0.183**
SUD	-0.068	0.068	0.037	0.081	-0.137*
SRA	0.059	0.166**	0.12*	0.011	-0.043
EVA	0.018	0.043	0.032	0.087	-0.117*
RNF	-0.011	0.028	-0.063	-0.065	0.055
AVT	0.109*	0.025	-0.014	0.082	0.048

** Correlation significant at the 0.01 level (2-tailed). * Correlation significant at the 0.05 level (2-tailed).

As seen on Table 5.2.2, there is a general negative correlation between F10.7 cm solar radio flux and RH, but this negative correlation is very strong in the coastal region of MSA as supported by the only significant correlation at the 0.01 level (2-tailed). The high level of humidity that is characteristic of the coastal region is certainly inversely influenced at the statistically significant levels by the coronal index F10.7 cm solar radio flux. The correlations between F10.7cm solar radio flux and MAT, MIT and RNF are all statistically insignificant.

F10.7 cm solar radio flux has negative correlation with WIS in KER and GRS. The negative correlations are significant at the 0.01 level (2-tailed); (Table 5.2). Positive variation of F10.7 cm solar radio flux with WIS is evident in NBI, KSM and MSA.

While the positive correlations in KSM and MSA are significant at the level of 0.05 (2-tailed), that of NBI is not significant. KER area with the lowest wind speeds and GRS area with the highest wind speeds due to their prevailing respective orography stated earlier, have their wind speeds influenced inversely by the corona through the index F10.7 cm solar radio flux. The large water body areas of KSM and MSA have their moderately high wind speeds influenced positively by the corona through the index F10.7 cm solar radio solar flux. NBI has its wind speed modified by the screening effect of the tall buildings, so the influence of the coronal index is not significant.

From Table 5.2, a pronounced negative correlation between F10.7 cm solar radio flux and SUD is notable in GRS as supported by the statistical significance at the 0.05 level (2-tailed). The other meteorological stations show correlations that are not significant. The unique variation of sunshine hours in GRS can therefore be attributed to the inverse influence of F10.7 cm solar radio flux and sunspot numbers as supported by the statistically significant negative correlation between each of the two solar parameters and SUD in GRS.

Positive correlation between F10.7 cm solar radio flux and SRA is evident in the meteorological stations except in GRS where an insignificant correlation is observed. Only two stations: NBI and KSM have the correlations that are statistically significant at the 0.01 and 0.05 levels (2-tailed) respectively. The central highland orography of NBI and its major city environment favor the statistically significant positive correlation

between F10.7 cm solar radio flux and SRA. On the other hand, KSM meteorological station at the shore of the lake, within the major city has comparatively high radiation values that are positively influenced by the coronal index F10.7 cm solar radio flux at the statistically significant level.

Only GRS meteorological station registers negative correlation between F10.7 cm solar radio flux and EVA that is statistically significant at the 0.05 level (2-tailed). The other stations show insignificant positive correlations between F10.7 cm solar radio flux and EVA. The steep decrease in evaporation after October through December with an increase from January and a maximum in March that is unique only to GRS meteorological station are attributable to the statistically significant inverse influence of F10.7 cm solar radio flux on EVA in GRS.

There is also a remarkable similarity in the trend of correlation between F10.7 cm solar radio flux and RNF to the correlation between sunspot numbers and RNF except at KER where F10.7 cm solar radio flux has negative correlation with RNF, but sunspot numbers has positive correlation with RNF. Just as is the case of sunspot numbers, none of the correlations between F10.7 cm solar radio flux and RNF is statistically significant.

Only KER meteorological station registers positive correlation between F10.7 cm solar radio flux and AVT that is statistically significant at the 0.05 level (2-tailed). The other stations show insignificant correlations between F10.7 cm solar radio flux and AVT. It is

evident here that the AVT values recorded in KER are to some extent due to the positive influence of the coronal index on AVT of KER.

5.2.3 Correlations between Mg II core-to-wing ratio and the climatic parameters

Table 5.2 3: Correlations between Mg II core-to-wing ratio and the climatic parameters

		Meteorological stations			
	KER	NBI	KSM	MSA	GRS
RH	-0.007	-0.045	0.041	-0.11*	-0.044
MAT	0.101	0.044	0.008	0.046	0.087
MIT	0.094	-0.049	-0.063	0.082	-0.04
WIS	-0.228**	-0.038	0.099	0.135*	-0.138*
SUD	-0.075	0.036	0.015	0.047	-0.103
SRA	0.1	0.162**	0.07	-0.042	-0.074
EVA	-0.015	-0.002	0.006	0.042	-0.07
RNF	0.008	0.026	-0.049	-0.062	0.022
AVT	0.138*	0.006	-0.021	0.065	0.034

** Correlation significant at the 0.01 level (2-tailed). * Correlation significant at the 0.05 level (2-tailed).

As seen on Table 5.2.3, there is a general negative correlation between Mg II core-to-wing ratio and RH, but this negative correlation is very strong in the coastal region of MSA as supported by the only significant correlation at the 0.05 level (2-tailed). The high levels of humidity that is characteristic of the coastal region is certainly inversely influenced at statistically significant levels by the chromospheric index Mg II core-to-wing ratio (hence the solar UV radiation) and the coronal index F10.7 cm solar radio flux; but not by the photospheric index sunspot numbers. Significance of influence of the coronal index is stronger at the 0.01 level (2-tailed) than the chromospheric index which is at the 0.05 level (2-tailed). The correlations between Mg II core-to-wing ratio and MAT, MIT, SUD and RNF are all statistically insignificant.

Mg II core-to-wing ratio has negative correlation with WIS in KER, NBI and GRS. Only the negative correlations in KER and GRS are significant at the 0.01 and 0.05 levels (2-tailed) respectively. This scenario is quite similar to the correlations between F10.7 cm solar radio flux and WIS in the two stations, except that the level of significance is higher between F10.7 cm solar radio flux in GRS than between Mg II core-to-wing ratio and WIS in GRS. Positive correlation between Mg II core-to-wing ratio and WIS is evident in KSM and MSA. While the positive correlation in MSA is significant at the level of 0.05 (2-tailed), that of KSM is not significant. KER area with the lowest wind speeds and GRS area with the highest wind speeds due to their prevailing respective earlier stated orography, have their wind speeds influenced inversely by the chromosphere and the corona through their respective indices, Mg II core-to-wing ratio and F10.7 cm solar radio flux. The photosphere through sunspot numbers has similar influence in the two stations except that the negative correlation between sunspot numbers and WIS in GRS is not significant. The large water body areas of KSM and MSA have their moderately high wind speeds influenced positively by the chromosphere through the index Mg II core-to-wing ratio. The positive influence is more pronounced in MSA as supported by the level of statistical significance. The larger water body of the Indian Ocean is in this case favoring the significant positive influence of the chromosphere on WIS.

Positive correlation between Mg II core-to-wing ratio and SRA is evident in NBI at the 0.01 level of significance (2-tailed). There are, however insignificant positive

correlations between Mg II core-to-wing ratio and SRA in KER and KSM. In MSA and GRS the insignificant negative correlations are observed. The central highland orography of NBI and its major city environment favor the statistically significant positive correlation between Mg II core-to-wing ratio and SRA.

Only KER meteorological station registers positive correlation between Mg II core-to-wing ratio and AVT that is statistically significant at the 0.05 level (2-tailed). The other stations show insignificant correlations between Mg II core-to-wing ratio and AVT. The influence is similar to that of F10.7 cm solar radio flux on AVT. It is therefore evident that the AVT values recorded in KER are to some extent due to the positive influence of the coronal and chromospheric indices on AVT of KER.

There is also a remarkable similarity in the trend of correlations between F10.7 cm solar radio flux and RNF to that between sunspot numbers and RNF; and also between Mg II core-to-wing ratio and RNF. Similarities in correlations between each of the three solar indices and RNF, and the fact that none of them is statistically significant testify to the fact that the correlation between any of the three solar indices and RNF can be positive, negative or even zero on short term observation in Kenya. Pederson, (2001) through Juan *et al.*, (2004) concluded the possibilities of positive, negative or even zero correlations between sunspot numbers and RNF based on long term (centennial) observations.

5.3 Power spectra and periodicities of Meteorological variables in relation to solar activities

Figures 5.2 – 5.6 show the results of power spectra (periodograms) of the various meteorological variables at all the stations as obtained from the spectral analysis stated in chapter 4. The prominent periodicities identified in the periodograms for various variables in each meteorological station are indicated in Table 5.3.

Figure 5.2: Power Spectra of Meteorological variables at Kericho

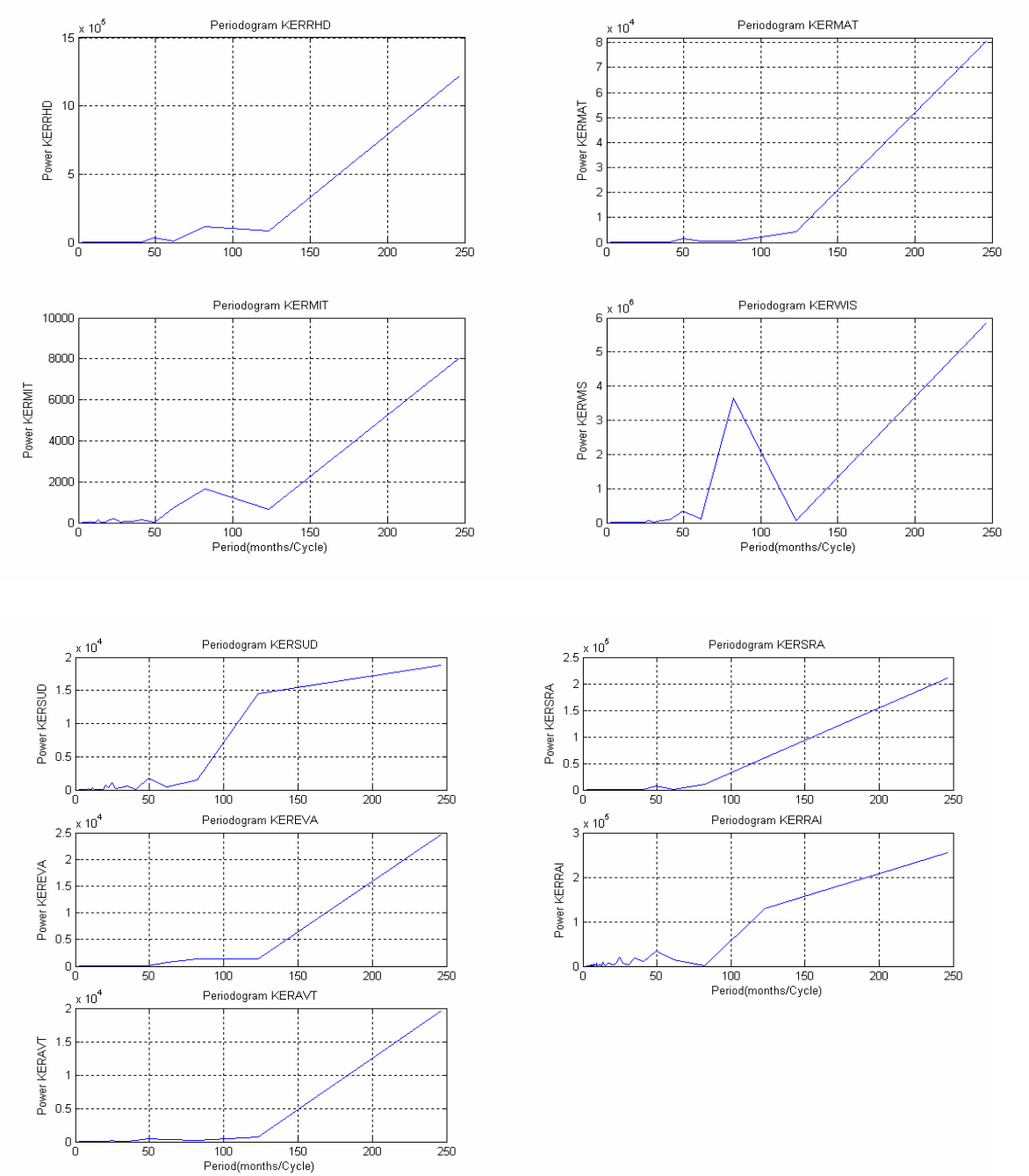

Figure 5.3: Power Spectra of Meteorological variables at Dagoretti Corner, Nairobi

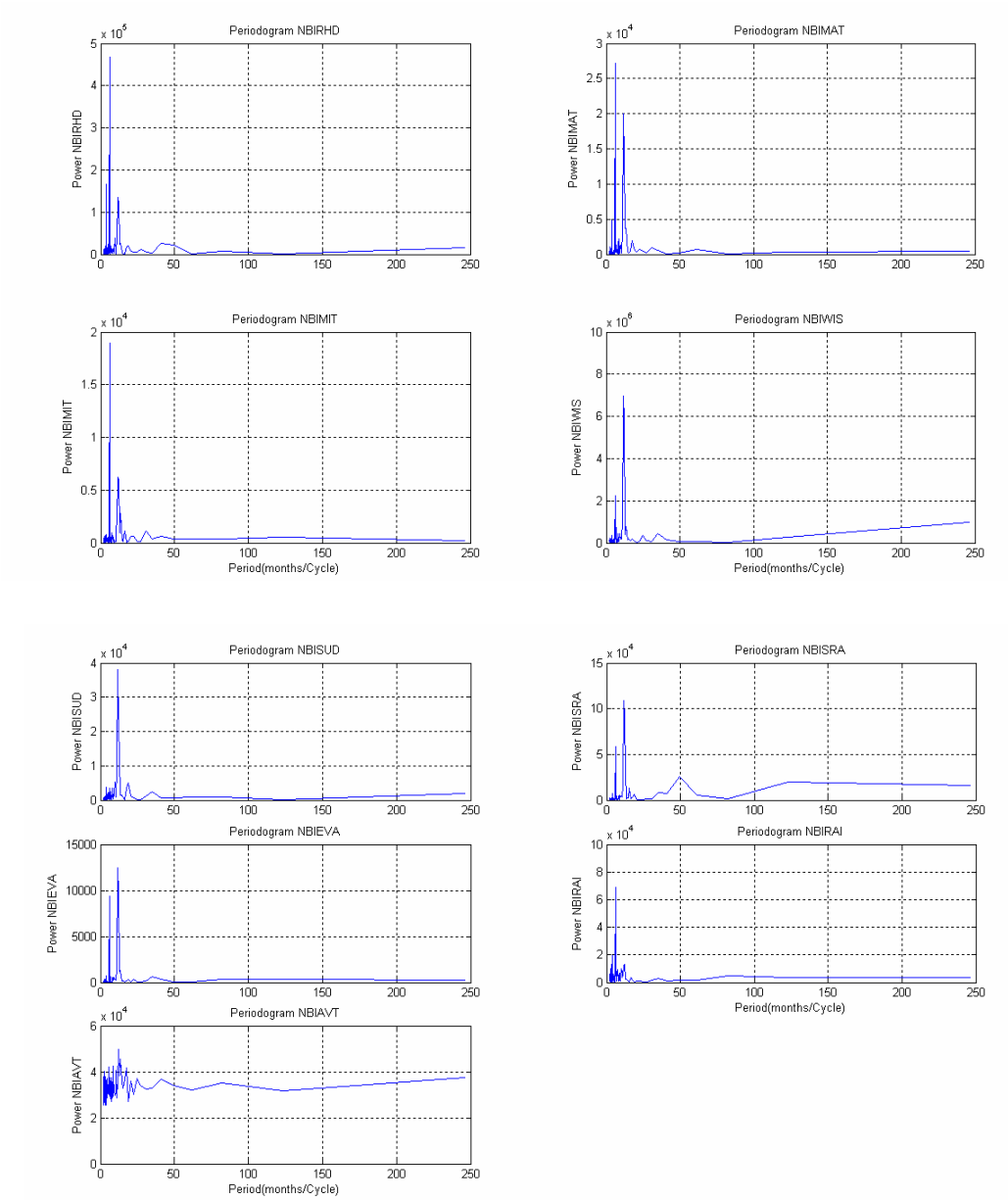

Figure 5.4: Power Spectra of Meteorological variables at Kisumu

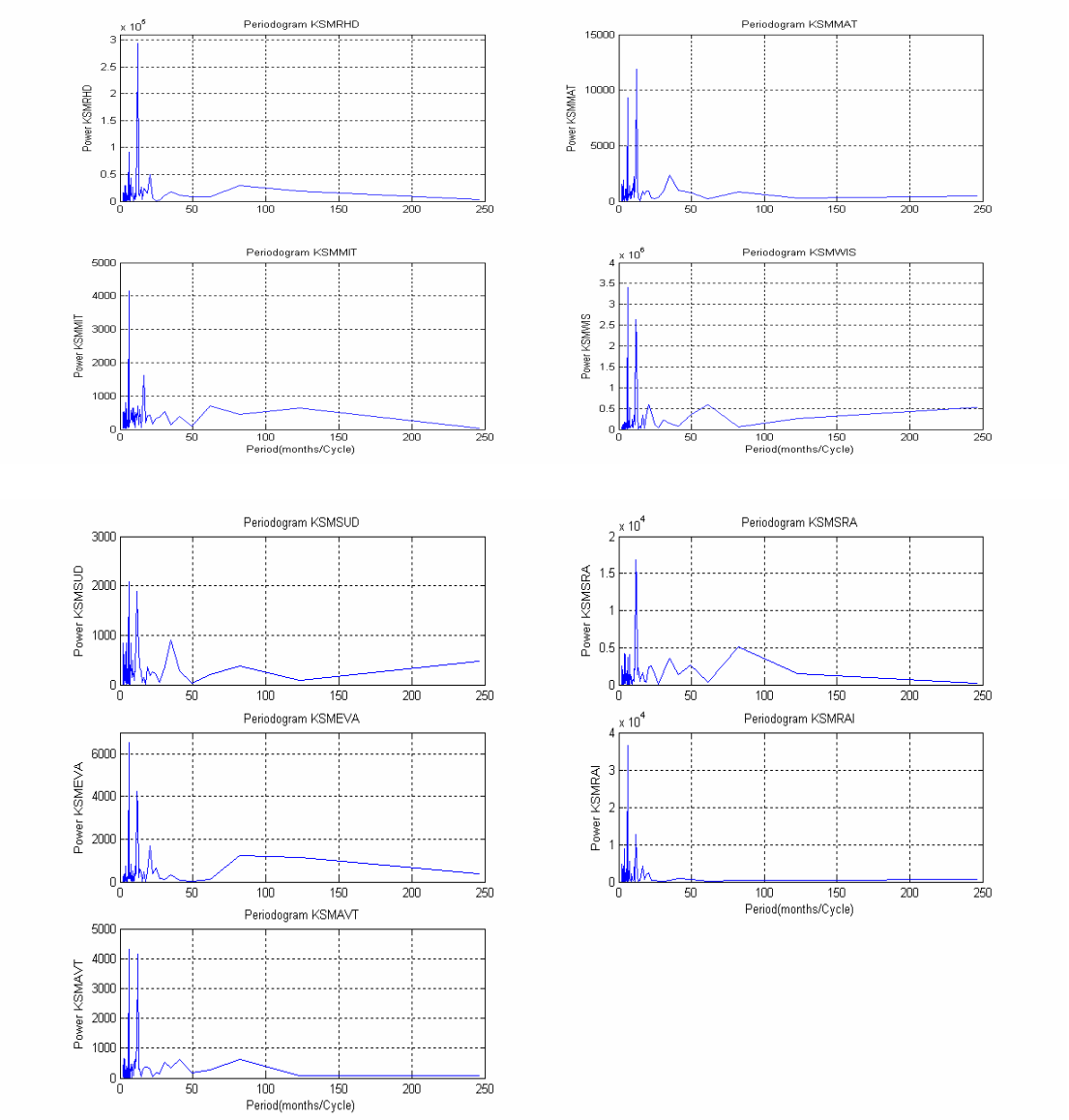

Figure 5.5: Power Spectra of Meteorological variables at Mombasa

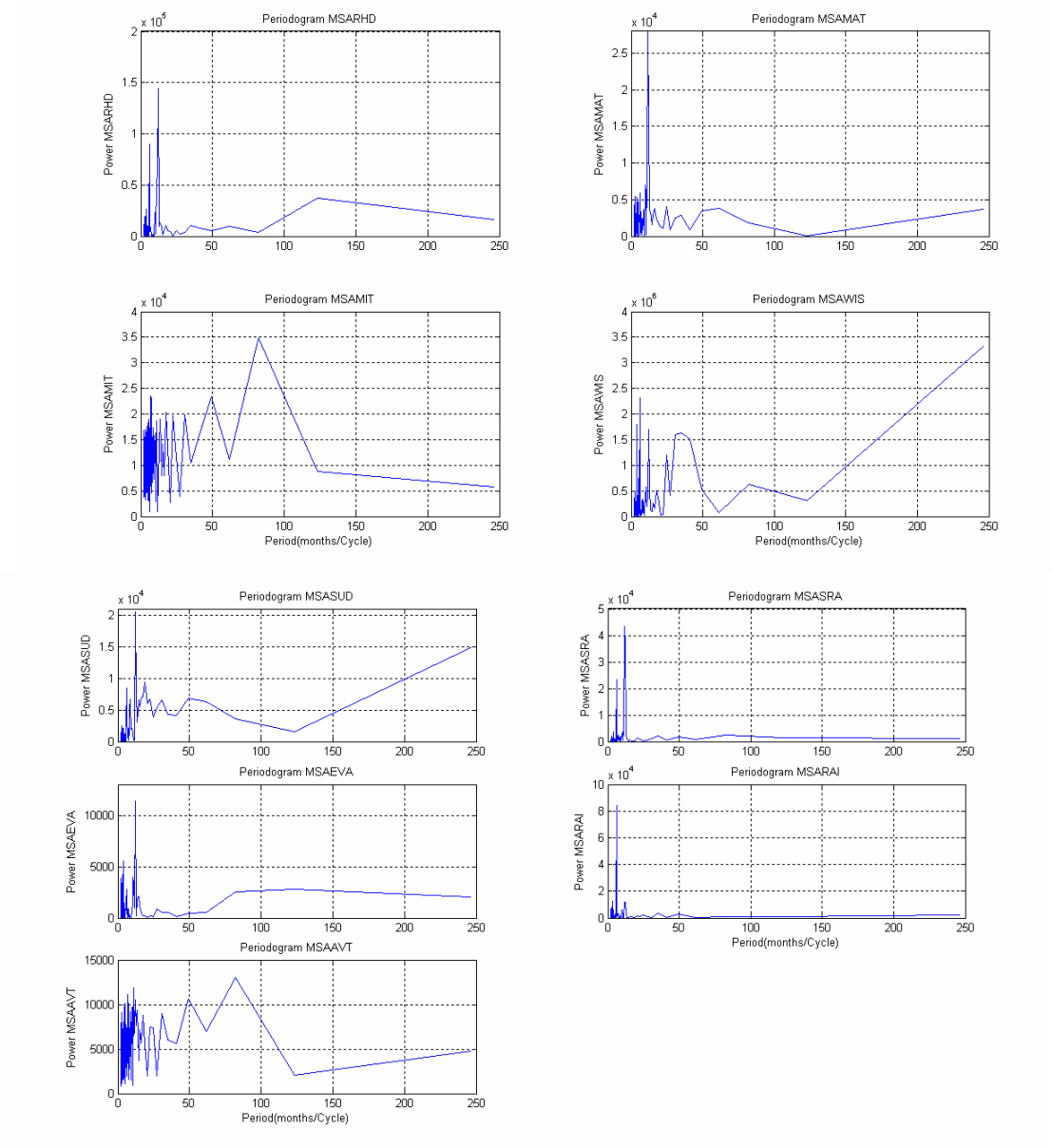

Figure 5.6: Power Spectra of Meteorological variables at Garissa

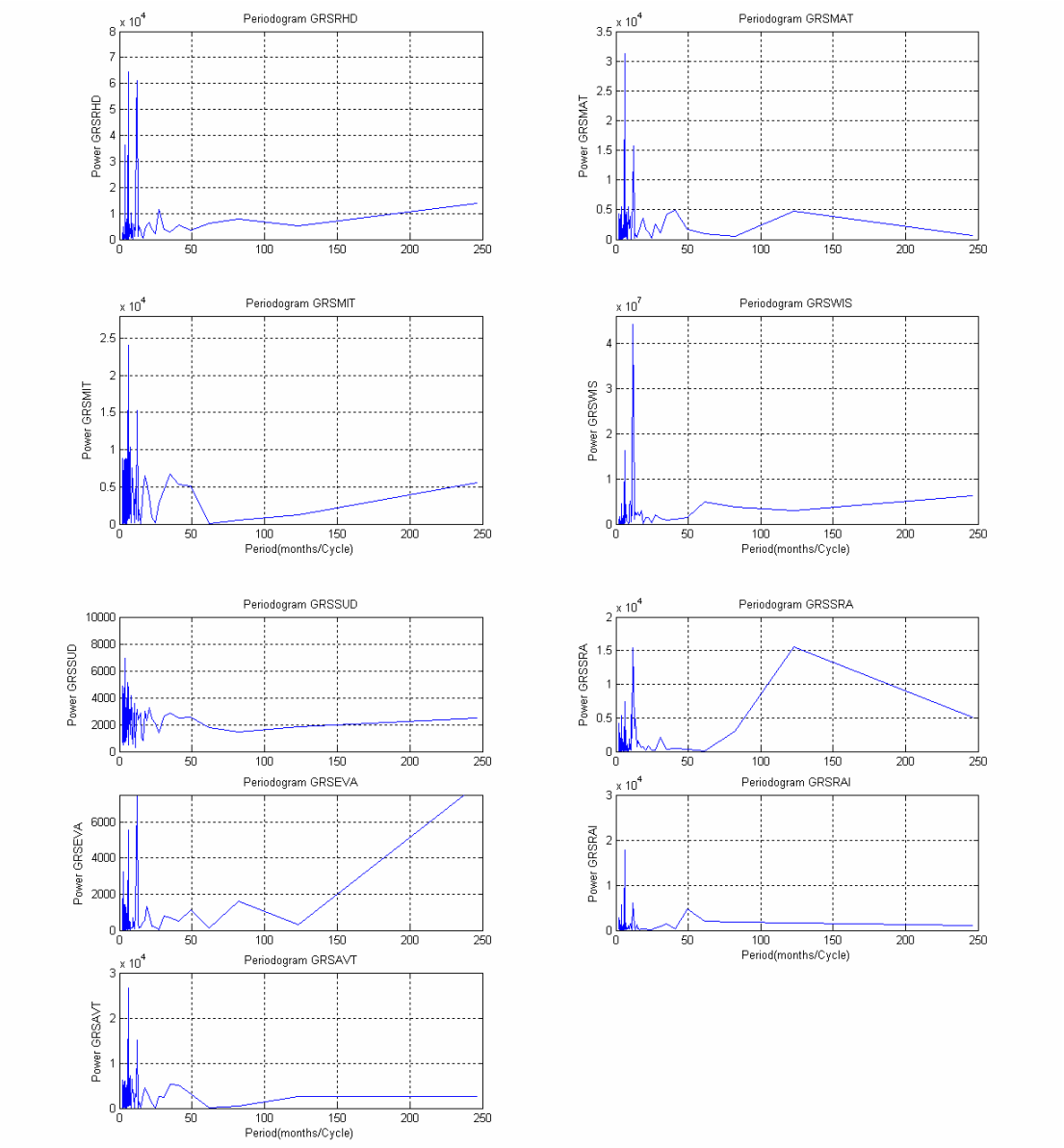

Table 5 3: Periodicities in months of different climatic parameters at different stations.

Climatic parameters	NBI	KER	KSM	MSA	GRS	MODE
RH	5, 12, 40.5	50, 86	3, 6, 12, 22 36, 85	3, 6, 12, 36, 62,125	3, 6, 12, 41, 82	3, 6, 12.
MAT	4, 6, 12.5	50	3, 6, 12, 36	3, 6,12, 16 35, 60	3, 6, 12, 18, 27.5, 40,122	3, 6, 12
MIT	5, 12.5	25, 86	3, 6, 12, 62 125	6,11, 12, 17, 22.5, 31, 50, 83	3, 6, 12,18, 36	6, 12
WIS	7.5, 12	50, 82	6, 12, 21, 31, 61	3, 6, 12, 35, 82.5	3, 6, 12, 22, 28, 62	3, 6, 12
SUD	12, 35	25, 50	1, 6, 12, 20, 25, 35, 85	3, 6, 7, 12, 32, 36, 50	3, 6, 7, 12, 21, 36	6, 12
SRA	6, 12, 50	50	3, 6, 12, 81	3, 6, 12, 50	3, 5, 6, 12, 32, 123	6, 12
EVA	6, 12		6, 12, 22, 35, 82.5	3, 6, 12, 80	3, 6, 12, 50, 82	6, 12.
RNF	3, 6, 12	25, 35, 50	3, 6, 17, 20, 40	3, 6, 12	3, 4, 6, 12, 50	3, 6, 12
AVT	3, 6, 7, 12 25	50	3, 6, 12, 82.5	3, 5, 6, 7, 12, 32, 50, 82.5	2, 3, 7, 37	3, 6, 12

Figures 5.2 – 5.6 show similarities in power spectra for the climatic parameters in the five stations with remarkable deviations in KER. The prominent periodicities in Table 5.4 show variability from one station to another. From the Table, model periodicities of 6 and 12 months/cycle are observed for all the climatic parameters at all the meteorological stations except Kericho. The modal 6 and 12 months/cycle for these parameters had been observed by Rabiu *et al*. (2007). However, a periodicity of 3 months / cycle is also quite prominent for RH, MAT, WIS, RNF and AVT at the stations apart from Kericho.

The prevailing climate in KER can account for their peculiar periods of 50 months and 82 months in some of the variables. The region is characterized by mountainous terrain that is rainy, with colder temperature throughout the year; Ogallo, (1989). The kind of climate in KER that is caused by the attendant orography can be the cause of the observed periods.

It is quite obvious that the meteorological variables consistently demonstrate modal periodicities of 6-month and 12-month values across the stations. The 6-month period is a demonstration of semiannual effect in the atmosphere, while the 12-month period is a manifestation of the annual effect. The semiannual changes in the atmosphere have been related to solar activity by Russell and McPherron, (1973) and Clua de Gonzalez *et al.,* (2001).

Rabiu, (2004) observed semiannual variation in the upper atmosphere and attributed this to the semiannual changes in the ionospheric heating and ionization; the IMF-effect in the solar wind-magnetosphere coupling; favored alignment of the magnetospheric boundary with respect to the solar wind interaction at equinoxes; and equinoctial/semiannual increase in solar wind speed. It is possible that the three separate and independent components, viz. a semiannual, an annual and a Sun-Earth-distance determined component, all of which can be accurately determined from solar-terrestrial geometry alone, discussed by Chaman-Lal (2000), can account for the observed modal periods.

Quasi-biennial periods of 25 months are also seen in Kericho meteorological station for: Minimum temperature, Sunshine duration and Rainfall. Georgieva, *et al*., (2000) have reported that Quasi-biennial oscillation of stratospheric winds (QBO) signals have been identified in a number of geophysical parameters, such as sea level pressure, ozone distribution, Earth's rotation, and that its existence has been shown in solar activity parameters as sunspot numbers, solar radio flux 10.7 cm, green coronal activity and solar neutrino flux.

The annual modal periodicity in the climatic parameters is also observed to some extent in the Sunspot number and F10.7 cm radio solar flux. This is an evidence of solar signature on terrestrial climate.

The 11 year solar cycle manifests as 125 months periodicity that appears in all the solar indices. The climatic parameters: MAT, SRA, all in GRS show similar periodicity. This is an indication that the semi arid region is prone to solar signature on these climatic parameters. RH in MSA also shows the same periodicity as the solar parameters. The coastal region of MSA registers the highest humidity levels of all the regions. Since RH depends on evaporation that in turn depends on radiation from the sun, it is therefore true that the unique humidity levels in MSA are due to the solar forcing in this region. We also have periodicity occurring in KSM for MIT that corresponds to the 11 year solar cycle.

5.4 Models and their validity

The equations (models) that relate the various climatic parameters to the solar indices are obtained from Tables 4.14 to 4.22. The models represented in equations 5.1 to 5.45 show the solar forcing of RH, MAT, MIT, WIS, SUD, SRA, EVA, RNF and AVT respectively. The RMSE values for the equations as seen on Tables 4.14 to 4.22 are approximately zero, and the MBE values are very low as recommended by Iqbal, (1993) and Halouani *et al*., (1993). This is an indication of good performance of the models and therefore validates them.

5.4.1 Relative Humidity (RH) and solar indices:

KER: $RH = -33.7938 - 0.1391R_s + 0.0628F10.7 + 382.59Mg\ II$ (5.1)

NBI: $RH = 18.3722 + 0.1385R_s - 0.1714F10.7 + 273.4407Mg\ II$ (5.2)

KSM: $RH = -50.4949 + 0.0894R_s - 0.1383F10.7 + 477.1217Mg\ II$ (5.3)

MSA: $RH = 58.5081 + 0.1140R_s - 0.1375F10.7 + 117.3244Mg\ II$ (5.4)

GRS: $RH = 167.7331 - 0.0454R_s + 0.0888F10.7 - 388.261Mg\ II$ (5.5)

The models presented in equations 5.1 to 5.5 show the solar forcing of the climatic parameter Relative humidity at all the stations. Models 5.2 to 5.4 for NBI, KSM and MSA indicate direct forcing of sunspot numbers and inverse forcing of F10.7 cm solar radio flux. In KER and GRS meteorological stations; equations 5.1 and 5.5 respectively, show that R_s has negative forcing of RH while F10.7 cm solar radio flux has positive forcing of RH. The uniqueness of KER is attributable to the orography of KER as has

been discussed on the basis of unique periodicities seen there. The lowland semi arid features of GRS favors the inverse forcing of RH observed.

Positive forcing of Mg II core-to-wing ratio on RH is evident in all the stations except GRS. GRS actually shows negative forcing of sunspot number and Mg II core-to-wing ratio on RH; But positive forcing of F10.7 cm solar radio flux on RH. This is attributable to the semi arid features characterizing that region. The high coefficient of Mg II core-to-wing ratio in the models is an indication that the forcing due to the chromosphere and hence the solar ultraviolet radiation is more prominent on RH compared to photosphere and corona. The kind of correlations that gave significance to the negative correlations in MSA on the basis of one solar parameter to RH at a time become different when all the solar parameters are together in the models.

5.4.2 Maximum Temperature (MAT) and solar indices:

KER: $MAT = 88.8943 + 0.0417R_s - 0.0061F10.7 – 251.6985Mg\ II$ (5.6)

NBI: $MAT = 57.8234 - 0.0545R_s + 0.0733F10.7 – 144.8584Mg\ II$ (5.7)

KSM: $MAT = 48.5030 - 0.0112R_s + 0.0198F10.7 - 75.5191Mg\ II$ (5.8)

MSA: $MAT = 6.1165 - 0.0495R_s + 0.0391F10.7 + 84.6753Mg\ II$ (5.9)

GRS: $MAT = 47.4955 - 0.0316R_s + 0.0447F10.7 – 60.0679Mg\ II$ (5.10)

The models presented in equations 5.6 to 5.10 show the solar forcing of the climatic parameter Maximum temperature at all the stations. All the models here indicate

reasonable positive constant. Models in equations 5.7 to 5.10 indicate negative forcing of sunspot number on maximum temperature. Model in equation 5.6 for KER indicates positive forcing of sunspot numbers on maximum temperature. Uniqueness of KER is seen in this case as was observed in relative humidity and periodicities.

All stations apart from KER indicate positive forcing of the coronal index F10.7 cm solar radio flux on maximum temperature. The uniqueness of KER in this case shows the consistency earlier observed.

The index of the chromosphere, Mg II core-to-wing ratio has negative forcing on maximum temperature in all the stations except in the case of MSA as demonstrated in equations 5.6 to 5.10. The unique case of MSA is attributed to the proximity of the Indian Ocean. The solar activities in the chromosphere, through Mg II core-to-wing ratio, hence solar ultraviolet radiation has positive forcing of the maximum temperatures recorded in the coastal region. High coefficients of Mg II core-to-wing ratio in all the models indicate its stronger influence than the other two solar indices.

5.4.3 Minimum Temperature (MIT) and solar indices:

KER: $MIT = 46.5722 + 0.0118R_s - 0.0003F10.7 - 139.1391Mg\ II$ (5.11)

NBI: $MIT = 11.7282 - 0.0232R_s + 0.0202F10.7 + 2.2811Mg\ II$ (5.12)

KSM: $MIT = 6.9808 - 0.0100R_s + 0.0031F10.7 + 39.07461Mg\ II$ (5.13)

MSA: $MIT = -53.8120 - 0.0057R_s - 0.0310F10.7 + 297.5030Mg\ II$ (5.14)

GRS: $MIT = 60.9028 - 0.0094R_s + 0.0305F10.7 - 149.5705Mg\ II$ (5.15)

The models presented in equations 5.11 to 5.15 show the solar forcing of the climatic parameter Minimum temperature at all the stations. The models in equations 5.12 to 5.15 indicate that the index of the photosphere, the sunspot numbers, has negative forcing of minimum temperature. In KER (equation 5.11) it has positive forcing. The same reason as stated for RH and MAT over KER applies here.

NBI, KSM and GRS stations indicate positive forcing of F10.7 cm solar radio flux on minimum temperature, while KER and MSA show inverse forcing. The coastal climate of MSA is the possible explanation to this deviation.

A high value of positive forcing of the index of the chromoshpere, Mg II is seen in equations 5.12 to 5.14 for NBI, KSM and MSA. The exact opposite is the case in KER and GRS. While the uniqueness of KER has been explained for the cases of RH and MAT, the GRS is attributable to the unique lowland semi arid climate there. One observation is quite clear that in all cases so far discussed, there are high coefficient values Mg II core-to-wing ratio as compared to the other solar parameters; hence it's dominant forcing.

5.4.4 Wind Speed (WIS) and solar indices:

KER: $WIS = -415.1341 + 0.1767R_s - 0.3321F10.7 + 2172.83781Mg\ II$ (5.16)

NBI: $WIS = 1267.7286 - 0.5733R_s + 1.0974F10.7 – 4600.6233Mg\ II$ (5.17)

KSM: $WIS = 335.8195 - 0.7290R_s + 0.8961F10.7 – 1019.3638Mg\ II$ (5.18)

MSA: $WIS = -435.5342 - 0.1853R_s + 0.0103F10.7 + 2206.1649Mg\ II$ (5.19)

GRS: $WIS = -3137.4157 + 1.0270R_s – 2.5723F10.7 + 13274.0143Mg\ II$ (5.20)

The models presented in equations 5.16 to 5.20 show the solar forcing of the climatic parameter Wind speed at all the stations. Models given by equations 5.17 to 5.19 for NBI, KSM and MSA stations indicate inverse forcing of the photospheric index, sunspot numbers on wind speed. In KER and GRS, however, positive forcing of sunspot numbers on wind speed is the case. The coefficients displayed here are quite high. This is an indication of high dependence of wind speed on sunspot numbers. Each of the three solar indices individually correlates with WIS negatively at very high statistical significance in KER as had been seen earlier, but the forcing changes to positive for sunspot numbers and Mg II core-to-wing ratio in the model (equation 5.16). F10.7 cm solar radio flux has negative forcing of WIS while sunspot numbers and Mg II core-to-wing ratio have positive forcing of WIS when the three parameters are all together in the model of equation 5.16. The uniqueness of the modal periodicities of 50 and 82 months are also observable in KER. KER area with the lowest wind speeds due to the prevailing mountainous terrain that act as barriers to the wind movement has its wind speed mainly

influenced inversely by F10.7 cm solar radio flux, and positively by sunspot numbers and Mg II core to wing ratio. The unique periodicities of the wind speed are also due to the solar activities that are evident in the forcing due to the solar indices.

Models in equations 5.17 to 5.19 for NBI, KSM and MSA show positive forcing of the coronal index, F10.7 cm solar radio flux on wind speed. Strong positive forcing of the coronal index, F10.7 cm solar radio flux on wind speed is evident in NBI and KSM from the high coefficients seen in equations 5.17 and 5.18. The fairly strong inverse forcing of F10.7 cm solar radio flux on wind speed observed in KER and GRS (equations 5.16 and 5.20) is attributable to the mountainous terrain in KER and the semi arid conditions in GRS area.

NBI and KSM indicate strong negative forcing of the chromospheric index Mg II core-to-wing ratio on wind speed as shown by the high negative coefficients in equations 5.17 and 5.18. Strong positive forcing of Mg II core-to-wing ratio is, however, seen in KER, MSA and GRS (equations 5.16, 5.19 and 5.20). The screening effects by the sky scrapers in the cities of Nairobi and Kisumu have effects on the wind speed leading to the negative forcing observed here. The other three stations are quite far from the city environments and as such are experiencing positive forcing of the chromospheric index on wind speed.

5.4.5 Sunshine Duration (SUD) and solar indices:

KER: $SUD = 40.6050 + 0.0234R_s - 0.0004F10.7 – 130.0465Mg\ II$ (5.21)

NBI: $SUD = 44.8362 - 0.0845R_s + 0.1063F10.7 – 168.3219Mg\ II$ (5.22)

KSM: $SUD = 12.4588 - 0.0179R_s + 0.0218F10.7 – 21.3620Mg\ II$ (5.23)

MSA: $SUD = -51.7240 - 0.0258R_s - 0.0003F10.7 + 229.2170Mg\ II$ (5.24)

GRS: $SUD = 11.4541 + 0.0281R_s – 0.0261F10.7 – 4.5036Mg\ II$ (5.25)

The models presented in equations 5.21 to 5.25 show the solar forcing of the climatic parameter Sunshine duration at all the stations. The three stations, NBI, KSM and MSA show inverse forcing of the photospheric index, sunspot numbers on sunshine duration as seen in the models of equations 5.22, 5.23 and 5.24 respectively. Positive forcing is, however, noted in KER and GRS as seen in models of equations 5.21 and 5.25. The kind of forcing patterns here is exactly opposite to the pattern seen for RH. Kericho's terrain with cloud cover that favors frequent rains here leads to the positive forcing; Garrisa's positive forcing can be linked to the semi arid condition which directly links the area to the sun.

The coronal index, F10.7 cm solar radio flux has positive forcing of sunshine duration in NBI, KSM and MSA as seen in models of equations 5.22, 5.23 and 5.24 respectively. Inverse forcing is however, seen in KER and GRS (equations 5.21 and 5.25). A similar explanation for the deviation in the two stations as in the last paragraph is applicable

here. Pattern of forcing of F10.7 cm solar radio flux on SUD is exactly opposite to forcing of F10.7 cm solar radio flux on RH.

Strong inverse forcing of the chromospheric index, Mg II core-to-wing ratio on SUD is evident in all the stations except MSA as seen in models of equations 5.21 to 5.25. MSA shows a positive forcing. So the sunshine duration in Indian Ocean environment is positively influenced by Mg II core-to-wing ratio index while sunshine duration in other places is influenced negatively by it. Forcing due to Mg II core-to-wing ratio is still stronger than those due to the other two indices.

5.4.6 Solar Radiation (SRA) and solar indices:

KER: $SRA = 91.1397 + 0.0617R_s - 0.0100F10.7 – 270.0257Mg\ II$ (5.26)

NBI: $SRA = -14.9340 - 0.1005R_s + 0.1048F10.7 + 104.1790Mg\ II$ (5.27)

KSM: $SRA = 56.8440 - 0.0385R_s + 0.0560F10.7 – 137.6061Mg\ II$ (5.28)

MSA: $SRA = 109.7347 - 0.0464R_s + 0.0898F10.7 – 358.3198Mg\ II$ (5.29)

GRS: $SRA = 32.4426 - 0.0327R_s + 0.0263F10.7 – 42.0080Mg\ II$ (5.30)

The models presented in equations 5.26 to 5.30 show the solar forcing of the climatic parameter solar radiation at all the stations. Inverse forcing of the photospheric index, sunspot numbers on solar radiation measured on the earth is evident in all the meteorological stations except KER as seen in the models. Uniqueness of KER station is consistent in all the parameters discussed so far and also in the observed prominent

periodicities discussed earlier. So the positive forcing in KER can be explained on the basis of the mountainous terrain that is responsible for cloud cover that absorbs the incoming solar radiation. The high coefficient values still point to the assertion that when the three solar parameters are together, Mg II core to wing ratio has dominant forcing of SRA compared to the other two.

Positive forcing of the coronal index, F10.7 cm solar radio flux on solar radiation measured on the earth is evident in all the meteorological stations except KER as seen in the models of equations 5.26 to 5.30. Uniqueness of KER station is consistent in all the parameters discussed so far and also in the observed prominent periodicities discussed earlier. So the negative forcing in KER noticed here can be explained as previously done.

The chromospheric index, Mg II core-to-wing ratio, however, shows negative forcing of solar radiation for all the meteorological stations except NBI as seen in the models of equations 5.26 to 5.30. The positive forcing seen in NBI is quite unique and can be attributed to the thick cloud cover often observed above NBI area.

5.4.7 Evaporation (EVA) and solar indices:

KER: $EVA = 41.0370 + 0.0261R_s - 0.0048F10.7 – 139.6113Mg\ II$ (5.31)

NBI: $EVA = 37.5828 - 0.0327R_s + 0.0048F10.7 – 136.2027Mg\ II$ (5.32)

KSM: $EVA = 16.2239 - 0.0198R_s + 0.0240F10.7 – 43.5316Mg\ II$ (5.33)

MSA: $EVA = -23.4720 - 0.0097R_s + 0.0009F10.7 + 107.2436Mg\ II$ (5.34)

GRS: $EVA = -35.6684 + 0.0068R_s - 0.0285F10.7 + 169.5269Mg\ II$ (5.35)

The models presented in equations 5.31 to 5.35 show the solar forcing of the climatic parameter Evaporation at all the stations. Inverse forcing of sunspot numbers on evaporation is evident in NBI, KSM and MSA while positive forcing is seen in KER and GRS (models of equations 5.31 to 5.35). The mountainous terrain of KER and the lowland semi arid features of GRS make the two areas susceptible to photospheric positive forcing of EVA through the index sunspot numbers.

Positive forcing of F10.7 cm solar radio flux on evaporation is evident in NBI, KSM and MSA while inverse forcing is seen in KER and GRS (models of equations 5.31 to 5.35). Physical features of KER and GRS stated in the last paragraph make them susceptible to coronal inverse forcing of EVA through the index F10.7 cm solar radio flux.

Significant inverse forcing of the chromospheric index, Mg II core-to-wing ratio on evaporation is evident in KER, NBI and KSM while significant positive forcing is evident in MSA and GRS as seen in models of equations 5.31 to 5.35. Chromosphere through Mg II core-to-wing ratio index, hence solar ultraviolet radiation interacts with the lowland semi arid region of GRS and the Oceanic environment of MSA in such a way that it has negative forcing of EVA. The high coefficients of this index indicate its dominant forcing compared to the other two solar indices.

5.4.8 Rainfall (RNF) and solar indices:

KER: $RNF = 8.0958 - 0.0323R_s - 0.0126F10.7 + 2.2351Mg\ II$ (5.36)

NBI: $RNF = 22.9796 - 0.0053R_s + 0.0079F10.7 – 75.7304Mg\ II$ (5.37)

KSM: $RNF = -1.8352 - 0.0147R_s + 0.0094F10.7 + 19.9973Mg\ II$ (5.38)

MSA: $RNF = 0.5408 + 0.0244R_s - 0.0307F10.7 + 16.6751Mg\ II$ (5.39)

GRS: $EVA = 22.0315 - 0.0057R_s + 0.0158F10.7 – 82.9950Mg\ II$ (5.40)

The models presented in equations 5.36 to 5.40 show the solar forcing of the climatic parameter Rainfall at all the stations. Inverse forcing of the photospheric index, sunspot numbers on rainfall is evident in all the stations except MSA as seen in the models of equations 5.36 to 5.40. MSA shows positive forcing that can only be explained in terms of the solar driven effects on rainfall patterns in the coastal region.

Referring to the same models we see inverse forcing of the coronal index, F10.7 cm solar radio flux on rainfall in the two stations: KER and MSA. But positive forcing is seen in NBI, KSM and GRS. The negative forcing in the two meteorological stations can be attributed to their geographical locations and the attendant climatic conditions.

The index of the chromosphere, Mg II core-to-wing ratio shows negative forcing on rainfall in NBI and GRS while it has positive forcing on rainfall in KER, KSM and MSA.

5.4.9 Average Temperature (AVT) and solar indices:

KER: $AVT = 67.7332 + 0.0267R_s - 0.0032F10.7 – 195.4188Mg\ II$ (5.41)

NBI: $AVT = -105.7111 - 0.0942R_s + 0.0239F10.7 + 472.5642Mg\ II$ (5.42)

KSM: $AVT = 27.7419 - 0.0106R_s + 0.0115F10.7 – 18.222Mg\ II$ (5.43)

MSA: $AVT = -23.8478 - 0.0276R_s + 0.0040F10.7 + 191.0892Mg\ II$ (5.44)

GRS: $AVT = 54.1991 - 0.0205R_s + 0.0376F10.7 – 104.8192Mg\ II$ (5.45)

The models presented in equations 5.41 to 5.45 show the solar forcing of the climatic parameter Average temperature at all the stations. Inverse forcing of sunspot numbers on average temperature is evident in all the meteorological stations except KER as seen in models of equations 5.41 to 5.45. KER shows positive forcing. The same reasons as earlier stated for other parameters can explain the unique case of KER.

Positive forcing of F10.7 cm solar radio flux on average temperature is evident in all the meteorological stations except KER. KER shows inverse forcing. The same reasons as earlier stated for other parameters can explain the unique case of KER.

Inverse forcing of Mg II core-to-wing ratio on average temperature is evident in KER, KSM and GRS but positive forcing in NBI and MSA. The positive forcing in the two major cities can be explained in terms of modifications by the Urban Heat Island effect.

Table 5.4 below gives a summary of all forcing signs (positive or negative) of the three solar indices: sunspot numbers, F10.7 cm solar radio flux and Mg II core-to-wing ratio on the climatic parameters discussed in this work. The summaries are obtained from the models in equations 5.1 to 5.45.

Table 5 4: Summary of signs of forcing of solar indices on the various climatic parameters in various stations

	Sunspot numbers R_s	F10.7 cm solar radio flux	Mg II core-to-wing ratio
RH	+ve: NBI, KSM, MSA -ve: KER, GRS	+ve: KER, GRS -ve: NBI,KSM,MSA	+ve: KER,NBI, KSM,MSA -ve: GRS
MAT	+ve: KER -ve: NBI,KSM,MSA,GRS	+ve: NBI,KSM,MSA,GRS -ve: KER	+ve: MSA -ve: KER,NBI,KSM,GRS
MIT	+ve: KER -ve: NBI,KSM,MSA,GRS	+ve: NBI,KSM, GRS -ve: KER, MSA	+ve: NBI, KSM, MSA -ve: KER, GRS
WIS	+ve: KER, GRS -ve: NBI, KSM, MSA	+ve: NBI,KSM,MSA -ve: KER, GRS	+ve: KER, MSA, GRS -ve: NBI, KSM
SUD	+ve: KER, GRS -ve: NBI, KSM, MSA	+ve: NBI, KSM -ve: KER, MSA, GRS	+ve: MSA -ve: KER,NBI,KSM,GRS
SRA	+ve: KER -ve: NBI,KSM,MSA,GRS	+ve: NBI,KSM,MSA,GRS -ve: KER	+ve: NBI -ve: KER,KSM,MSA,GRS
EVA	+ve: KER, GRS -ve: NBI, KSM, MSA	+ve: NBI, KSM, MSA -ve: KER, GRS	+ve: MSA, GRS -ve: KER, NBI, KSM
RNF	+ve: MSA -ve: KER,NBI,KSM,GRS	+ve: NBI, KSM, GRS -ve: KER, MSA	+ve: KER, KSM, MSA -ve: NBI, GRS
AVT	+ve: KER -ve: NBI,KSM,MSA,GRS	+ve: NBI,KSM,MSA,GRS -ve: KER	+ve: NBI, MSA -ve: KER, KSM, GRS

5.4.10 Correlations between the predicted and observed values of the climatic parameters

When the models were subjected to test by using the monthly solar indices data from January 2006 to October 2007 (20 months data), the correlation coefficients between the observed and predicted climatic parameters that were obtained per meteorological station are given in Appendix 1. In Appendix 2, we have the correlations between the observed and predicted values when data from all the stations are pooled, not station wise. This is for longer data of 100 months for all the five stations, each having the 20 month climatic parameters data.

From appendix 1, the positive correlations between the observed and predicted RH are quite strong in KER (r = 0.67) and KSM (r = 0.52) at the 0.01 and 0.05 levels of significance respectively. No other station has significant correlation, although MSA gives a fair correlation at r = 0.5). This is an indication that the RH model can best be used in the western highland rift valley of KER and close to the large water bodies in KSM and MSA.

Only the negative correlation between observed and predicted MAT in KER (r = -0.68) is statistically significant at the 0.05 level (2-tailed). Though not significant, some substantial positive correlation between observed and predicted MAT are in NBI (r = 0.52) and MSA (r = 0.58). Other stations show low and statistically insignificant correlations between observed and predicted MAT. This shows that the MAT model is

best applied in the low temperature area of the western highlands of rift valley, and the coastal and central highland areas to a limited extent.

The correlations between the observed and predicted values of MIT, WIS, SUD, RNF and AVT are not significant, however, there is some statistically insignificant, but substantial positive correlation between observed and predicted WIS in KSM and MSA ($r = 0.6$). The WIS models can therefore be applied in the areas of large water bodies only.

The observed and predicted values of SRA correlate in NBI ($r = -0.6$) and KER ($r = 0.45$) significantly at the 0.01 and 0.05 levels (2-tailed) respectively. No correlations are shown for the other stations due to lack of observed meteorological date for comparison. It is notable that the SRA model predicted values show negative correlations with the observed values in the central highland areas of NBI at very good significance level; but a negative correlation in the western highland area of KER. The models can be used in the two highland areas.

The observed and predicted values of EVA correlate negatively in MSA ($r = -0.44$) at the 0.05 significant level (2-tailed). Other stations give insignificant correlations between the observed and predicted values. So the model can be applied to some extent in the coastal region to predict evaporation values.

From Appendix 2, we see that when we have long time data, the predicted values for all parameters, except RNF are statistically significant at the 0.01 level (2-tailed). The model works best for temperature (MAX, MIN, and AVT) with the correlation coefficient of 0.9. This is followed by EVA (r = 0.66), RH (r = 0.64) then WIS (r = 0.55). The model can be used to predict values of SRA when we have longer data period, but not as well as the other climatic parameters. It shows negative correlation between the observed and predicted SRA values. RNF cannot be predicted with the models. The correlation between climatic variables and the solar indices using statistical tools depended on the degree of confidence. We used 95% of confidence to validate the models; this does not mean that there are insignificant correlations between the solar indices and climatic variables in the stations.

5.5 Periodicities of drought occurrence and solar periodicities

The spectral characteristics of drought occurrences at all the meteorological stations and the spectral characteristics of sunspot number as obtained from the fast Fourier transform are shown in Figure 5.7. The prominent peak periodicities identified in the spectral characteristics of the meteorological variables are tabulated in Table 5.5.

Figure 5.7: Spectral characteristics of drought at the five stations; and spectral characteristics of sunspot numbers.

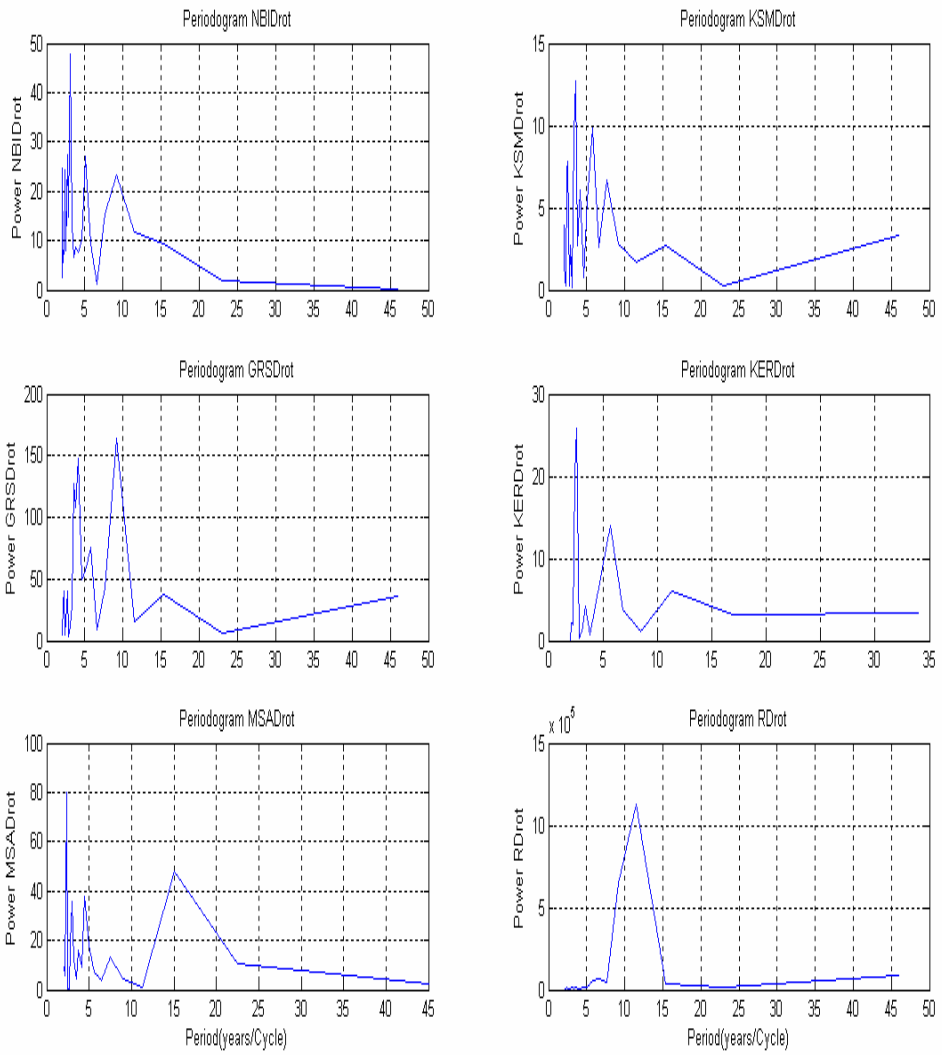

Table 5 5: Prominent peaks in periodicities of drought indices

Station	Period (years)
KER	2.6, 6, 11
NBI	3, 5, 9
KSM	3.5, 6, 8
MSA	2.4, 4, 7.5, 15
GRS	4, 9.2

From Table 5.5, an average of the most frequently occurring drought period is about 3.5 years as observed across the stations. Short periodicities of 3.5 - and 5.6 years have been reported by Rao, (1973) for solar activities. The short periodicities in the drought occurrence that are obtained in this work when the short time data are used are therefore in correspondence with the short periodicities in solar activities that have been reported by Rao, (1973). We also observe prominent periodicities of 9 to 11 years in drought occurrences that relate to the 11 year solar cycle periodicity shown by the sunspot numbers.

5.6 Discussion of results of models from stepwise regression analysis of the lagged solar indices on climatic variables

Results of multiple regressions using the stepwise method in SPSS for the lagged solar indices on the climatic variables are shown on Table 5.6. The lag period is up to 3 months backwards. Hence the number 1 in parenthesis for the solar parameter implies the last one month. The number 2 in the parenthesis means the previous two months lag. The number 3 in the parenthesis indicates the previous three month value.

Table 5 6: Results of stepwise regression of lagged solar indices on climatic parameters

Relative Humidity (RH)

Station	Standardized model	
Mombasa (MSA)	$RH = 1.429R_s\ (1) – 2.142F10.7\ (1)$	(5.46)

Maximum Temperature (MAT)

Station	Standardized model	
Nairobi (NBI)	$MAT = -1.236R_s\ (1) + 1.231F10.7\ (1)$	(5.47)
Kericho (KER)	$MAT = -0.986R_s + 0.924F10.7$	(5.48)
Garissa (GRS)	$MAT = -1.576R_s\ (2) + 1.689F10.7\ (2)$	(5.49)

Minimum Temperature (MIT)

Station	Standardized model	
Nairobi (NBI)	$MIT = -1.255R_s\ (1) + 1.137F10.7\ (1)$	(5.50)
Kisumu (KSM)	$MIT = -0.673R_s + 0.575Mg\ II$	(5.51)
Garissa (GRS)	$MIT = -1.033R_s + 0.923F10.7$	(5.52)

Wind Speed (WIS)

Station	Standardized model	
Kericho (KER)	$WIS = -0.298R_s$	(5.53)
Kisumu (KSM)	$WIS = -1.358R_s\ (1) + 1.515F10.7\ (1)$	(5.54)
Mombasa (MSA)	$WIS = -0.504R_s\ (1) + 0.613Mg\ II\ (1)$	(5.55)
Garissa (GRS)	$WIS = 1.063R_s - 1.530F10.7 + 0.325Mg\ II\ (3)$	(5.56)

Sunshine Duration (SUD)

Station	Standardized model	
Kericho (KER)	$SUD = -0.612R_s\ (1) + 0.507Mg\ II\ (2)$	(5.57)
Garissa (GRS)	$SUD = -0.645R_s\ (1) + 0.503\ Mg\ II\ (1)$	(5.58)

Solar Radiation (SRA)

Station	Standardized model	
Nairobi (NBI)	$SRA = -1.326R_s\ (1) + 1.349F10.7\ (1)$	(5.59)
Kericho (KER)	$SRA = -0.347R_s + 1.059Mg\ II – 0.688\ R_s\ (1)$	(5.60)
Kisumu (KSM)	$SRA = -1.228R_s + 1.941F10.7 – 0.558Mg\ II\ (3)$	(5.61)
Garissa (GRS)	$SRA = 1.190\ F10.7\ (2) - 1.367Mg\ II\ (3)$	(5.62)

Average Temperature (AVT)

Station	Standardized model	
Kericho (KER)	$AVT = -1.071R_s\ (2) + 0.796F10.7\ (2)$	(5.63)

5.6.1 Relative Humidity and the lagged solar indices

The model in equation 5.46 is unique to MSA meteorological station. Being at the Eastern Coast, MSA has the lowest altitude of the five stations, and it experiences high average temperatures throughout the year, with generally higher Relative humidity records. These features of MSA apparently make it have the relationship between RH and the solar parameters. It can be inferred that for MSA, relative humidity varies directly with the first lagged values of Sunspot number, and inversely with the first lagged values of F10.7 cm solar radio flux. That is, the previous month values of R_s and F10.7 cm solar radio flux determine the current month value of relative humidity in Mombasa area.

5.6.2 Maximum temperature and the lagged solar indices

For the three meteorological stations with the models (equations 5.47 to 5.49) here, the Sunspot number, R_s and MAT correlate inversely, while F10.7 cm solar radio flux and MAT correlate directly. However, the models show the following disparities: For NBI, the previous values of Sunspot numbers R_s and F10.7 cm solar radio flux determine the current month value of MAT. For KER, the non lagged values of the solar parameters cause variations of MAT. It is to say that the current values of the two solar parameters determine the current values of Maximum temperature. As per the GRS model the average January values of Sunspot numbers and F10.7 cm solar radio flux will determine the average March value of Maximum temperature for the same year. Higher

values of F10.7 cm solar radio flux lead to higher maximum temperatures. Lack of models in KSM and MSA can be attributed to the fact that the two stations are located at the shores of large water bodies. The convection currents due to these water masses directly affect the maximum temperature patterns; hence neutralize effects of the solar parameters on the maximum temperatures recorded by the ground instruments.

The fact that some solar parameters show significant correlations with the climatic parameters independently but are not predictors of the same climatic parameters when more predictors are used is possible in statistical analysis. In presence of preferred predictors, the less preferred ones are naturally left out in the competitive selection.

5.6.3 Minimum temperature and the lagged solar indices

From the models (equations 5.50 to 5.52), generally minimum temperature varies inversely with sunspot numbers, R_s and it varies directly with F10.7 cm solar radio flux. For NBI, the current month values of minimum temperature are determined by the previous month values of sunspot numbers, R_s and F10.7 cm solar radio flux. For KSM, the direct values of R_s and Mg II core-to-wing ratio determine the values of minimum temperature. Since Mg II core-to-wing ratio is highly correlated with F10.7 cm solar radio flux, it may be necessary to use the later instead. For GRS, a scenario similar to the one of NBI is indicated, but with non lagged values of the solar parameters for GRS.

KER and MSA meteorological stations do not show models of minimum temperature with the solar parameters. KER has the highest altitude of the five meteorological stations, and it is in hilly irregular and forest landscape with constant rains most of the year. It is therefore possible that the minimum temperatures are more due to these climatic and geographical features than the solar parameters. The MSA case can be argued in the line of argument adopted for maximum temperature and the solar parameters. However, one may cite a contradiction for KSM case when this line of argument is adopted. But it is noteworthy that the water mass in KSM is much less than that of MSA and the advections in KSM are quite different from those of MSA. From the results of models in equations 4.12 to 4.14, it can be inferred that, in general higher sunspot numbers lead to lower minimum temperatures. The current values of F10.7 cm solar radio flux will lead to higher values of minimum temperature.

5.6.4 Wind speed and the lagged solar indices

From models in equations 5.53 to 5.56, an increase in sunspot numbers decreases wind speed, and an increase in F10.7 cm solar radio flux increases wind speed. For KER, the current month values of sunspot numbers decrease the current month values of wind speed. For KSM, the previous month values of sunspot numbers and F10.7 cm solar radio flux determine the current month values of wind speed. The MSA model resembles that of KER except for the previous month values of Mg II core-to-wing ratio appears instead of the previous month values of F10.7 cm solar radio flux. But due to the

high positive correlation between the two solar indices we can use the later instead of the former.

The model (equation 5.56) for GRS is unique. GRS is located within the lowland semi arid areas of the country. The wind patterns recorded in this region are much higher in this area. There is a lot of heating over the Chalbi desert, coupled with the fact that the East African low jet is due to temperature differentials, the sun has a definite effect on these winds. Therefore, the inverse effect of the solar activities on wind speed noticed here can be attributed to the interactions of the solar activities and the semi arid effects.

NBI meteorological station is situated within the city of Nairobi, and surrounded by tall buildings. The screening effects of the tall buildings and the tall trees in this area can bring about the low values of the wind speed recorded and used in this research. It is therefore possible that the artificial screening overshadows the effects of the solar activities on wind speed in this area. Hence no model is recorded by the statistical indicators.

5.6.5 Sunshine duration and the lagged solar indices

For KER and GRS meteorological stations, sunshine duration varies linearly but negatively with the first lagged values of sunspot numbers, it also varies linearly but directly with the Mg II core-to-wing ratio. However, for KER station the variation is with lag 2 (model in equation 5.57), while it is with lag 1 (model in equation 5.58) for

GRS. On examination, Mg II (1) and Mg II (2) correlate very strongly for both the stations and we can therefore adopt Mg II (1) instead of Mg II (2) for this model. Failure to get statistically acceptable models in the remaining three stations (NBI, KSM and MSA) makes it inconclusive as to forcing of Mg II core-to-wing ratio and sunspot numbers on sunshine duration when stepwise regression analysis is applied. It is notable though that the three stations are in major cities; which can be a factor in failure to have the models.

5.6.6 Solar radiation and the lagged solar indices

From the above models (equations 5.59 to 5.62) it can be seen that sunspot numbers vary inversely with solar radiation, and F10.7 cm solar radio flux varies directly with solar radiation. There is something quite important to note between equation 5.46 on one hand and equations 5.59 to 5.61 on the other hand. The solar parameters correlate with RH in an inverse manner in the model of equation 5.46 as compared to the variation in models of equations 5.59 - 5.61. That is, there is positive correlation between RH and R_s (equation 5.46), while there is negative correlation between SRA and R_s (equations 5.59-5.61). Also, there is negative correlation between RH and F10.7 cm solar radio flux (equation 5.46) and a positive correlation between SRA and F10.7 cm solar radio flux (equations 5.59-5.61). This important result is confirmed by the results of interrelationship between Relative humidity and Solar radiation for Kenya reported by Ndeda *et al.,* (2006). This confirmed a negative correlation between RH and SRA. Inclusion of Mg II core-to-wing ratio in the models (equations 5.60 to 5.62) of SRA can

be explained on the basis of its high positive correlation with the other solar indices and their lagged values. So Mg II core-to-wing ratio can be replaced with F10.7 cm solar radio flux or sunspot numbers where necessary.

Evaporation (EVA) and Rainfall (RNF) do not show models in any of the stations. They do not show significant correlation with any of the solar parameters and/or their lagged values. The two parameters have models when the Fast Fourier method is used, but not when stepwise regression analysis is done. EVA models given by Fast Fourier method with good predictions, reveals that the method is more applicable in determining the solar forcing of climate than the stepwise regression method. The models of rainfall obtained by Fast Fourier method do not give good predictions, so it is confirmed that there is no direct connection between the solar indices and rainfall. If there is any relationship between rainfall and solar indices, then it is not linear.

5.6.7 Average temperature and the lagged solar indices

The only model (equation 5.63) is for KER meteorological station. It gives inverse variation of the second lagged values of sunspot numbers with average temperature, and positive variation of the second lagged values of F10.7 cm solar radio flux with average temperature. Going by model result of KER meteorological station, the previous two months values of sunspot numbers will inversely vary the current month values of average temperature. And the previous two months values of F10.7 cm solar radio flux will directly vary the current values of average temperature.

When these models were subjected to post data testing using monthly solar indices data from January 2006 to October 2007 so as to generate the predicted values, the resulting time plots for the observed and the predicted values had no observable relationships. That is to say that the observed and predicted values did not give any correspondence in all the cases. But periodicities in climatic parameters are found to correspond to the periodicities in solar activities as earlier explained. This is a clear indication that analyses of periodicities in climatic parameters and solar variability reveal more inherent connections between solar variability and climatic parameters. Also, employment of fast Fourier method gives the better models, with better predicted values than when the stepwise regression method is used.

CHAPTER 6

CONCLUSIONS AND RECOMMENDATIONS

6.0 Introduction

This chapter states the conclusions drawn from the results; while also providing the recommendations to researchers for possible future work, and to relevant government institutions for implementation. Conclusions drawn from the various methods adopted in the research are in section 6.1. Finally, the recommendations are in section 6.2.

6.1 Conclusions

6.1.1 Conclusions drawn from the Mean Monthly and seasonal variations of the Meteorological parameters

1. High values of Relative humidity are experienced during the long rains and dry cold periods in Kenya except for the semi arid regions where the patterns are different. The coastal regions bordering the Indian Ocean show the highest values of RH.

2. Temperatures are related to rainfall in the country except in the semi arid regions, where there is no relation between temperature and rainfall. Maximum temperatures are notable from the onset of the long rains; but maximum temperature values correlate with rainfall values negatively, while minimum temperature correlates with rainfall positively.

3. High wind speed values are prevalent during the onset of the long rains in the country except in the semi arid regions. Very low wind speeds are obtained during the cold periods, but higher trends during the hot and rainy periods. Lowest wind speeds are in the highland areas while the desert areas have the highest wind speeds in comparison to the other regions.

4. It can be concluded that rains are preceded by higher values of temperature, sunshine duration, solar radiation and evaporation.

6.1.2 Conclusions drawn from correlations between the solar indices and the climatic parameters

1. The lake influence in KSM and the mountainous terrain of western highlands of Rift Valley in Kericho make the two areas susceptible to little direct influence of the photospheric index, Sunspot number on RH, while the Indian Ocean influence in MSA and the low land semi arid orography of GRS make these areas susceptible to little inverse correlation between R_s and RH.

Negative correlation between the coronal index F10.7 cm solar radio flux and RH is evident in Kenya, particularly in the coastal regions where MSA meteorological station is located. Lake Victoria modifies the correlation in KSM area to a slight positive value. Mg II core-to-wing ratio, hence the solar UV radiation has dominant positive correlation with RH in most parts of Kenya, particularly in the coastal region of MSA where RH is

comparatively higher. Effect of Lake Victoria is that the correlation between Mg II core-to-wing ratio and RH is positive as observed in KSM. The correlation pattern of Mg II core-to-wing ratio with RH is quite similar to that between F10.7 cm solar radio flux and RH, and to that between sunspot numbers and RH, except in KER where sunspot numbers has a positive instead of negative correlation with RH unlike the other two.

2. It can be generally stated that sunspot numbers has negative correlation with temperature in most parts of the country, except in the western rift valley highlands of KER where the mountainous terrain influences positive variation between them.

Positive variation of the coronal index with temperature is dominant in Kenya, particularly in the western highlands of Rift valley area of KER. However, the high temperature range areas of KSM and GRS whose respective climates are modified by Lake Victoria and the low land semi arid condition have their minimum temperatures influenced inversely by the coronal index. The effect of the chromosphere through Mg II core-to-wing ratio, hence the solar UV radiation is similar in pattern to the effect of the corona through F10.7 cm solar radio flux on temperature in Kenya.

3. Proximity of the water bodies in KSM and MSA influence wind pattern in such a way that some positive correlation of sunspot numbers with the wind speed is detectable. In

the highland areas of KER and NBI; and in the low land semi arid areas of GRS, the pattern of the winds is that there is some negative correlation between R_s and WIS.

KER area with lowest wind speeds and the GRS area with the highest wind speeds due to their prevailing respective orography earlier mentioned, have their wind speeds influenced inversely by the corona through the index F10.7 cm solar radio flux. The large water body areas of KSM and MSA, have their moderately high wind speeds influenced positively by the corona through the index F10.7 cm solar radio flux. NBI with moderate wind speeds also registers positive influence of the coronal index, though without statistical significance.

The correlation pattern between Mg II core-to-wing ratio and WIS is quite similar to that between sunspot numbers and WIS, though the positive correlation between Mg II core-to-wing ratio and WIS in MSA, and the negative correlation between the two parameters in GRS are statistically significant at the 0.05 level (2-tailed). But, the analogous correlations between sunspot numbers and WIS in the two areas (MSA and GRS) are not significant at any acceptable levels.

4. The sunspot numbers (R_s) has some negative correlation with SUD in most parts of the country, especially in the low land semi arid areas of GRS. The coastal regions on the other hand indicate slight positive correlation between R_s and SUD.

The western highlands of rift valley area of KER and the lowland semi arid area of GRS have their sunshine duration inversely influenced by the corona through the index F10.7 cm solar radio flux. The negative influence is stronger in the semi arid region of GRS. The central highland area of NBI and the areas within the proximity of large water bodies such as KSM and MSA have their sunshine duration positively, but weakly influenced by the corona through the index F10.7 cm solar radio flux.

The trend of correlation between the chromospheric index Mg II core-to-wing ratio, hence solar UV radiation and SUD is similar to the trend of correlation between the coronal index F10.7 cm solar radio flux and SUD at all the stations, however, the positive correlation between F10.7 cm solar radio flux and SUD in GRS is statistically significant at the 0.05 level (2-tailed) while the correlation between Mg II core-to-wing ratio and SUD in GRS is not significant at any acceptable level.

5. The sunspot numbers (R_s) has some negative correlation with SRA in most parts of the country, especially in the lowland semi arid area of GRS. The central highland area of NBI and the lake influence in KSM make the two areas have positive correlation between R_s and SRA.

Corona through the index F10.7 cm solar radio flux correlates with SRA positively in most parts of the country. The positive correlation with SRA is strong in the lake region of KSM, but strongest in the central highland area of NBI. The correlation between F10.7 and SRA is, however, inverse in the lowland semi arid region of GRS.

The trend of correlations between Mg II core-to-wing ratio and SRA is similar to the trend of correlations between F10.7 cm solar radio flux and SRA at all the stations except at MSA where F10.7 cm solar radio flux has a positive correlation with SRA but the inverse correlation between Mg II core-to-wing ratio and SRA is the case. A slight difference in KSM where the positive correlation between the corona and SRA through the index F10.7 cm solar radio flux is significant at 0.05 level (2-tailed) while the analogous correlation between the chromosphere and SRA through Mg II core-to-wing ratio is not significant at any level.

6. A general negative correlation between R_s and EVA is evident in Kenya. The coastal influence brings about the little positive correlation between R_s and EVA in MSA.

Corona through the index F10.7 cm solar radio flux correlates with EVA positively in most parts of the country. The correlation between F10.7 cm solar radio flux and EVA is, however, inverse in the lowland semi arid region of GRS. The inverse correlation with EVA is very strong in this region.

The chromosphere through Mg II core-to-wing ratio, just like the photosphere through the sunspot numbers correlates negatively with EVA in the western highlands of rift valley area of KER, central highlands of NBI and in the lowland semi arid area of GRS. The chromosphere through Mg II core-to-wing ratio and the corona through F10.7 cm

solar radio flux have some positive correlations with EVA in the areas near large water bodies of KSM and MSA due the influence of the proximity of the large water bodies.

7. The orography of highland areas (KER and NBI) and the low land semi arid area of GRS favor the positive correlations between sunspot numbers and RNF; and between Mg II core-to-wing ratio and RNF. On the other hand, proximity of large water bodies of KSM and MSA favor the negative correlations between the two solar parameters and RNF. F10.7 cm solar radio flux has similar variations with RNF as the other two solar indices with RNF, except at KER where it correlates with RNF negatively instead of positively as the other two. KER has the highest rainfall values being in the western highlands of rift valley with dense forest coverage. The physical features favor cloud formation that result in frequent rainfall. The kind of orography here favors negative correlation between the coronal index and RNF in the area. It is, however, conclusive that the correlation between the three solar indices and rainfall is complex, and can be positive, negative or even zero in the country based on my short term observations; a similar scenario by Pederson (2001) based on long term (centennial) observations as reported by Juan (2004) states that the correlation between sunspot numbers and precipitation may be positive, negative, or even zero.

6.1.3 Conclusions drawn from the significant periodicities in climatic parameters

1. The modal 6 and 12 months (the semiannual and annual) periodicities observed in all the climatic parameters in NBI, KSM, MSA and GRS are due to solar activity forcing as

supported by reports of Russel and McPherron (1973), Charman-Lal (2000), Clua de Gonzalez *et al.* (2001) and Rabiu (2004).

2. The Quasi-biennial periodicities of 25 months/cycle observed in Minimum temperature, Sunshine duration and rainfall in Kericho are due to solar activity whose parameters such as sunspot numbers, solar radio flux 10.7 cm, green coronal activity and solar neutrino flux have also shown Quasi-biennial Oscillation signals as reported by Georgieva *et al.,* (2000).

3. The 11 year solar cycle that is evident in all the solar indices, is also observable in MIT and RH for KSM and MSA respectively as 125 months/cycle; it is also close to the 122 and 123 months/cycle for MAT and SRA respectively in GRS. This is still a conclusive evidence of solar control on climate.

6.1.4 Conclusions drawn from the empirical linear models obtained

All the models in equations 5.1 to 5.45 show solar indices forcing of the climatic parameters. The statistical indicators MBE and RMSE validate the models as recommended by Iqbal, (1993) and Halouani *et al.,* (1993). The following conclusions can be drawn from the models:

1. The photosphere through its index, the sunspot number has positive forcing of Relative humidity (RH); while the corona, through its index F10.7 cm solar radio flux

has negative forcing of RH in Kenya, except for KER and GRS meteorological stations where the scenario is opposite. Solar Ultraviolet (UV) radiation through the proxy Mg II core to wing ratio which is the index of the chromosphere has positive forcing of RH in Kenya. The lowland semi arid region of north Eastern Kenya influences the opposite trend of forcing. The models give predicted values that correlate well with the observed values for KER, KSM and MSA when short time data are used (Appendix 1); but they give predicted values that correlate better with observed values when longer duration data are used (Appendix 2).

2. The photosphere through its index, the sunspot number has negative forcing of Temperature (Maximum, Minimum and Average temperatures); while the corona, through its index F10.7 cm solar radio flux has positive forcing of Temperature in Kenya, except for KER meteorological station. Solar UV radiation through the proxy Mg II core-to-wing ratio, which is the index of the chromosphere has negative forcing of MAT in Kenya, except for MSA where there is negative forcing. Mg II core-to wing ratio, however, shows general negative forcing of MIT and AVT in majority of the stations considered in this study. Positive forcing is, however, prevalent in KER and GRS for MIT; and in NBI and MSA for AVT. The Maximum temperature model for KER gives predicted values that correlate well with observed values when short time data are used (Appendix 1); but they give predicted values that correlate better with observed values ($r = 0.89$) when longer duration data are used (Appendix 2). From Appendix 2, it is also clear that longer period predictions can be done for minimum and average temperature

($r \geq 0.9$ between predicted and observed values when longer time data are used in model testing).

3. The photosphere through its index; the sunspot number has negative forcing of Wind speed, Sunshine duration, solar radiation and evaporation in Kenya, except for KER meteorological station where positive forcing is noted. The positive forcing seen in GRS for SUD and EVA are unique due to the lowland semi arid conditions there.

The corona, through its index F10.7 cm solar radio flux has positive forcing of Wind speed, Sunshine duration, solar radiation and evaporation in Kenya, except for KER and GRS meteorological stations where negative forcing is noted for WIS, SUD and EVA. Negative forcing of SRA is only in KER.

Solar UV radiation through the proxy Mg II core-to-wing ratio, which is the index of the chromosphere has negative forcing of WIS in NBI and KSM but positive forcing in the rest of the stations. The positive forcing in NBI and KSM is attributable to the screening effect of the tall buildings that modify the wind speed. However, a clear negative forcing of SUD, SRA and EVA is evident in the country save for MSA in the cases of SUD and EVA, NBI in the case of SRA and GRS in case of EVA. Negative forcing of these three climatic parameters can be concluded for Kenya.

From appendix 2, it is clear that longer period predictions can be done for wind speed (r = 0.55 between predicted and observed values when longer time data are used in model testing). However, SUD and SRA models give predicted values that do not have very high correlation coefficients with the observed values although the correlations are highly significant (Appendix 2). The models for EVA also give predicted values that correlate well with observed values (r ~ 0.7 at high significance level) when longer duration data is used in post data model testing (Appendix 2).

4. The photosphere through its index, the sunspot number has negative forcing of Rainfall in Kenya, except for the positive case noted in MSA. F10.7 cm solar radio flux has negative forcing of Rainfall in KER and MSA, while it has positive forcing in NBI, KSM and GRS. Mg II core-to-wing ratio has negative forcing of rainfall in NBI and GRS, while it has positive forcing in KER, MSA and KSM. It is evident that the nature of forcing the three solar indices have on rainfall can be positive, negative or even zero just as was noticed in the correlations between each of the three solar indices and rainfall. Pederson, (2001) based on long term (centennial) observations as reported by Juan, (2004) confirms this scenario. The models of rainfall are not applicable as can be seen in the poor correlation coefficients between predicted and observed values when post data testing of the models are done (Appendixes 1 and 2).

6.1.5 Conclusion drawn from the periodicities of drought occurrences versus the solar periodicities

Solar signature is in the drought occurrence in Kenya as observed in the model short time periodicities of 3.5 years that directly correspond to solar activity periodicities that have been reported by Rao, (1973). The well known 11 year solar cycle and a fairly close periodicity of 9 to 11 years in drought occurrence obtained in this work further confirm this signature.

6.1.6 Conclusion from the models of stepwise regression of the lagged solar indices

The stepwise multiple regression method of the lagged values of the solar indices on the climate parameters gives some models that do not give reliable results when the post data testing of the models are done. So it is conclusive that the fast Fourier analysis method gives better models with good results when post data testing of the models are done. Appendixes 1 and 2 confirm statistically significant correlations between observed and predicted values of climatic parameters obtained from Fast Fourier analysis models.

6.2 Recommendations

6.2.1 Recommendations to researchers for further work

1. There is need to investigate lack of annual and semiannual periodicities of climatic parameters in Kericho, and why we get the 50 and 82 months periodicities only in this

station. Uniqueness of Kericho in all the cases discussed earlier is recommendable for further studies.

2. Kericho's uniqueness in the solar indices forcing of RH and Temperature, WIS, SUD, SRA, EVA and RNF needs further investigation as to how the prevailing orography there is responsible. Similarly, the coastal climate can be studied to establish how it is responsible for positive forcing of the chromospheric index Mg II core-to-wing ratio on MAT.

3. I also recommend studies to investigate possibility of shorter periodicities in solar activities in any of the many solar parameters that can be related to the 3 months periodicities that are seen in the climatic parameters: RH, MAT, WIS, RNF and AVT in all the meteorological stations apart from Kericho.

4. Further studies are also necessary for longer climatic data period. The climatic data period for Kenya could not go longer than what I had for this work. The longer data period will be essential in establishing how solar cycles are related to climatic variability and changes on decadal to centennial scales. Non linear models need to be tried, especially for rainfall. Development of accurate models can help in generating climatic data from as far back as when the solar data records are available. The accurate models can help in forecasting the climatic parameters because the solar parameters' data for the future are well estimated. Also there is a need to consider more meteorological stations

so as to attain more comparable results in the different topographic locations of the country.

6.2.2 Recommendation to the Kenya Meteorological Department.

There is a need to forecast the other climatic elements such as Relative Humidity, Temperature, Wind speed, Sunshine duration, solar radiation and Evaporation by looking at the solar forcing. This is going to take climate and weather forecast steps higher from the traditional weather forecast by looking at rainfall patterns.

6.2.3 Recommendation to the Government of Kenya

The government needs to institute policies that enable the scientific communities to have direct access to the satellite data for this kind of research. There is a need to link up the local researches to advanced nations with the observatories and satellites in space for ease of research activities in this area. It is necessary for us as a country to start planning for our own observatories and satellites; there are uncountable solar events that have direct influence on activities on the earth. Some of these events are harmful and we can only be safe from them if we can have adequate knowledge of them in advance.

REFERENCES

1. Agwata, J.F. (2003). A review of indices used to study drought. Proceedings of the Sixth Kenya Meteorological Society workshop on meteorological research, applications and services, Mombasa, Kenya, pages 108-112.
2. Akasofu, S and Chapman, S. (1972). Solar Terrestrial Physics, Clarendon press Oxford England.
3. Alusa, A. (2003). Early warning, prevention-preparedness and response continuum in the management of hydromteorological disasters. Proceedings of the Sixth Kenya Meteorological Society workshop on meteorological research, applications and services, Mombasa, Kenya, pages 23-26.
4. Aming'o, P.O. (2005). Potential Causes and Predictability of the Space – Time patterns of the Decadal Rainfall Variability Modes over East Africa. M Sc thesis; Department of Meteorology, University of Nairobi.
5. Anderson, R.Y. (1982). Long geoclimatic record from the Permian: Journal of Geophysical Research, v. **87**, pages 7285–7294.
6. Bai, T. (2003). Periodicities in Solar Flare Occurrence: Analysis of Cycles 19-23; (bai@quake.stanford.edu.) ApJ, April 8, 2003.
7. Basalirwa, C. P. K., Odiyo, J. O., Mngodo, R. J. and Mpeta E. J. (1999). The climatological regions of Tanzania based on rainfall characteristics. Intl. J. Climatol. Vol. **19**, pages 69-80.
8. Bhatnagar, A. (2006). Why study the sun? Journal of Astrophysics and Astronomy, vol. **27**, pages 59-78.
9. Bourke, P., (1996). (http://astronomy.swin.edu.au/_pbourke/other/correlate/.). February 23, 2007.
10. Brijlal and Subramahmanyam, N. (1982). Heat and Thermodynamics; S. Chand &Company Ltd publishers, Ram Nagar, New Delhi-110055.
11. Chaman-Lal (2000). Sun-earth geometry, geomagnetic activity, and planetary F2 layer ion density. Part 1: Signatures of magnetic reconnection, *Journal of Atmospheric and Solar-Terrestrial Physics*, vol. **62**, pages 3-16.

12. Climate and Weather of the Sun – Earth System (CAWSES), 2004-2008: an international program sponsored by Scientific Committee on Solar Terrestrial Research (SCOSTEP).
13. Clua de Gonzalez, A. L., Silbergleit, V. M., Gonzalez, W. D., and Tsurutani, B. T. (2001). Annual variation of geomagnetic activity, *Journal of Atmospheric and Solar-Terrestrial Physics, vol.* **63**, pages 367-374.
14. Dean, W. E. (2006). Sun and Climate **(**http://greenwood.cr.usgs.gov/pub/fact-sheets/fs-0095-00/). April 4, 2007.
15. Dewan, E. M and Shapiro, R. (1991). Are sunspot-weather correlations real? J. *Atmos. Terr. Phys*. Vol. **53**, pages 171-174.
16. Dickinson, R. E. (1975). Solar variability and the lower atmosphere, Bull. Amer. Met. Soc. Vol. **56,** pages1240-1248.
17. Dilley,(http://www.livingwithclimate.fi/linked/en/Dilley-cross_cutting_issues). June 18, 2008
18. Dendrochronology - Wikipedia, the free encyclopedia. **(**http://en.wikipedia.org/wiki/Dendrochronology). March 12, 2008.
19. Duffie, A. J. and Beckman A. W. (2006). Solar Engineering of Thermal Processes, Third Edition: Copyright © by John Wiley & Sons, Inc., Hoboken, New Jersey.
20. Eddy, J. A. (1977). Climate and the changing sun, *Clim. Change***,** vol. **1,** pages 173-190.
21. El-Metwally, M. (2005). Sunshine and global solar radiation estimation at different sites in Egypt. Journal of Atm. and Solar-Terrestrial Physics, vol. **67**, pages 1331–1342.
22. Falayi, E. O. (2005). M.Tech Thesis, Federal University of Technology, Akure.
23. Fernandez, J. H., *et. al*. Abstract book of UN/NASA Workshop on International Heliophysical Year (IHY) and Basic Space Science, Bangalore India. November 27-December 1, 2007. Web-site: (http://www.iiap.res.in/ihy)

24. Foukal, P. and Lean, J. (1990). A model of total solar irradiance variation between 1874-1988, Science, vol. **247,** pages 556-558.

25. Fox, P. A., Fontenla, J. M., and White, O. R. (2004). Solar irradiance variability-comparison of models and observations. *Advances in space Research***,** vol. **34,** pp 231-236.

26. Fremming, D. (1970). Notes on Easterlies disturbances affecting East Africa. *E. A. Met. Dept. Tech. Memo.*, No. 13.

27. Friis-Cristensen, E., and Lassen, K. (1991). The length of the solar cycle: an indicator of solar activity closely associated with the terrestrial climate, *Science,* vol. **254**, pages 698-700.

28. Friis-Cristensen, E. (2001). Do Solar Variations Affect Our Climate? ESA Space Weather Workshop: Looking towards a European Space Weather Programme ESTEC.

29. Georgieva, K., Tsanev, V., Kirov, B. (2000). Solar asymmetry, QBO and Climate, In: Proceedings of the SPARC 2000, Second Assembly of the SPARC/WCRP Project. (www.aero.jussieu.fr/Sparc/SPARC2000new/PosterSess3/Session_3/Georgieva/doklad.htm).

30. Glossary of the Solar-Terrestrial terms; NOAA/Space Weather prediction Center. (http://www.swpc.noaa.gov/info/glossary.html). January 1, 2008.

31. Győri, L., Baranyi, T., Turmon, M. and Pap, J. M. (2004). Study of differences between sunspot area data determined from ground-based and space-borne observations, Advances in Space Research, vol. **34**, pages 269-273.

32. Haigh, J.D. (1994). The role of stratosphere in modeling the solar radiative forcing of climate. Nature, vol. **370**, pages 544-546.

33. Halouani, M., Nguyem, C. T and Ngoc, D. (1993). Calculation of monthly average global solar radiation on horizontal surface using daily hour of bright sunshine solar energy, vol. **50**, pp. 247-258.

34. Hansen, J. E. and Lacis, A. A. (1990). Sun and dust versus greenhouse gases: an assessment of their relative roles in global climate change, Nature, vol. **346**, pp 713-719.

35. Heath, D.F. and Schlesinger, B.M.(1986). The Mg II 280nm doublet as a monitor of changes in solar Ultraviolet Irradiance. J. Geophysics. Res. Vol. **91**, pages 8672-8682.

36. Iqbal, M. (1993). An introduction to solar radiation. Academic press. New York, pp 59-67.

37. ISO 21348 information; Space environment Technologies. spacenvironment@spacevironment.net http://SpaceWx.com February 20, 2008.

38. Jona Lendering; **(**http://www.livius.org/dedh/dendrochronology/dendrochronology.html) July 14, 2007.

39. Juan, Z, Yan-Ben H, Zhi-An L. (2004). The Effect of Solar Activity on the Annual Precipitation in the Beijing Area. Chinese Journal of Astronomy and Astrophysics. Vol. **4**. No. 2; pp189-197 (http://www.chjaa.org or http://chjaa.bao.ac.cn).

40. Kilcik, A. (2005). Regional sun–climate interaction. Journal of Atmospheric and Solar-Terrestrial Physics, vol. **67**, pages 1573–1579.

41. Kitheka, S.K. (2003). The challenges of climate variability to sustainable agriculture in semi-arid Kenya. Proceedings of the Sixth Kenya Meteorological Society workshop on meteorological research, applications and services, Mombasa, Kenya, pages 126-129.

42. Kyle, L. Climatology Interdisciplinary Data Collection update on Total Solar Irradiance (Temporal coverage Nov 1978-Dec 1997).

43. Makabana J. R. (2003). The experience of the Kenya meteorological services in early warning, disaster preparedness and mitigation in Kenya. Proceedings of the Sixth Kenya Meteorological Society workshop on meteorological research, applications and services, Mombasa, Kenya, pages 1-3.

44. Makarova, L. N. and Shirochkov, A. V. (2004). The Sun and the solar wind variability of different time-scales and the climate dynamics, Advances in Space Research, vol. **34**, pages 432-435.

45. Mathur, D. S. (1980). Elements of Properties of Matter; Shyam Lal Charitable Trust Ram Nagar publishers, New Delhi-110055.

46. Mehul, M. (2005). Solar coronal rotation and phase of solar activity cycle. Bull. Astr. Soc. India, vol. **33**, pages 323-325.

47. Micolich, A. (2006). Lectures 6: Thermodynamics in the Atmosphere. "PHYS2060 Thermal Physics Lecture 6". (www.ausgo.unsw.edu.au/PHYS2060/pdf/).

48. Mungai, J.G. and Mukabana, J.R. (2003). The current status of NWP model application in forecasting at regional meteorological centre – Nairobi. Proceedings of the Sixth Kenya Meteorological Society workshop on meteorological research, applications and services, Mombasa, Kenya, pages 51-54.

49. Nag, T.K. & Das, T.K., Periodicity in various kinds of solar activity. Institute of Radio Physics & Electronics, Kolkata - 700009. Email: tukada2@vsnl.net. August 15, 2007.

50. Ndeda, J. O. H., Rabiu, A. B., Ngoo, L. H. M. and Ouma G. O. (2006). Inter-Relationships between Solar Radiation Intensity and Relative Humidity in Kenya. Abstract bookof 2nd UN/NASA WORKSHOP on International Heliophysical Year and Basic Space Science, Bangalore India.

51. Ndeda, J. O. H., Rabiu, A. B., Ngoo, L. H. M. and Ouma G. O. (2007). Stepwise Multiple Regression of the Climatic Parameters on Solar Parameters: Sunspot Numbers(R_s), F10.7 cm Solar Radio Flux, Mg II and their lagged Values for Kenya. Abstract book of 2nd International Heliophysical Year-Africa and SCINDA

52. Ndeda, J.O.H., Rabiu, A.B., Omeny, P., Ouma, G. and Ngoo, L.M. (2007). Solar signature in the Drought Occurrence in Kenya, East Africa. Abstract book the First International Academy of Astraunatics (IAA) African Regional Conference in Abuja, Nigeria.

53. NGDC, Boulder, Colorado;(http://www.ngdc.noaa.gov/stp/SOLAR/ftpsolar(uv or radio).html). March 27, 2006.

54. Nikolashkin, S. V., Ignatyev, V. M., and Yugov, V. A. (2001). Solar activity and QBO influence on the temperature regime of the subauroral middle atmosphere, *J. Atmos. and Solar-Terrestrial Physics,vol* **63**, pp853-858. *www.elsevier.nl/locate/jastp*.

55. Njau, L. N (1982) : Tropospheric wave disturbances in East Africa. *M. SC. Thesis, Dept. Of Met., University of Nairobi.*

56. Nyakwada, W. (2003). Climate risk and vulnerability in Kenya. Proceedings of the Sixth Kenya Meteorological Society workshop on meteorological research, applications and services, Mombasa, Kenya, pages 35-43.

57. Ogallo, L. J. (1980). Regional classification of East Africa rainfall stations into homogeneous groups using the method of principal component analysis, statistical Climatology, Developments Atmospheric Science, vol.**13**, pp.255-266.

58. Ogallo, U. (1989b). The spatial and temporal patterns of the East African rainfall derived from PCA. Inter J. Climatology. Vol. **9**, pages 145-167.

59. Okoola, R. E. A. (1996). Space-time characteristics of the ITCS over equatorial eastern Africa during anomalous rainfall years. *Ph.D. Thesis, Dept. of Meteorol.,University of Nairobi, Kenya.*

60. Oritz, A., Dimingo V., Sanahuja B. Department d'Asronomia i Meteorologia. Universitat de Barcelona. Spain *(http://www.am.ub.es/~blai/sol-constant-UB.html)* Solar irradiance variations. January 20, 2008.

61. Ouma, G. O. (2000). Use of Satellite Data in Monitoring and Prediction of Rainfall over Kenya. Ph. D thesis; Department of Meteorology, University of Nairobi. August.

62. Palmer, M.A., Gray L.J., Allen M.R. and Norton, W.A. (2004). Solar Forcing of Climate: Model Results. Advances in Space Research, vol. **34**, 343-348.

63. Quark Soup: Reflections on the wave function of the universe; September 2004, Haiti. http://www.nasw.org/users/appell/Weblog/indexold.html.

64. Rabiu, B. A., Ndeda, J. O. H., Ngoo, L. H. M. and Ouma, G. O. (2007). Spectral Characteristics of the Meteorological Variables over Kenya, East Africa; Proceedings of the International Conference on the Impacts of Exreme Weather and Climate on Socio-Economic Development in Africa. 11-15 November, Akure, Nigeria, Pages 132-135.

65. Rabiu, A. B., Adeyemi, B. and Ojo, J. (2005). Variability of solar activity and surface air temperature variation in tropical region. Journal of the African Meteorological Society, vol.**6**. No.3, pages 83-91.

66) Rabiu, A. B., And Omotosho, T. V. (2003). Solar activity and total column ozone variation in Lagos, Nigeria. J. Pure and Applied phys. vol. **2**, pages 17-20.

67) Rabiu, A. B., **(**2004). Semiannual variation of geomagnetic activity Ak index and its response to solar activity. Zuma Journal of Pure and Applied Sciences, ZJPAS, vol. **6.** No. 1, pp 40-47.

68) Rao K. R. (1973). Short periodicities in solar activity. Solar Physics journal Vol. **29**, No. 1. March, pages 47-53.

69) Raspopov, O.M., Dergachev, V.A., Shumilov, O.I., Kolström, T., Lindhholm, M., Meriläinen, J., Eggersston, O., Vasiliev, S.S., Kuzmin, A.V., Kirtsidey, I.Y., Kasatkina, E.A. (2001). Dendrochronological evidence of long-term variations in solar activity and climate (oleg@omr..izmi.ras.spb.ru). International conference Tree rings and people. Davos.

70) Riley, P. and Crooker, N.U. (2004). Kinematic treatment of coronal mass ejection evolution in the solar wind. Astrophys. J. Vol. **600**, page 1035.

71) Rolf, P., Bruno, D., Marty, C., Atsumu, O., Martin, W. (2005). Radiative forcing – measured at Earth's surface – corroborate the increasing greenhouse effect. GRL, VOL. **31**, L03202, doi:10.1029/2003GL018765.

72) Russell, C. T. and McPherron, R. L. (1973). Semi-annual variation of geomagnetic activity, *J. Geophys. Res. Vol.* **78**, pages 92-108.

73) Ruzmaikin, A., Lawrence, John K. and Cadavid, A. C. (2004).A simple model of solar variability influence on climate, Advances in Space Research, vol. **34**, pages 349-354.

74) Scargle, J. D. (1982). Studies in astronomical time series analysis. II. Statistical aspects of spectral analysis of unevenly spaced data, Astrophys. J., vol. **263**, pp 835-853.

75) Schwabe, H. (1843). Excerpts from solar observations during 1843. Astronomische Nachrichten, vol. **20**, No 495.

76) Shah, G. N, Mufti S. (2005). Anti-podal Geomagnetic activity, Sea surface temperature and long- term solar variations. 29th International Cosmic Ray Conference Pune **00**, pages 101-104.

77) Solanki, S. K. and Fligge, M. (2001). ETHZ IfA: Reconstruction of Past Solar Irradiance Variations. Institute of Astronomy ETH Zurich. (http://www.astro.phys.ethz.ch/research/fligge/paleo_nf.html)

78) Solar Filaments and Prominences. January 1, 2008. **(**http://solar.physics.montana.edu/YPOP/spotlight /Tour/imagemap/docs/hfilaments2.html).

79) Solar Irradiance and Long-Term Climatic Variability. January 1, 2008. **(***http://www.Org/revgeophysics/reidoo/model2.html)*.

80) Solar Spectra: Air Mass Zero. (http*://rredc.nrel.gov/solar/specra/amo/*). February 29, 2005.

81) Solar Structure. January 1, 2008. (http://www.columbia.edu/~ah297/unesa/sun/sun-chapter1.html).

82) Solar Ultraviolet Spectral Irradiance. National Geophysical Data Centre (NGDC). January 1, 2008. (http:www.ngdc.noaa.gov/stp/SOLAR/ftpsolaruv.html).

83) Tamara S., Ledley *et. al.*, (1999). Climate Change and Greenhouse Gases. EOS vol. **80**, No. 39, pp.453.

84) The Australian Space Weather Agency (IPS Radio and Space Weather Sciences); Sept 12 2006. (http://www.ips.gov.au/Solar/1/6).

85) The Structure of the Sun. January 1, 2008. (http://www.cs.berkeley.edu/~barreno/classes/projects/sun/struct.html).

86) The Sun and Space Weather. (soho.nascom.nasa.gov/spaceweather/lenticular). January 1, 2008

87) This is the Sun in ultraviolet light! January 1, 2008. **(**www.nasa.gov, soho.nascom.nasa.gov).

88) Thompson, B. W. (1957): Some reflections of equations and tropical forecasting. *E. A. Met. Dept. Tech. Mech.,* No. 7.

89) Tobiska, W. K. **(**2002). New developments in solar irradiance proxies for operational space weather. TIGER Virtual Symposium Proceedings.

90) Tobiska, W. K., Woods, T., Eparvier, F., Viereck, R., Floyd, L., Bouwer, D., Rottanman, G. and White, O. R. (2000). The SOLAR2000 empirical solar irradiance model and forecast tool. *Journal of Atmospheric and Solar-Terrestrial Physics* **62**, pages 1233-1250.

91) Tracking a solar storm by NASA; Why do Sunspots and CMEs occur? January 1, 2008. (http://son.nasa.gov/tass/content/occur.html).

92) Udo, S. O. A. (2003). Modeling of Infrared Radiation for all Skies from Easy-to-measure Meteorological parameters at Tropical Location: Ilorin Nigeria. Turk J Phys. Vol. **27**, pp 61 – 68.

93) US National Report to JUGG, 1991-1994. Rev. Geophysics vol. **33** Supp,@1995 American Geophysical Union.

94) Varotsos, C. O. and Cracknell, A. P.(2004). New features observed in the 11-year solar cycle. Int. j. remote sensing, vol. **25**, NO. 11, 2141-2157.

95) Viereck, R. A., Puga, L., McMullin, D., Judge D., Weber M. and Tobiska W. K. (2001). The Mg II Index: A proxy for Solar EUV., G RL, vol. **28**, No.7, pp1343-1346.

96) Viereck, R. A., and Puga, L. C. (1999). The NOAA Mg II core-to-wing solar index: Construction of a 20-year time series of chromospheric variability from multiple satellites, JGR, vol. 104, pp9995-10005.

97) Viereck, R. A., L. E. Floyd, P. C. Crane, T. N. Woods, B. G. Knapp, G. and Rottman, M. (2004). Laboratory for Atmospheric and Space Physics. Activity Report. University of Colorado at Boulder.

98) Weather review during June 2007 and the Forecast for July 2007 of the KMD (Ref. No. Met/ 7/26. (http://www.meteo.go.ke). July 4, 2007.

99) Wilson, R. C., NGDC/STP-Solar Irradiance Data Archived at NGDC – Daily Total SolarIrradiance (Oct1991-Dec1993). **(***http://www.Ngdc.noaa.gov/stp/SOLAR/IRRADIANCE/irrad.hHtml)*. Feb 12, 2004.

100) Zeilik, M. and Gregory, S. (1998). Introductory Astronomy and Astrophysics, 4th Ed. Saunders College publishing, a division of Harcout Brace College publishers.

INTERNATIONAL MEETINGS WHERE VARIOUS RESULTS OF THE WORK ARE REPORTED:

(1) 2nd UN/NASA Workshop on the International Heliophysical Year and Basic Space Science: Bangalore - India (27 November – 1 December 2006)

(2) 7th Workshop on the Applicability of Environmental Physics and Meteorology in Africa: Gaborone – Botswana (26 February – 2nd March 2007)

(3) 3rd UN/ESA/NASA Workshop on International Heliophysical Year and Basic Space Science: Tokyo – Japan (June 18 – 22, 2007)

(4) 2nd International Heliophysical Year/SCINDA - Africa Workshop: Addis Ababa – Ethiopia (11 – 16, November 2007)

(5) Proceedings of the International Conference on the Impacts of Extreme Weather and Climate on the Socio-Economic Development in Africa. 11 – 15 November, 2007, Akure, Nigeria.

(6) 1st African Regional Conference of the International Academy of Astronautics (IAA) : Abuja – Nigeria (3rd – 5th December 2007)

APPENDICES

APPENDIX 1

Table of correlations between the predicted and observed values of the climatic parameters for each station

Climatic parameters		Meteorological stations			
	NBI	KER	KSM	MSA	GRS
RH	-0.15	0.67**	0.52*	0.52	0.33
MAT	0.52	-0.68*	0.29	0.58	-0.08
MIT	0.21	0.21	-0.3	0.14	0.26
WIS	-0.02	-0.03	0.59	0.59	No data
SUD	-0.37	0.4	-0.03	-0.46	0.26
SRA	-0.6**	0.45*	No data	No data	No data
EVA	-0.28	0.24	0.4	-0.44*	No data
RNF	-0.28	-0.52	-0.24	0.53	-0.47
AVT	-0.35	0.34	0.34	0.02	0.26

** Correlation significant at the 0.01 level (2-tailed). * Correlation significant at the 0.05 level (2-tailed).

APPENDIX 2

Table of correlations between the predicted and observed values of the climatic parameters with all stations' data used

Climatic parameter	Corr. Coeff
RH	0.64**
MAT	0.89**
MIT	0.96**
WIS	0.55**
SUD	0.35**
SRA	-0.45**
EVA	0.66**
RNF	-0.18
AVT	0.90**

** Correlation significant at the 0.01 level (2-tailed). *Correlation significant at the 0.05 level (2-tailed).